Année 2014 N° d'ordre : 41630

Université Lille1 Sciences et Technologies

Laboratoire Génie Civil et géo-Environnement

Ecole doctorale Sciences Pour l'Ingénieur

THÈSE

Pour l'obtention du grade de

Docteur de L'Université des Sciences et Technologies de Lille

Discipline : Génie Civil

Sous le titre de :

Analysis of the stability of slopes submitted to water infiltration using advanced models :

Coupled hydro mechanical model and Nonlinear Dynamic Method

Présentée et soutenue publiquement par

Mohammad IHSAN

Le 24 Novembre 2014 devant le jury :

Isam SHAHROUR	Professeur, Université de Lille 1	Directuer de thèse
JAOUAD Zemmouri	Professeur, Université de Lille 1	Co- Directuer de thèse
HAGE CHEHADE Fadi	Professeur, Université Libanaise	Rapporteur
ARAB Ahmad	Professeur, Université de Chlef	Rapporteur
Ali ZAOUI	Professeur, Université de Lille 1	Examinateur
Alia HATEM	Ingénieur Etude, ARCADIS	Examinateur

Table of Content

List of Figure

Résumé

Ce travail de thèse porte sur l'analyse des glissements de terrain, qui constituent un risque naturel majeur responsable de pertes humaines élevées ainsi que de grands dommages aux structures, des infrastructures et de l'environnement naturel. Cette question revêt une importance particulière, en raison du changement climatique, qui augmente le risque de fortes pluies ainsi que la sécheresse, et par conséquent le risque d'instabilité des pentes due à l'environnement.

Généralement, l'analyse de la stabilité des talus est réalisée en utilisant l'approche de l'équilibre limite. Comme cette théorie ne tient pas compte du processus de mobilisation du frottement, elle pourrait conduire à une surestimation du facteur de sécurité. Une analyse fiable de la stabilité des talus, en particulier dans les sols hétérogènes soumis à l'action de l'eau, nécessite l'utilisation de méthodes numériques avancées. Deux méthodes ont été utilisées dans cette recherche: la méthode de couplage hydromécanique et la méthode dynamique non linéaire.

La thèse est organisée en trois chapitres:

Le premier chapitre présente l'état de l'art sur la stabilité des pentes. Il présente l'influence de l'eau sur la stabilité des talus, l'utilisation de l'approche d'équilibre limites et des méthodes plus avancées.

Le deuxième chapitre présente l'utilisation de la méthode de réduction de la force mise en œuvre dans un modèle hydromécanique couplé. Les analyses sont effectuées à l'aide du programme FLAC3D. Elles couvrent un grand nombre de configurations des caractéristiques des sols et de la nappe phréatique.

Le dernier chapitre traite de l'utilisation de la méthode dynamique non linéaire pour l'analyse de la stabilité des pentes. Les analyses sont effectuées sur diverses configurations en utilisant l'équation d'équilibre ou une approche basée sur l'énergie. Des abaques sont construits pour la détermination du domaine d'instabilité d'une configuration simplifiée de talus.

Mots clés : stabilité des pentes, glissements de terrain, modèle hydromécanique couplé, méthode dynamique non linéaire

Abstract

This research concerns analysis of landslides, which constitute a major natural risk responsible for high human losses as well as large damages to structures, infrastructure and natural environment. This issue becomes particularly important, because of the climate change, which increases the risk of heavy rains as well as severe drought and consequently the risk of slope instability due to the environment change.

Generally, analysis of slope stability is conducted using the limit equilibrium theory. As this theory does not take into consideration the process of mobilization of the friction, it could lead to an overestimation of the safety factor. A reliable analysis of the slope stability, in particular in heterogeneous soils submitted to the water action, requires the use of advanced numerical methods. Two methods were used in this research: the coupled hydro-mechanical method and the nonlinear dynamic method.

The thesis is organized in three chapters:

The first chapter presents the state of the art on slope stability. It presents the influence of the water on the slope stability, the use of the limit equilibrium methods and the use of more advanced methods such as the Strength Reduction Method implemented in a coupled hydro-mechanical model.

The second chapter presents the use of the Strength Reduction Method implemented in a coupled hydro-mechanical model for the analysis of the slope stability. Analyses are conducted using the FLAC3D program. They cover a large number of configurations of the soil characteristics and the water table position.

The last chapter deals with the use of the Nonlinear Dynamic Method for the slope stability analysis. Analyses are conducted on various configurations using the equilibrium balance or a more advanced energy approach. Charts are constructed for the determination of the domain of instability of a simplified slope configuration.

Key word : slope stability, landslide, coupled hydro-mechanical model , nonlinear dynamic method

General Introduction

Landslides constitute a major natural risk, which could cause high human losses and large damages to structures, infrastructure and natural environment. Landslides result from many factors, which could be related to the environment or to human action. Water infiltration and flow are responsible of a large number of landslides. Because, generally the water infiltration leads to a reduction of the shear strength related to suction accompanied by addition forces resulting from water flow. The climate change increases the risk of heavy rains alternated with drought. These conditions present high risk for slope stability.

Landslide is submitted to major landslides risk, which caused in the period (1815-2014) 2778 destructive events and about 4372 victims.Flood is responsible for 5454 destructive events and 18 869 victims, while earthquakes are responsible for 298 destructive events and 15518 victims(Keefer, 1984; Harpe et al, 1991. Jibson et al, 1994. Harp and Jibson, 1996; Khazai and Sitar, 2004). The landslide in *Kanagarian Tandikek Padang Pariaman* damaged 3 villages and caused 675 victims. It was due to the Padang Earthquake (September 30, 2009), which was preceded by heavy rain falls during several days.

Slope Stability using the conventional methods

Thanks to important research works, the analysis of landslides has made great progress. Generally, landslides analysis is conducted using the limit equilibrium theory, which is based on the determination of the safety factor: the ratio between resisting forces (friction at the sliding surface) and driving forces (self weight, environmental loading). As this theory does not take into consideration the mobilization of the friction forces with the soil movement, it could lead to an overestimation of the safety factor for multilayer soils with different laws of friction mobilization. Indeed, in some cases, the maximum stress is not mobilized simultaneously in all the soil layers.

Need for more advanced analysis methods for the slope stability

Analysis of the slope stability particularly in heterogeneous soils submitted to the water action requires the use of methods, which take into account the action of water as well

as the deformation process and the mechanism of mobilization of the shear stresses. Two methods could be used for this analysis:

- The coupled hydro-mechanical method
- The nonlinear dynamic method.

Coupled hydro-mechanical method

The coupled hydro-mechanical method is used in geotechnical engineering for the analysis of several issues concerned by the water –skeleton interaction and the nonlinear behaviour of the soil material. Commercial programs offer large facilities for the use of this approach. In this work we will use the Strength Reduction Method implemented in the FLAC3D program.

The nonlinear dynamic method

The nonlinear dynamic method provides a powerful tool for the analysis of discontinuous phenomena, such as landslides (Thom (972). Chau (1995) and Qin et al. (2000,2005) used this method for the analysis of landslides including planar-slip slope. The sliding surface was divided into two parts: elastic – brittle and strain softening. The water action was neglected.

Research Objectives and thesis organization

This work aims at the analysis of the slope stability considering the water flow. Analyses are conducted using the two advanced methods:

- The Strength Reduction Method implemented in a coupled hydro-mechanical model
- The nonlinear dynamic method.

The thesis is organized in three chapters:

The first chapter presents the state of the art on slope stability. It presents the influence of the water on the slope stability, the use of the limit equilibrium methods and the use of more advanced methods such as the Strength Reduction Method implemented in a coupled hydro-mechanical model.

The second chapter presents the use of the Strength Reduction Method implemented in a coupled hydro-mechanical model for the analysis of the slope stability. Analyses are conducted using the FLAC3D program. They cover a large number of configurations of the soil characteristics and the water table position.

The last chapter deals with the use of the Nonlinear Dynamic Method for the slope stability analysis. Analyses are conducted on various configurations using the equilibrium balance or a more advanced energy approach. Charts are constructed for the determination of the domain of instability of a simplified slope configuration.

CHAPTER 1: Literature review slope stability analysis

1.1 Introduction

This chapter presents a literature review of researches conducted on slope instability (land sliding). The influence of the rain and the water table fluctuation on the slope stability is considered, because the water has a major responsibility in land sliding. Indeed heavy rainfalls could induce landslides in particular in the case of unsaturated slopes. In this case, landslides are governed by the following soils properties: the soil–water characteristic curve, the saturated coefficient of permeability and the unsaturated permeability, and the soil unsaturated soil resistance. Landslides appear generally in unsaturated slopes at the top of the slope and at inclinations higher than the soils friction angle. The stability of the slope is ensured by the positive effect of the matrix suction on the soils shear strength.

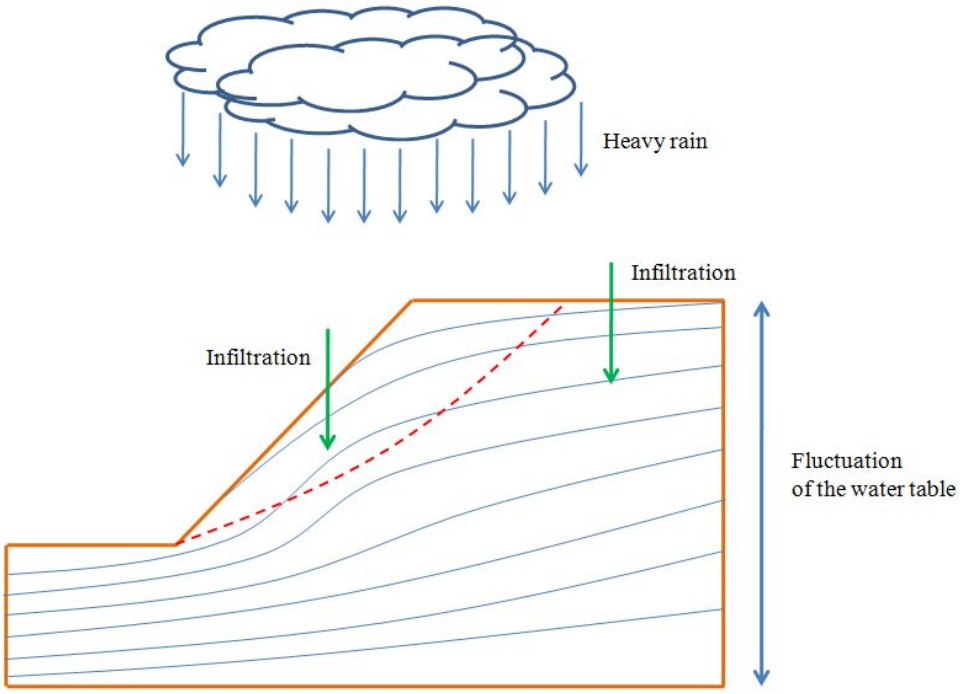

Figure 1.1 : Schematic Slope Failure Mechanism

The complexity of the landslide phenomena leaded to the development of engineering simplified methods, which are largely used in engineering practice. Since these methods do not take into consideration, the "soil deformation', they could miss some "instable states". In this chapter, we present two methods, which could take into account the soil deformability : the fully coupled hydro-mechanical model and the nonlinear dynamic method.

1.2 Hydro – mechanical approach

1.2.1 Influence of rainfall on the slope stability

Slope stability analysis of unsaturated slopes requires an extensive and detailed seepage analysis, because the slope failure in unsaturated soils is generally related to rainfall and water infiltration. The water infiltration in the soil induces:

- A loss of the soil strength related the negative pore–water (suction).
- Additional forces resulting from the water flow.

The contribution, of the soils suction $(u_a - u_w)$ to the increase in the soils strength can be accounted for by a simple extension of the Mohr-Coulomb criterion (Fredlund and Rahardjo 1993):

$$\tau = c' + (\sigma_n - u_a)\tan\phi' + (u_a - u_w)\tan\phi^b \quad (1.1)$$

In the unsaturated zone, a very small suction is often enough to ensure high safety factors. Indeed, the low conductivity of the unsaturated soil, even during the most intense rainfall events, usually prevents the water infiltration in the soil. Consequently, soils remain in unsaturated state. During dry periods, the soil loses a part of its water content, mainly by evaporation, favored in many cases by the presence of vegetation: as a consequence, only intense rain storms occurring after prolonged rainy periods may lead the soil to such wet conditions as to trigger slope instability. It is very hard to draw general conclusion concerning the soil stability under rainfall, because of the high complex slope-climate interaction (Sulem, 2010).

The determination of the change in the water suction and saturation due to the water infiltration requires the use of a water flow model in unsaturated soils as well as the knowledge of the environmental conditions.

The determination of the consequences of the change in the water saturation and pressure on the soil strength requires the use of researches developed in the field of unsaturated soils. For the seek of simplicity, we will use the simplified approach for the unsaturated soils implemented in FLAC3D program. This model will be presented in the 2nd chapter.

1.2.2 Strength Reduction Technique

The "Strength Reduction Technique" is used for the analysis of the stability in geotechnical engineering. In slope analysis, it consists in the reduction of the soil shear strength to values corresponding the slope limit equilibrium. This method is commonly used with the Mohr-Coulomb criterion (Figure 1.2) (Zienkiewicz et al. 1975, Naylor 1982, Donald and Giam 1988, Matsui and San 1992, Ugai 1989, and Ugai and Leshchinsky 1995). The values of the soil cohesion and friction angle are reduced as follows:

$$c^{\text{trial}} = \frac{1}{F^{\text{trial}}} c \tag{1.2}$$

$$\phi^{\text{trial}} = \arctan\left(\frac{1}{F^{\text{trial}}} \phi \right) \tag{1.3}$$

The tensile strength σ_t could also be considered in this method by the application of the reduction factor as in equation (1.1).

The use of this method in the analysis of the slope stability requires the conduction of a series of simulations with different values of the factor F_{trial}. Simulations should lead to large deformations, which could correspond to the system instability.

The Strength Reduction Method leads always to a valid solution. Unstable physical system will show "continuing" motion, because the solution corresponds to a dynamic process, for which a continuous motion is as a valid equilibrium solution.

The detection of the boundary between physical stability and instability is generally based on the use of the Mohr Coulomb criterion. This boundary is determined by conducting a series of runs with different strength-reduction factors. Each run is then checked to determine whether equilibrium or a continuing plastic

flow is reached. The point of failure can be determined to any required accuracy (typically 1%) by successive bracketing of the strength-reduction factors.

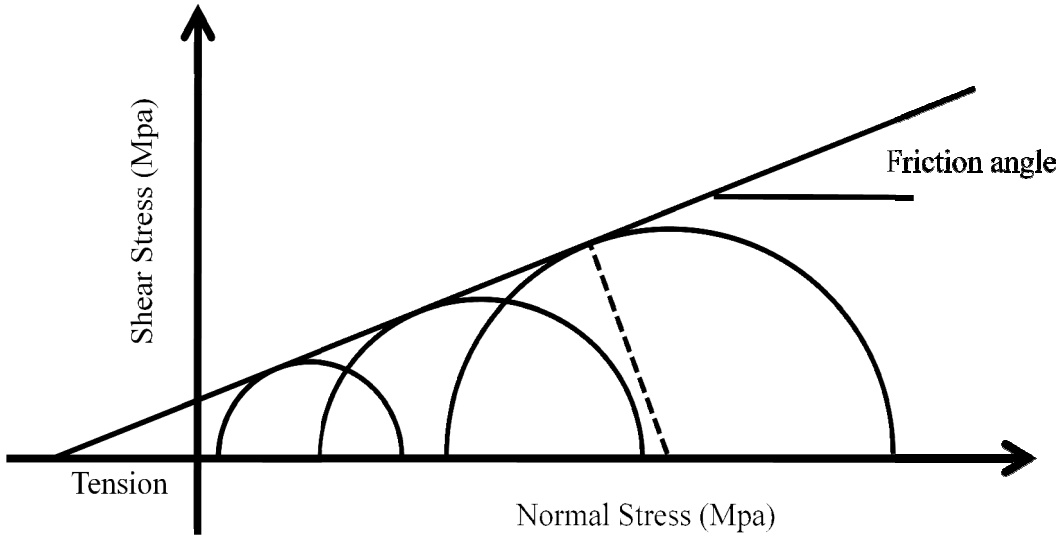

Figure 1.2 : Mohr Coulomb failure surface

1.3 Nonlinear dynamic theory

1.3.1 Statement

Analysis of the slope stability is generally conducted using the well-established Mohr-Coulomb's criterion, which includes tow parameters: the friction angle ϕ and the cohesion c. The use of this criterion includes strong assumption, because the slope stability results from a more complex process including the nonlinear soil response in the deformation domain.

Based on the theoretical studies of material stability developed by Hadamard (1903) for elastic materials and extended by Thomas (1961), Hill (1962) and Mandel (1966) for inelastic materials, instability can be predicted from the pre-failure behavior of the material. The conditions for the onset of localization are established by seeking the possible critical conditions for which the constitutive equation of the material (in the pre-localized stage) may lead to a bifurcation point for which the deformation mode could localize in a planar band (Rice 1976; Vardoulakis, 1976).

The mathematical modeling of the nonlinear and irreversible behavior of soils constitute a hard task, in particular for softening soils exhibiting important change in the plastic surface. Consequently, analysis of slope instability still uses simplified constitutive relations, which could not be able to describe the complex behavior of soils.

Since the slope instability involves common traits with some physical phenomena including jump change in the system behavior in response to a smooth change in the external conditions, the nonlinear dynamic theory could be used for the analysis of this phenomenon. Below we present this theory.

1.3.2 Nonlinear dynamic theory

The concepts and mathematical technique associated with the nonlinear dynamical system theory have been widely applied in divers scientific disciplines. Thom (1972) presented the catastrophe theory. Phillip (1992) presented the chaos concept, the fractal geometry and the catastrophe theory. Chau (1995) analysed the bifurcation of a creeping slope. Phillips (1993), Qin (2000) and Keilis-Borok, (1990) used the bifurcation theory for the analysis of landslides. In Figure 1.3 we can see evolution condition stable continue to bi stability until chaotic.

The origin of the catastrophe theory lies in the Whitney's theory of singularities of smooth mappings and Poincare and Andropov's theory of bifurcation of dynamical systems. Singularity theory is a generalization of the functions analysis at maximum and minimum point. In Whitney's theory, functions are replaced by mappings of multi-variables functions. Lyapunov (1892) presented theoretical results concerning the evolution in the time domain of the perturbation of a mechanical system. Physically, a system is stable if a little disturbance of the initial conditions does not induce a large influence on its response.

Bifurcation is used in a broad sense for designating all sort of qualitative reorganizations or metamorphoses of various systems resulting from a change in their governing parameters. Catastrophes are abrupt changes arising as a sudden response of a system to a smooth change in the external conditions.

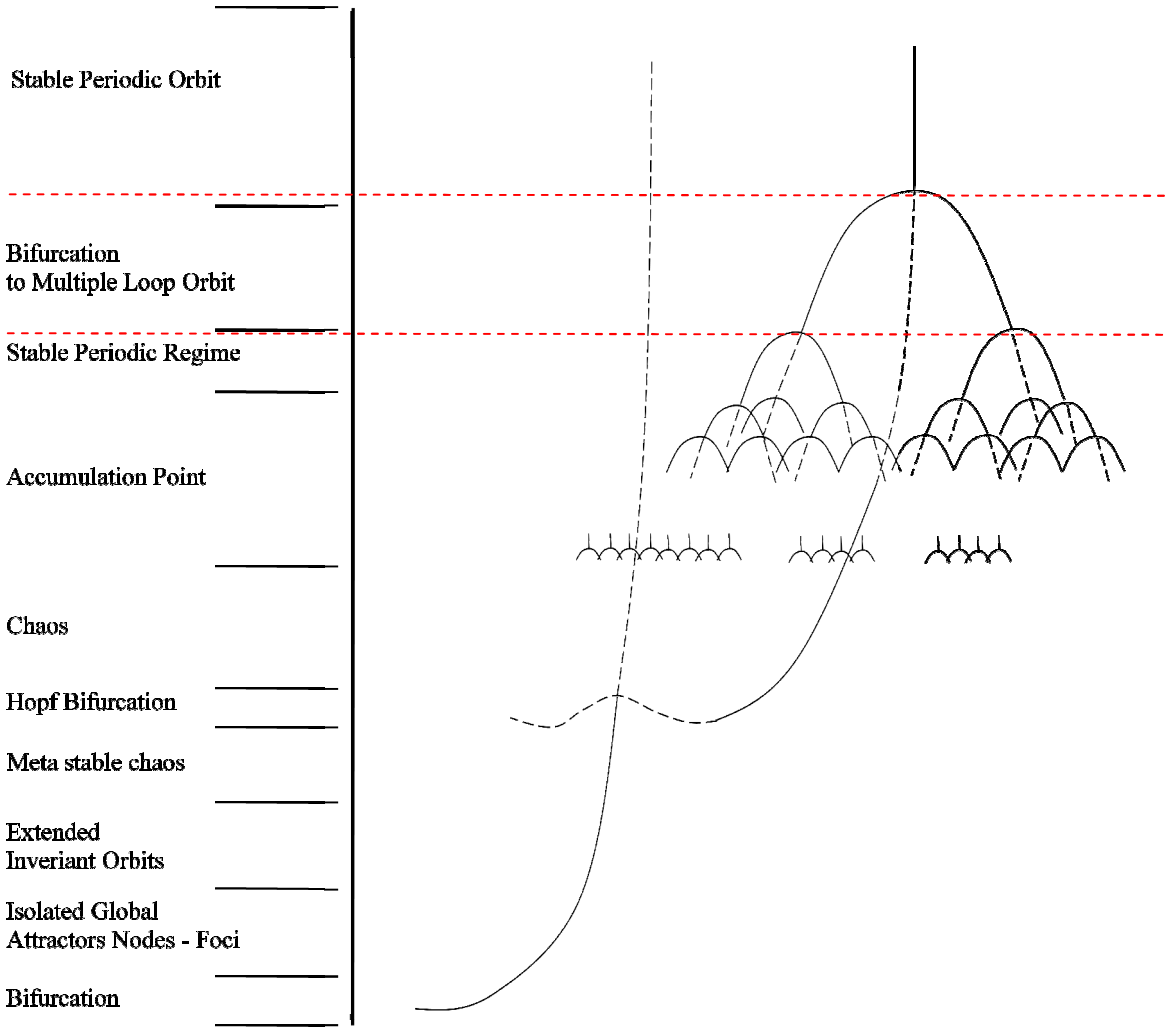

Figure 1.3 : The qualitative properties of the stable attractor of the Lorenz equations (K.A. robbins SIAM J. Appl. Math 1979)

The Bifurcation means forking and used in a broad sense for designating all sort of qualitative reorganizations or metamorphoses of various entities resulting from a charge of the parameters on which they depend. Catastrophes are abrupt changes arising as a sudden response of a system to a smooth change in external conditions. In order to understand what catastrophe theory is about one must first become acquainted with the elements of Whitney's singularity theory.

1.4 Bifurcation

Bifurcation theory concerns mathematical analysis of changes in continuous or discrete systems. It is mainly used in the analysis of dynamic systems. Bifurcation occurs when a small smooth change in a governing parameter of a system causes a sudden 'qualitative' change in its behavior.

In continuous systems, bifurcation corresponds to the annulations of the real part of an Eigen value of the system equilibrium. In discrete systems, bifurcation corresponds to a fixed point having a Floquet multiplier with modulus equal to one. In both cases, the system equilibrium is non-hyperbolic at the bifurcation point.

In figure 1.4 illustrates the bifurcation process of a system governed by the following equation at the equilibrium state were V is potential of the system:

$$\frac{dV}{dx} = x^3 + ax + b = 0 \tag{1.4}$$

a change in the parameter a or b induces change in V. b is control parameter of the system. Depending on a , the system may have one or three solutions. In the case of a single solution, the system is in a stable state but in the case of three solutions, the system has two stable solutions and an unstable solution.

The annulations of the 2^{nd} derivate of the equation (1.2) occurs at the two values:

$$x = \pm\sqrt{-\frac{a}{3}} \tag{1.5}$$

These two values x_1 and x_2 give the limit of three solutions area of equation (1.2). On the other hand, these two values don't depend on b and exist only if a is negative parameter.

In figure 1.4, we present in the next 3 figures evolution of x versus b for $a = 1$, $a = 0$ and $a = -1$

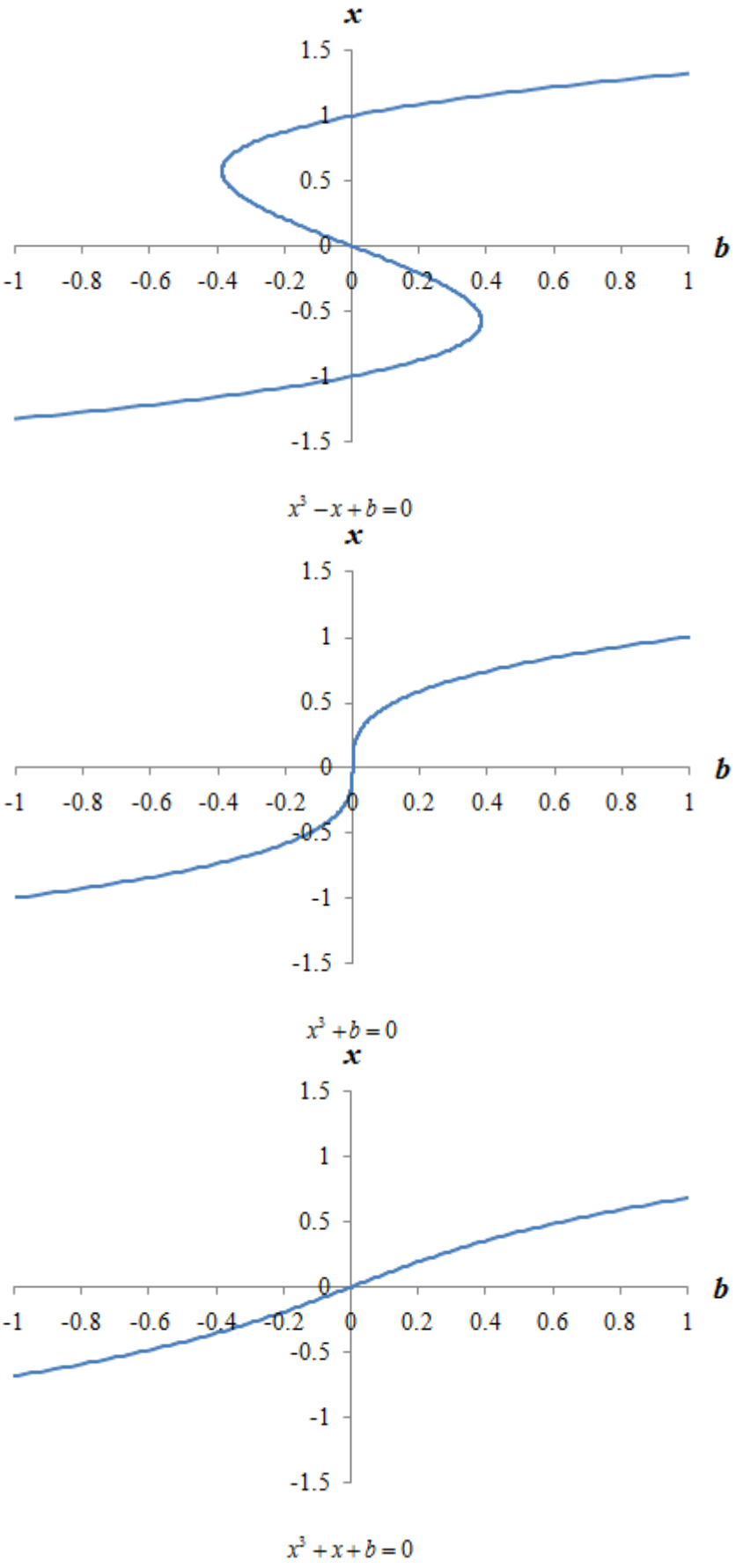

Figure 1.4 : Evolution of function bifurcation

Let us now analyse evolution of x with growing b for these three cases of a.

Case of a > 0 :

The slope of curve is always positive and then for all value of b we have only one corresponding value of x. Whatever the initial value of x, x growth monotonically with b and we don't expect any jumping of the system. We can conclude that evolution of b don't leads to any catastrophic change of the system.

Case of a < 0 :

In this case we have three branches and two branches with positive slope and one branch between $A1$ and $B1$ with negative slope.

Initial value of x defines evolution of system. Take of example that for $b = 0$, initial value of $x = -\sqrt{-a} = 1$x. By growing b from 0, x grows up $x1$ and jump at $B1 = \frac{2}{3}\sqrt{3}$ to higher branch at $A1$. Near $b = B1$, a very low change in b gives catastrophic change in x. The other case if we decrease b from $b = 0$ and $x = 1$. x decreases and at $b = B2$, x jump to the lower branch at $B1$.

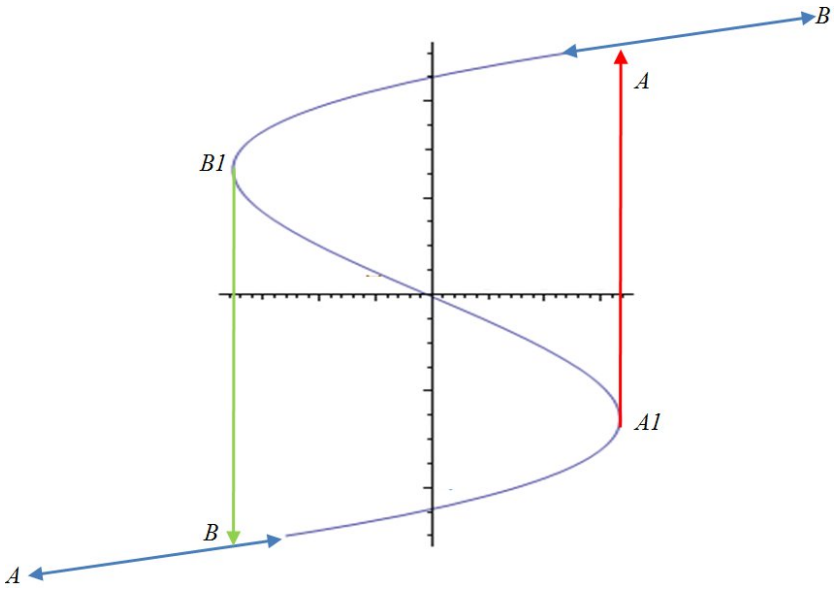

Figure 1.5 : Change in bifurcation system

A1 and *B1* are named turning points because at these points, system jumps if *b* is swept adiabatically i.e. sweeping time is higher than all characteristic times of the system.

System never access to the branch with negative slope by adiabatic sweeping of control parameter *b* because the branch *A1* and *B1* is unstable. Moreover, if system placed at $x = 0$ and $b = 0$ (unstable state), without perturbation, system remain in this state but under very low perturbation, system jump to a stable state. This condition describe with potential behaviour curve in figure 1.6.

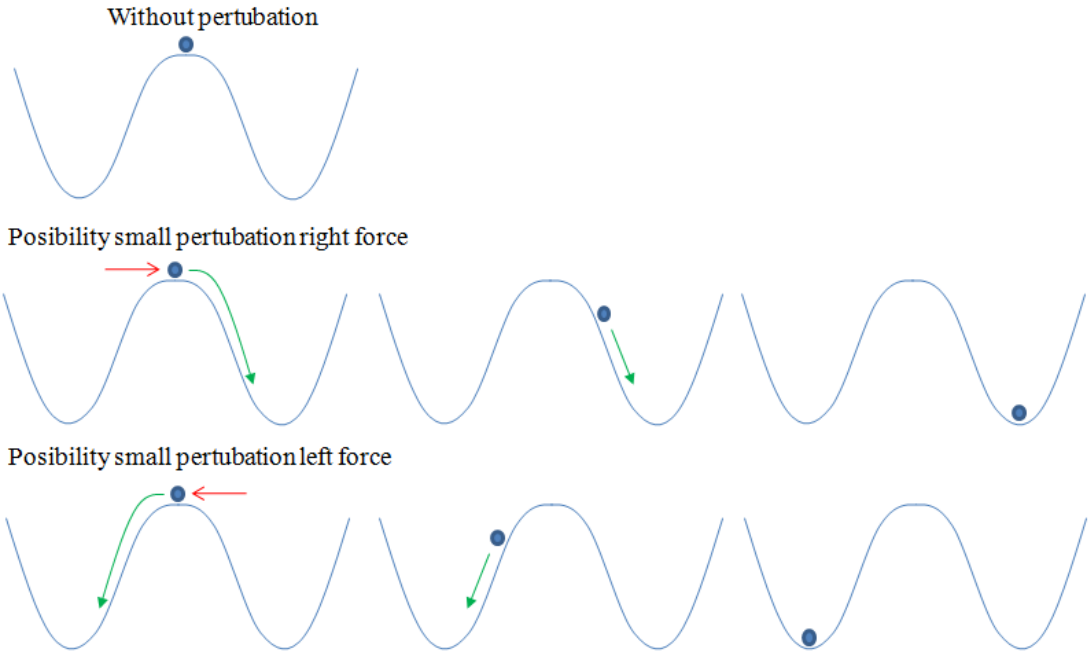

Figure 1.6 : Potential behaviour bifurcation without and posibility with pertubation

This behaviour appear for all points of negative slope but probability of transition to lower branch is higher for $b > 0$ and increases as b increases. In the same manner, probability of transition to higher branch is higher if $b < 0$ and increases as *b* decreases. In the next figure (figure 1.6) we consider positive perturbation in case 1 and negative perturbation in case 2. Without perturbation the system remain in unstable state.

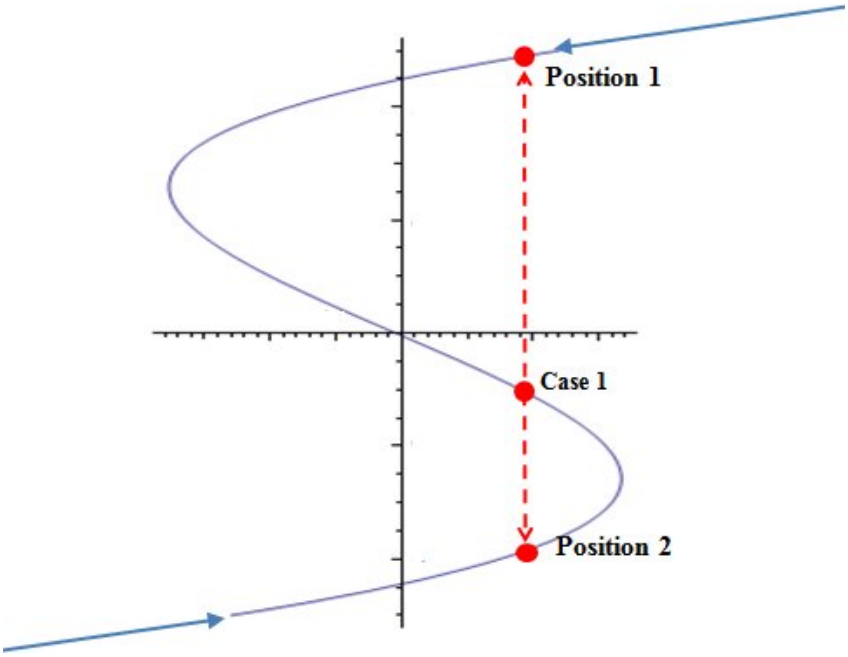

Figure 1.7 : Case 1 Bifurcation in small pertubation

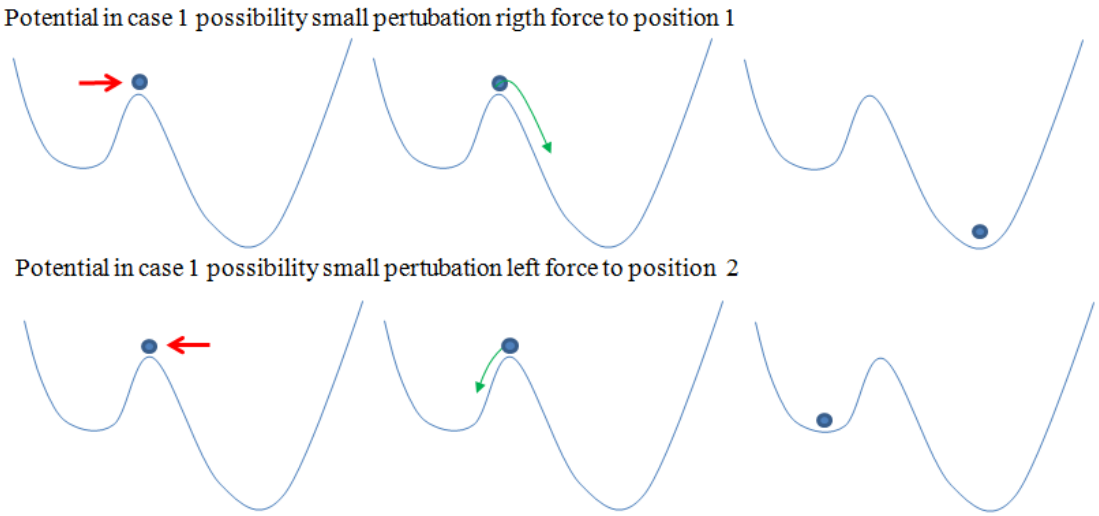

Figure 1.8 : Potentiale evolution of commutation fromnear unstable state

In Case 1, near points *A1* and *B1*, a very low change of *b* can lead to very big change of *x*. In interval between *x1* and *x2*, system is called bi stable because of existence of two stable branches and outside this interval the system is called mono stable.

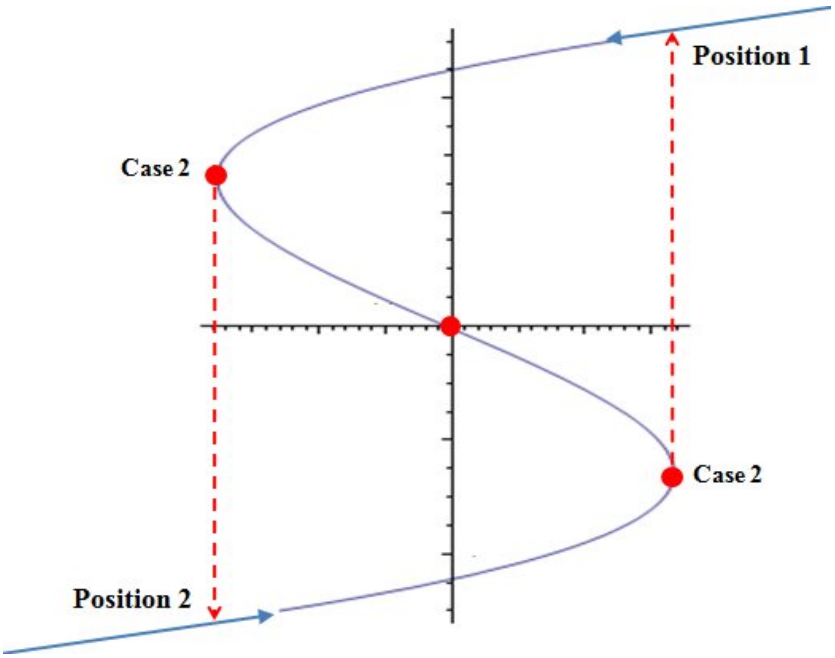

Figure 1.9 : Case 2 Bifurcation in critical slowing down

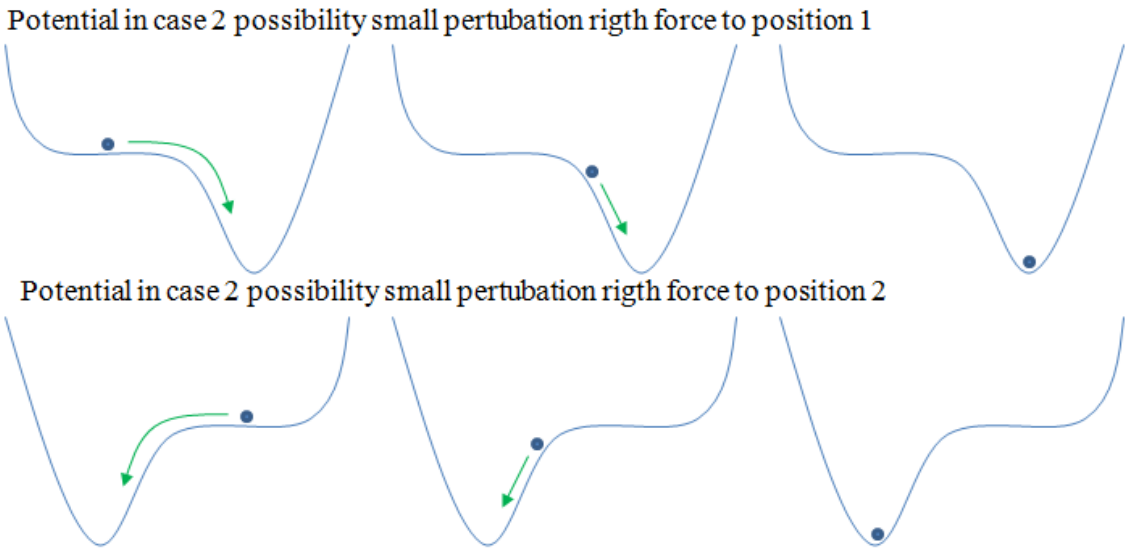

Figure 1.10 : Potential description of critical slowing down

In Case 2, in points *A1* and *B1*, a very low change of *b* can lead to very big change of *x*. Around these point we can obtain critical slowing down, or in landslide event call by creeping landslide because need long time to change in the other condition. Critical slowing down appears if system commutates under slow perturbation and then, system needs long time to commutation other state.

Case a = 0

This a particular case for witch equation (1.2) has one solution as case of $a > 0$ (mono stable situation) and 3rd derivative of V becomes zero at $b = 0$. This point is frontier between stable system and unstable one. Note that, 3rd derivative of V becomes zero only if unstable situation exist or at the frontier of system instability.

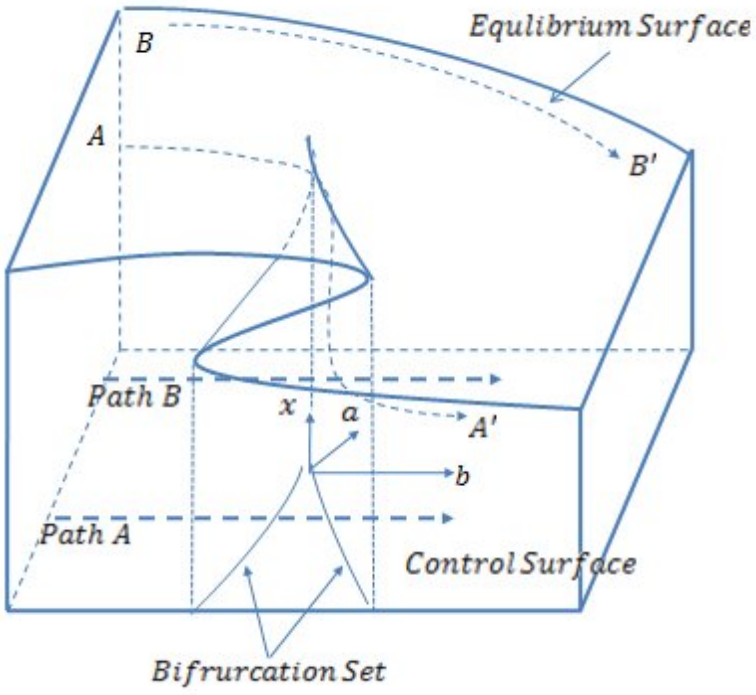

Figure 1.11 Gives schematic representation of global behaviour of $x^3 + ax + b = 0$

Equation 1.2 is very low nonlinearity leading to bi stability behavior. In more complex systems, behaviors described in the case of equation 1.2 will be found in the same manner. In particular case we can find several solutions, which correspond to multi-stable system (Figure 1.12).

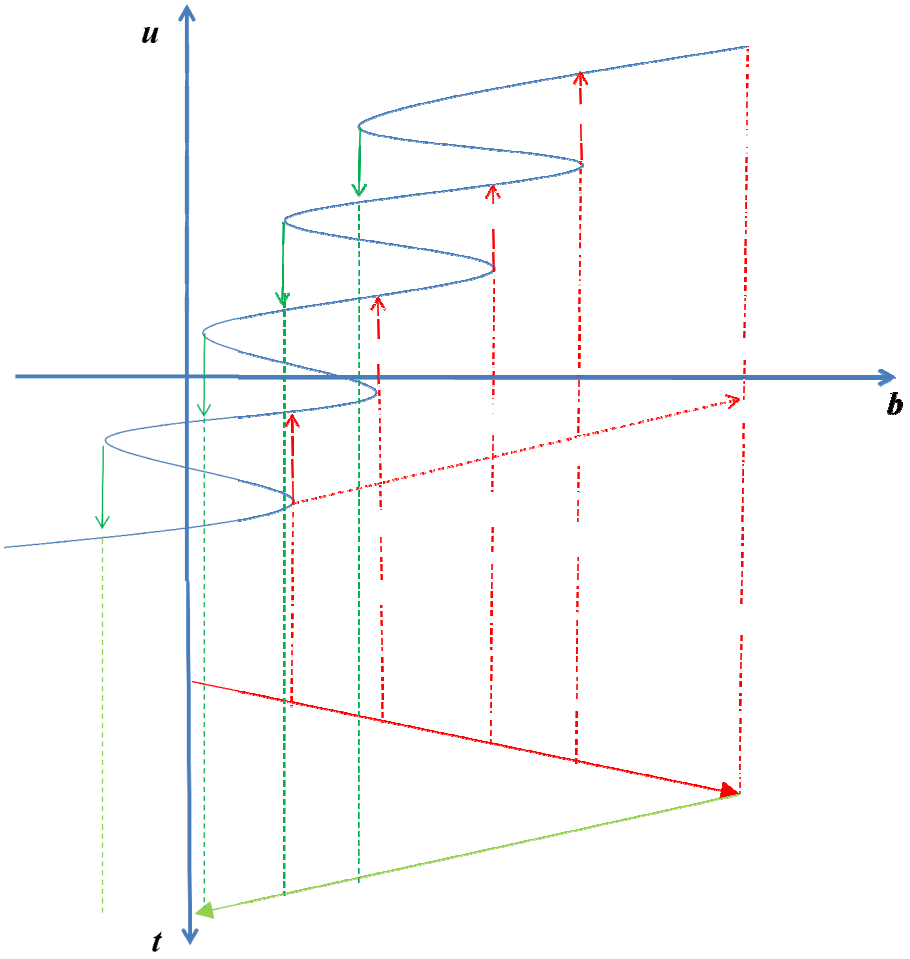

Figure 1.12 : Multi Stability system

The application of external forces could accelerate the system instability. Below the governing equations of a system submitted to a periodic load. Figure 1.13 shows that this force could lead to the system instability.

$$x^3 + ax + b + \alpha \frac{dx}{dt} = 0 \qquad (1.6)$$

If all equation 1.6 divided α, result equation 1.7 function standard cups catastrophe model of the stationeries condition with time function

$$\frac{x^3}{\alpha} + \frac{ax}{\alpha} + \frac{b}{\alpha} = -\frac{dx}{dt} \qquad (1.7)$$

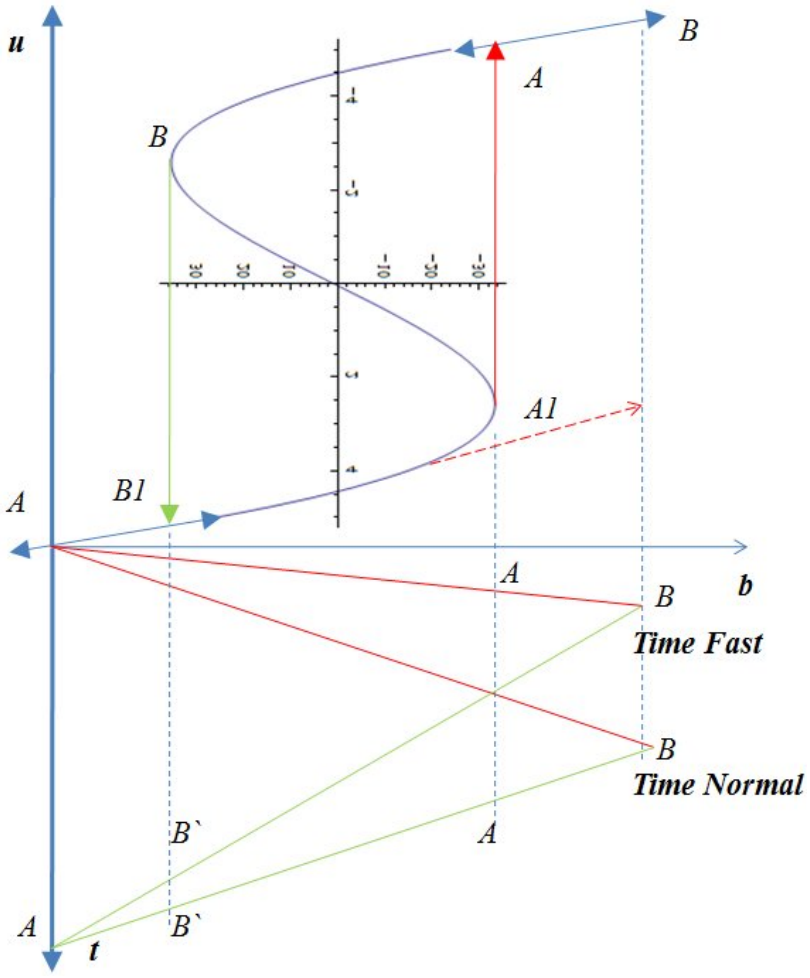

Figure 1.13: Time Function in bifurcation

1.5 Possibility in Bifurcation

To analyze the dynamics of the first order system $\dot{x} = f(x)$, we use the system potential energy. Figure 1.14 shows the path of a particle on the wall of a potential well. The potential $V(x)$ is defined by the equation:

$$f(x) = -\frac{dV}{dx} \tag{1.8}$$

The particle is heavily damped; consequently its inertia is negligible compared to the damping force. The variable *x* depends on time (*t*). Calculation of the time derivative leads to

$$\frac{dV}{dt} = \frac{dV}{dx}\frac{dx}{dt} \tag{1.9}$$

Which leads to

$$\frac{dV}{dt} = -\left(\frac{dV}{dx}\right)^2 \leq 0 \tag{1.10}$$

Consequently, $V(t)$ decreases along trajectory and the particle moves toward the lower potential. Result, if the particle is at equilibrium point where $dV/dx = 0$, then V remains constant. This is to be expected, since $dV/dx = 0$ implies $\dot{x} = 0$. Equilibrium occurs at the fixed point of the vector fields. But that local minima of $V(x)$ correspond to the stable fixed point, as expect intuitively the local maxima correspond to unstable fixed point.

Figures 1.15 and 1.16 show the phenomena at a critical point in mono and multi-stable systems, respectively. Figure 1.9 shows the situation of a system subjected to harmonic loading, which could lead to instability where controlling by function dynamic harmonic. Example in equation 1.10 where value of *b* is :

$$b = b_0 + b_1 \cos \omega t \tag{1.11}$$

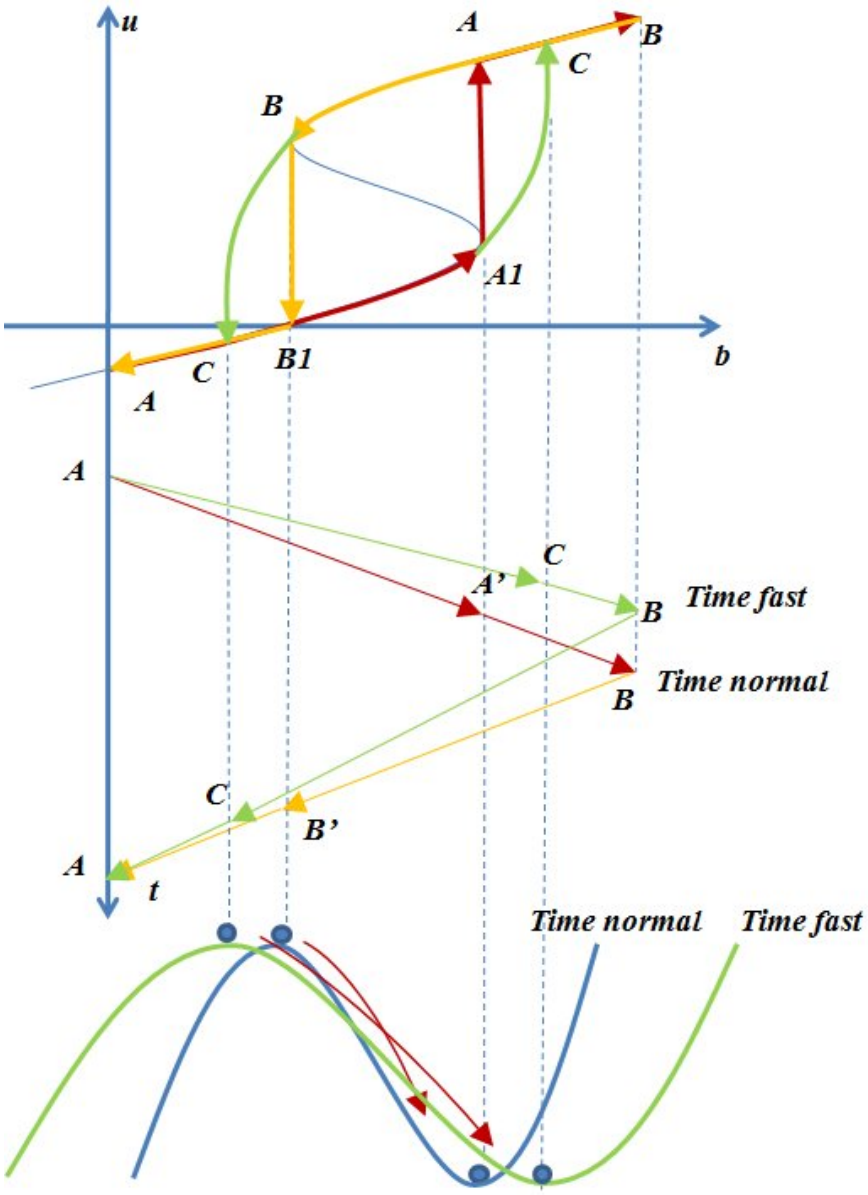

Figure 1.14 : Potential behaviour in time function

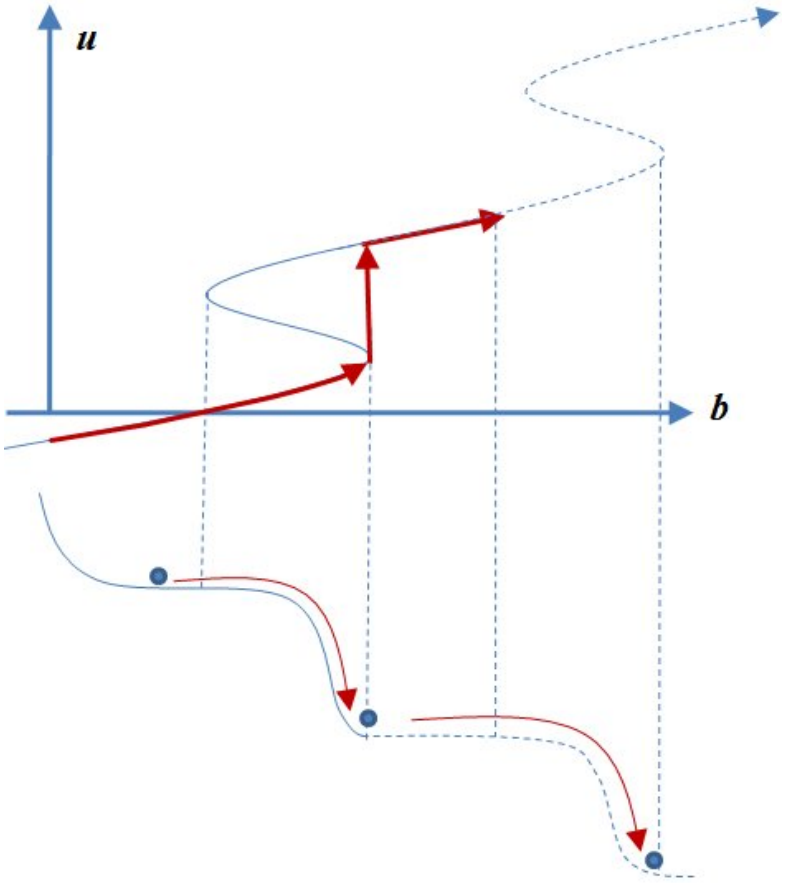

Figure 1.15 : Catastrophe in multi stability system

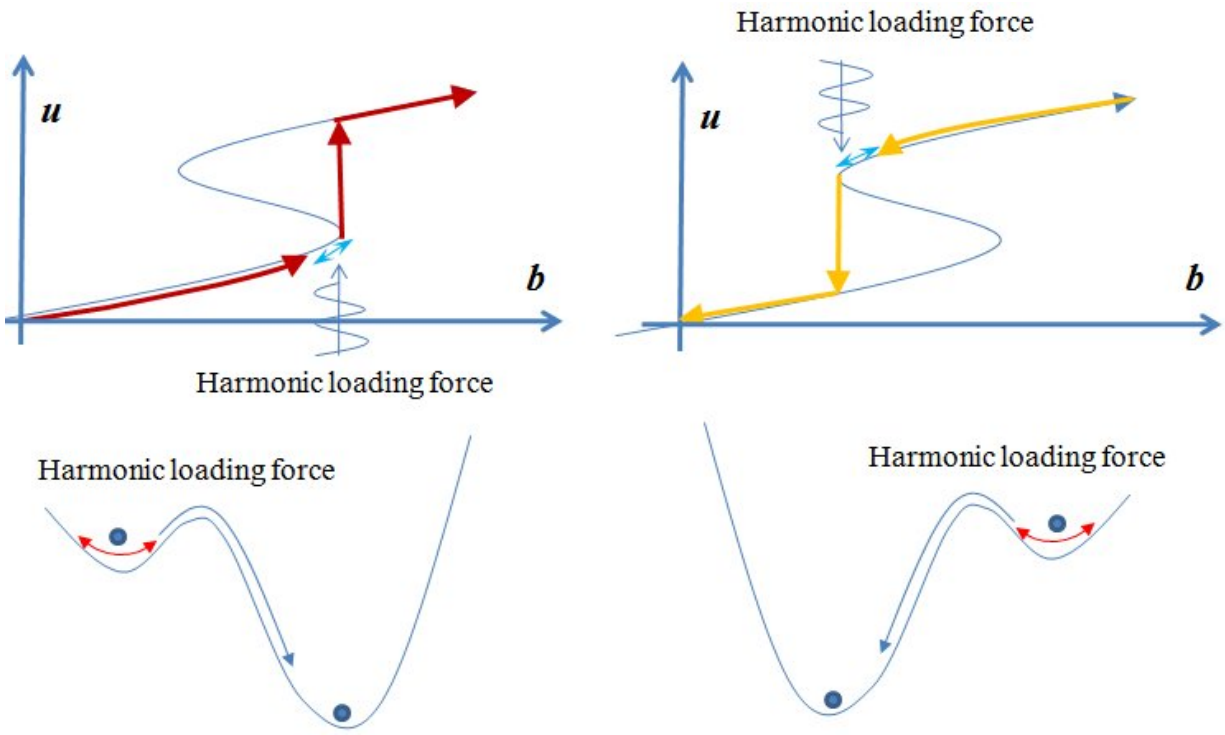

Figure 1.16 : Catastrophe in harmonic Loading Force

Figure 1.17 this explain if external force is random, this condition not pass in point critical slowing down, but it will be pass where can be go back to initial condition or can down in the catastrophe. Example when earthquake its happened, landslide can be occur or not depends on the frequency of normal earthquake. This behaviour appear if the sign of *b* or *x* change under random force. It is equivalent to fluctuation on parameter b or x new in the turning point *A1* and *B1*.

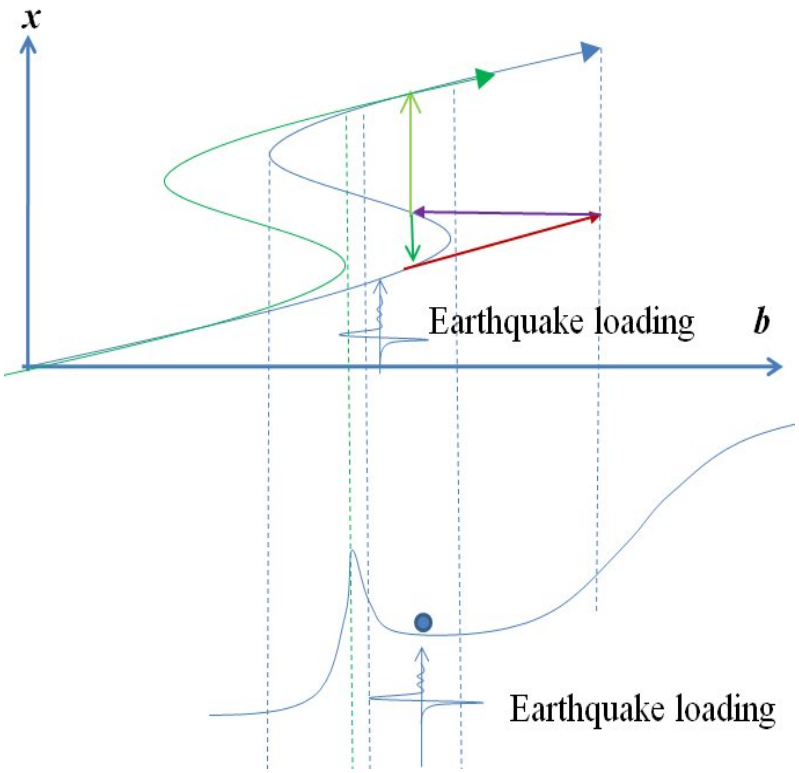

Figure 1.17 : Catastrophe in random external force like earthquake

1.6 Conclusion

This chapter included a literature review of some issues related to slopes instability (landslide), which constitutes a major concern in geotechnical engineering.

The chapter included a particular focus on the influence of rains on land sliding, because it constitutes a major cause of land sliding, which could result from the reduction of the soil strength related to the soils' partial saturation or to the additional forces related to the water flow.

Conventional slope stability analysis is based on the limit analysis methods, which do not consider the soils deformability or hardening.

The conventional methods are convenient for engineering analysis, but the simplifications could lead to missing some instable states. In order to improve the slope stability analysis, we could use tow approaches:

- The Strength Reduction method, which is used in geotechnical engineering for the determination of the safety factors by conduction a series of "deformation" analyses with reduced strength parameters. For the consideration of the effect of water infiltration, this method should be implemented in a coupled hydro-mechanical model.
- The non-linear dynamic, which is used for the analysis of instability of any physical system governed by non linear equations.

In the following, we will present the use of these approaches for the analysis of the slope stability subjected to a fluctuation of the water table. The 2nd chapter will deal with the coupled hydro-mechanical approach, while the 3rd chapter will focus on the use of the nonlinear dynamic theory for analysis of slope instability.

CHAPTER 2: Analysis of the slope stability using a coupled hydro- mechanical model

2.1 Introduction

This chapter presents a numerical analysis of the stability of a soil slope submitted to the variation of the water table. Below the water table, the soil is fully saturated, while above the water table the soil is assumed partially saturated. Analyses are conducted using a full-coupled hydro-mechanical model. The soil behaviour is governed by the non-associated Mohr-Coulomb criterion. Analyses are conducted using FLAC3D program. The Factor of Safety (FoS) is determined using the Strength Reduction Method. Analyses are conducted for different values of both the water table level and the slope inclination. The influence of the soil strength is also considered. The results are illustrated through the distribution of the pore pressure as well as the lateral and vertical displacements.

2.2 Problem statement

This section deals with the analysis of the stability of a slope submitted to the self-weight and the action of the water. A simplified geometrical configuration will be considered. The soil mass is supposed to be homogeneous and underlined by a stiff and impermeable media. The slope is inclined β to the horizontal axis. The lateral boundary is supposed to be far enough from the slop and with zero lateral displacement. The water table level is imposed at the lateral boundary. The water free surface is determined according to the governing hydro-mechanical model. The soil behaviour is supposed to be governed by an elastic-plastic behaviour. This chapter aims at the analysis of the influence of an increase in the water table, resulting from rain infiltration, on the slope stability using a full coupled hydro-mechanical model.

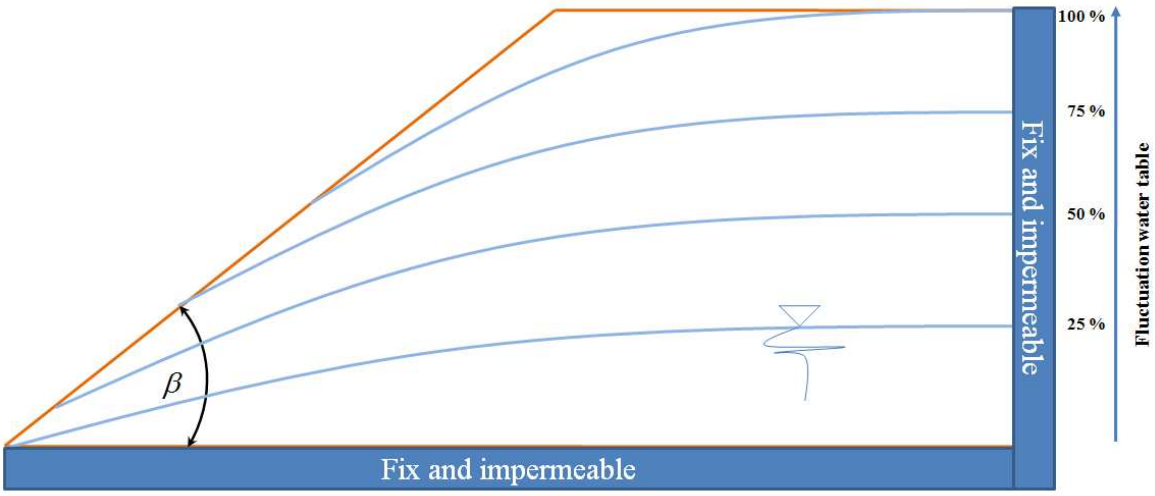

Figure 2.1: Slope stability analysis –problem statement

2.3 Numerical model

2.3.1 General presentation

Analyses are conducted using FLAC3D software, which is well adapted for the analysis of coupled hydro-mechanical problems with nonlinear constitutive relation. This software uses explicit finite difference method for analysis of a wide range of geotechnical engineering problems. The program includes nonlinear constitutive relations for the soil material. It also offers the possibility to implement users constitutive relations.

The soil mass is represented by elements or zones, which form a grid of the media to be modelled. This software offers interesting facilities to deal with geotechnical problems, in particular (i) it uses an explicate numerical scheme which allows to deal with large geotechnical problems using moderate computation means (ii) it is based on large-strain deformation formulation (iii) it takes into account the presence of interface and joint elements (iv) it deals with groundwater flow, including full coupled analysis (including negative pore pressure, unsaturated flow, and phreatic surface calculation) (v) it allows the consideration of structural elements such as soil- reinforcement elements (iv) it offers a variety of constitutive relations for both the soil and structural elements.

FLAC3D software is generally used with Mohr-Coulomb model with non-associated flow rules (Figure 2.2). It also offers the possibility to use a tension cut off (tension yield function). It could take into consideration changes in the mechanical properties such as Young's modulus, cohesion, friction, dilation and tensile strength, which could result from material transformation, hardening or softening.

This software is also used for stability analysis using the Strength Reduction Method, which was presented in the first chapter. Thanks to the dynamic explicit formulation, FLAC3D allows the determination of the displacement field, which results from the reduction of the strength parameters and consequently determine the reduction factor (Factor of Safety), which causes large deformations.

Saturation is defined as the ratio of pore volume occupied by fluid to total pore volume. The pore pressure is set to zero if the saturation is less than 1.

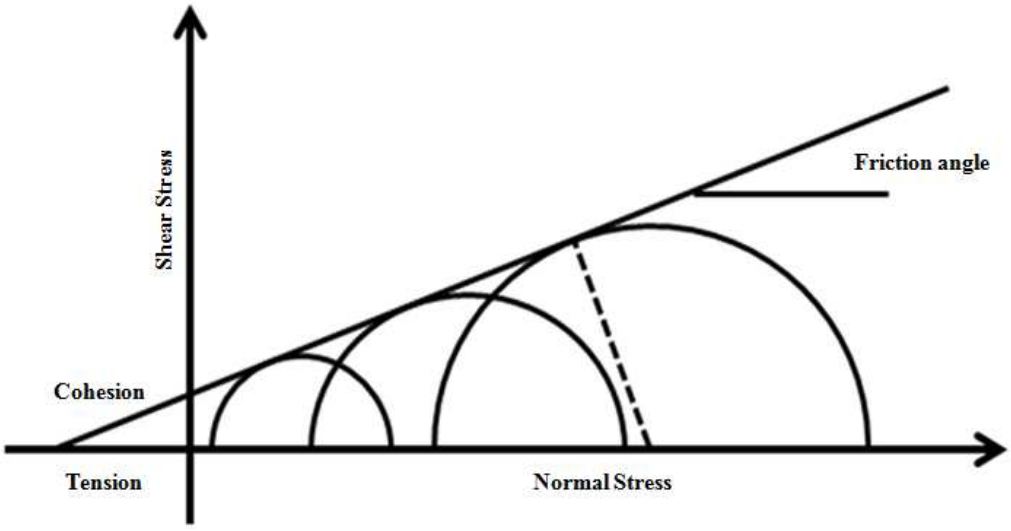

Figure 2.2 : Mohr – Coulomb failure surface

2.4 Analysis of the slope stability in neglecting the interacting with the underline layer

Figure 2.3 presents the slope configuration used in this stud. The height of the soil mass is equal to H = 10m.

2.4.1 Boundary condition

The soil mass is supposed to be underlined by a stiff media, consequently the displacement as well as the water flow are equal to zero. The lateral boundary is supposed to be far from the slope; consequently the lateral displacement at this boundary is equal to zero. The boundary is submitted to linear increasing pressure under the water table. The other boundaries (the top of the soil mass and the slope) are free. For the water condition in the soil mass, the water is assumed to flow with free surface.

2.4.2 Initial conditions

The soil mass is submitted to stresses resulting from the gravity forces under the boundary condition presented previously.

2.4.3 Loading

In addition to the gravity forces, the soil mass is subjected to the action of water flow which results from the increase in the water table at the lateral boundary. The water table will separate the soil mass into two zones: saturated zone below the water table and partially saturated zone above the water table.

In the model the fluid is isotropic with gravitational acceleration -10 m/sec^2. The isotropic permeability coefficient, k ($m^2/(Pa/sec)$ is equal to 1×10^{-4} Pa/m. Porosity (n) is a dimensionless number defined as the ratio of void volume to total volume of an element. It is related to the void ratio, in this model value of porosity is 0.5.The initial fluid modulus is equal to 500 kPa. When the fluid modulus Kf is given, the Biot modulus is computed internally using Kf equation for incompressible grains. In this calculation, the porosity is evaluated at the nodes using the nodal volume averaging. Pressure and saturation changes are computed using the current values of the saturation and whether the fluid has fallen below the tensile limit.

Analyses were conducted with the following properties : bulk modulus = 3.5714×10^8 Pa, shear modulus = 1×10^8 Pa, dilatation = 0 and masse density of soil=19.230 kg/m^3.

2.4.4 Results

Analyses were conducted with the following configurations (Figure 2.3):

- Three values of the slope inclination: β = 30, 40, 50 and 60 °
- For each slope, analyses were conducted for 9 values of the height of the water table (h_w/H = 0, 0.25, 0.50, 0.65, 0.67, 0.68, 0.69, 0.75 and 1). The density of values around (h_w/H = 0.67) resulted from a preliminary analysis for the determination of the water-table critical height.

The Factor of Safety (Strength Reduction Factor) was determined for each configuration.

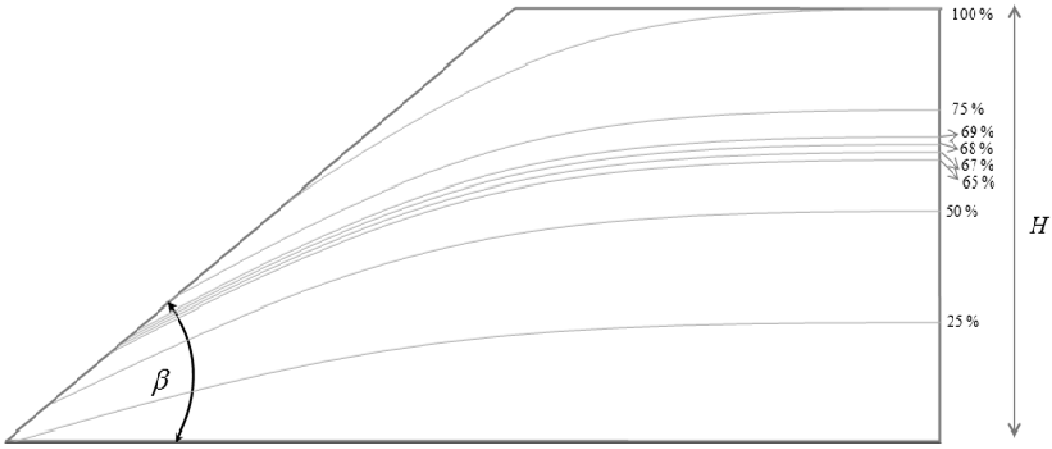

Figure 2.3: Configuration used in the analysis of the safety factor

Results of analyses are illustrated in table 2.1 and figure 2.3. It could be observed that the for each slope inclination, the increase in the water table level leads to a decrease in the factor of safety. For the slope included 30° to the horizontal, the slope is stable in the absence of the water (*FoS* = 1.86), the increase in the water table to 0.5 H (H = the slope height) induces a decrease in FoS to 1.32. The instability of the slope occurs when the water table attains 0.68 H (*FoS* = 1). After this value, the safety factor decreases very quickly and attains 0.27 when *hw* = *H*. The same trends are observed for other inclinations, with a slight decrease in the factor of safety with the increase in the slope inclination. The moderate influence of the slope inclination

on the *FoS* indicates a dominant role of cohesion in the slope stability. Since the soil cohesion is subjected to large variation, the results of this analysis should be considered with high attention in engineering practices.

Figure 2.4 shows the variation of the *FoS* with the variation in both the slope inclination and the water level. This figure clearly shows a decrease in the *FoS* with the increase in the water table with an amplification of this decrease for values of h_w/H between 0 and 0.5 and between 0.7 and 1. We can also observe the influence of the slope inclination on the *FoS*, but this influence is moderate regarding the influence of the water -table.

Table 2.3:Influence of the slope inclination (β) and water table level (h_w/H) on the Factor of Safety.

β / hw/H	**30**	**40**	**50**	**60**
0	*1.86*	*1.84*	*1.81*	*1.77*
0.25	1.64	1.66	1.66	1.63
0.50	1.32	1.34	1.35	1.3
0.65	1.07	1.06	1.06	1.05
0.67	1.03	1.02	1.02	1.01
0.68	1.01	1	0.99	0.99
0.69	1	0.99	0.98	0.97
0.75	0.85	0.87	0.89	0.86
1.0	0.27	0.27	0.27	0.26

In order to illustrate the limit of stability for the soil slope, we present in figure 2.5 the value of the water table level, which causes the slope instability. This figure could be used in order to determine for each slope the critical water level, that causes instability. This figure could be extended to cases encountered in engineering practices by the construction of charts of the slope stability.

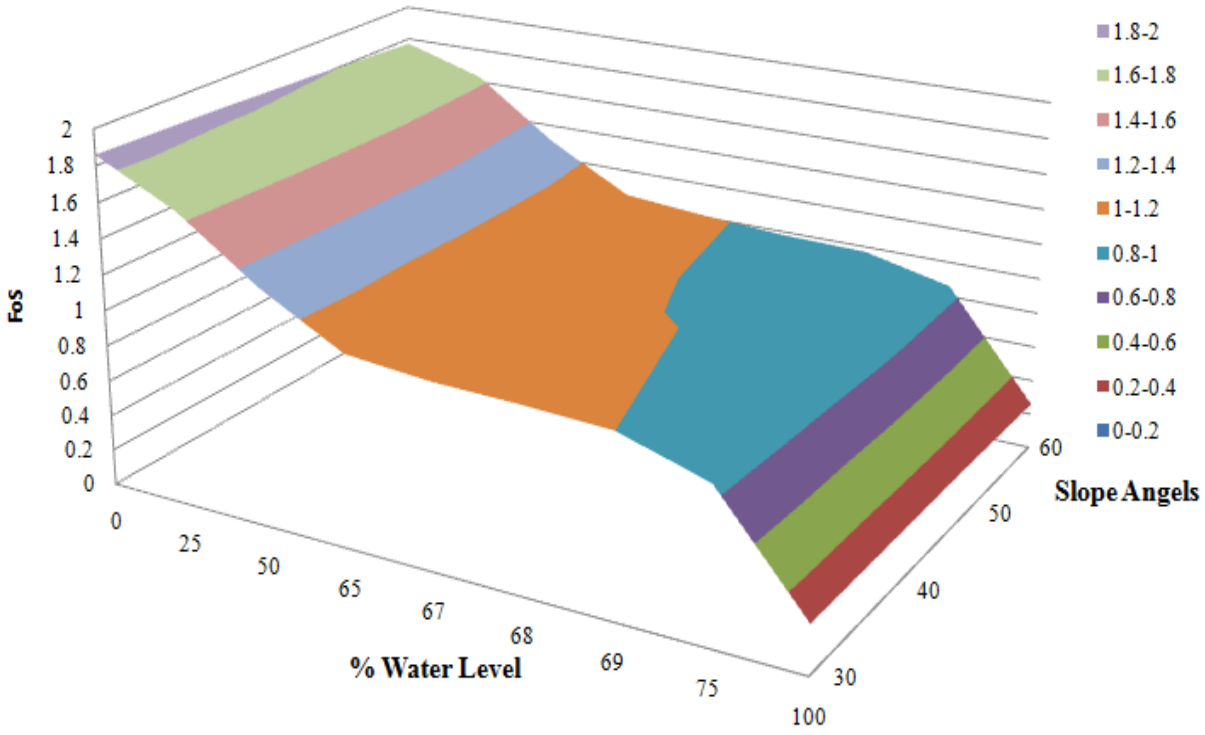

Figure 2.4: Influence of the slope inclination (β) and water-table level (h_w/H) on the Factor of Safety

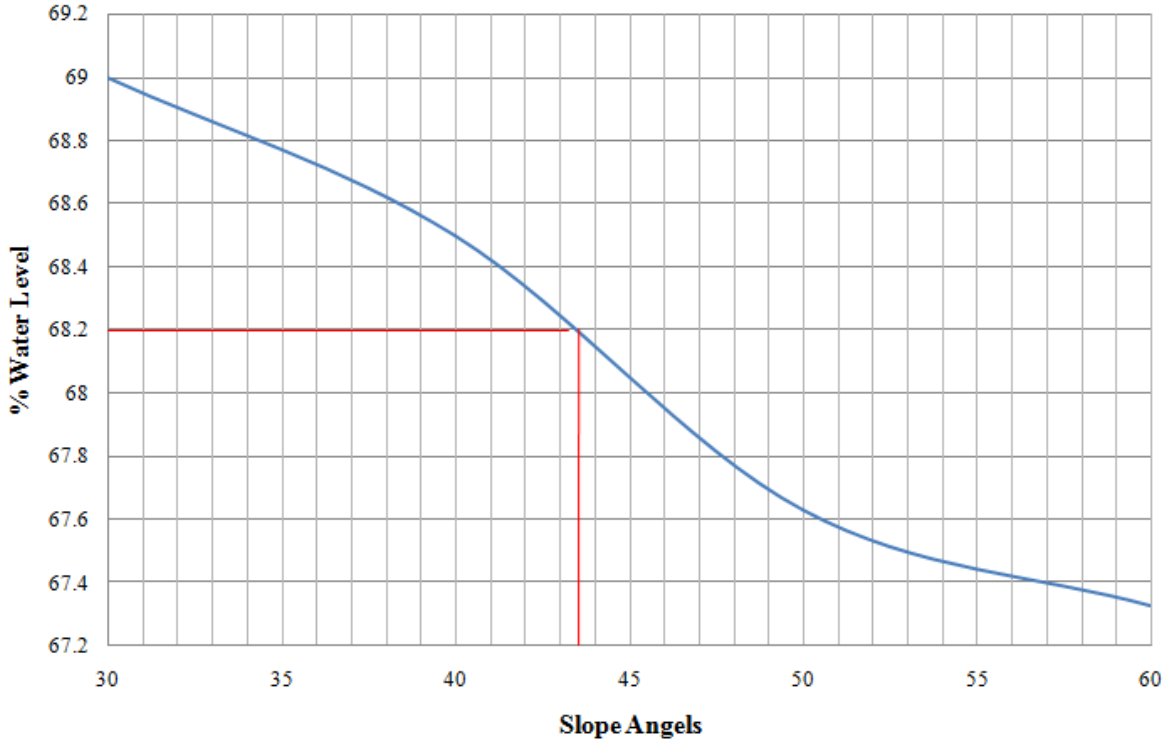

Figure 2.5: Limit of stability of the soilslope (Factor of Safety = 1)

2.5 Analysis of the slope stability in considering the interacting with the underline layer

2.5.1 Presentation

Analyses were conducted on a modified configuration, which takes into account the interaction of the underline layer. Figure 2.6 shows this configuration. It is similar to that presented in the previous section, but it includes 5 *m* of the underline layer. The initial and boundary conditions are similar to that used in the previous section. The left lateral boundary is assumed to be impervious with zero lateral displacement.

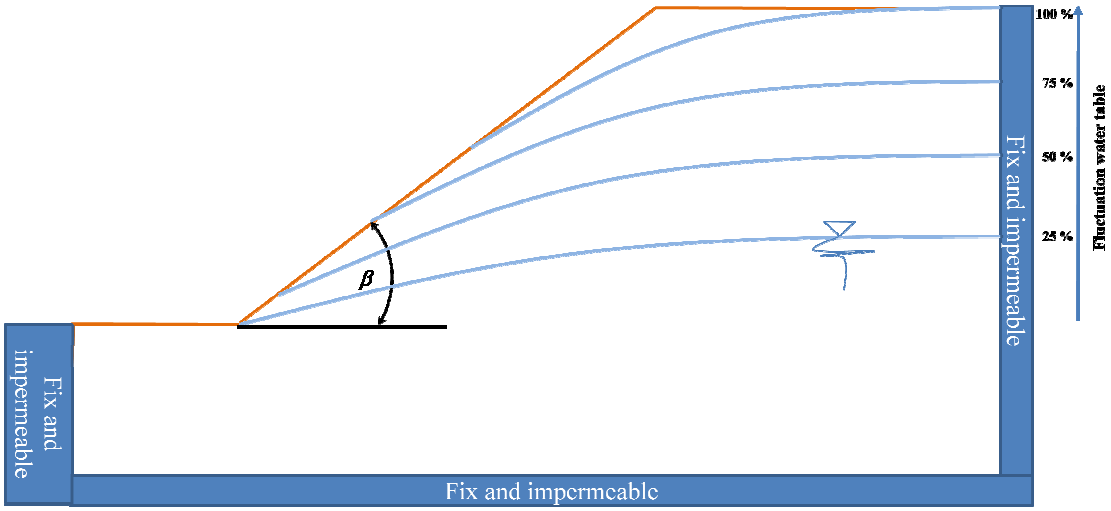

Figure 2.6: Configuration of the case used in the deformation analysis

Analyses were conducted for the following configurations :

- Three values of the slope inclination: β = 30, 35 and 40°
- For each slope, analyses were conducted for 5 values of the height of the water table (h_w / H = 0, 0.25, 0.50, 0.75 and 1).

Concerning the soils characteristics, we considered 4 cases:

- Case 1: Cohesion c = 5 *kPa* in the saturated zone and 10 *kPa* in the unsaturated zone, with full tensile strength (100 *kPa*).
- Case 2: Cohesion c = 5 *kPa* in the saturated zone and 10 *kPa* in the unsaturated zone, with zero tensile strength.
- Case 3: Cohesion c = 5 *kPa* in the saturated zone and 20 *kPa* in the unsaturated zone, with full tensile strength (100 *kPa*).
- Case 4: Cohesion c = 5 *kPa* in the saturated zone and 10 *kPa* in the unsaturated zone, with zero tensile strength.

2.5.2 Safety factor

Figure 2.7 shows a typical shear strain distribution in the soil mass. We observe a high concentration of the shear strain around a bloc limited by an inclined line in the soil mass with a slope higher than that of the soil slope and a horizontal line at the bottom of the soil mass.

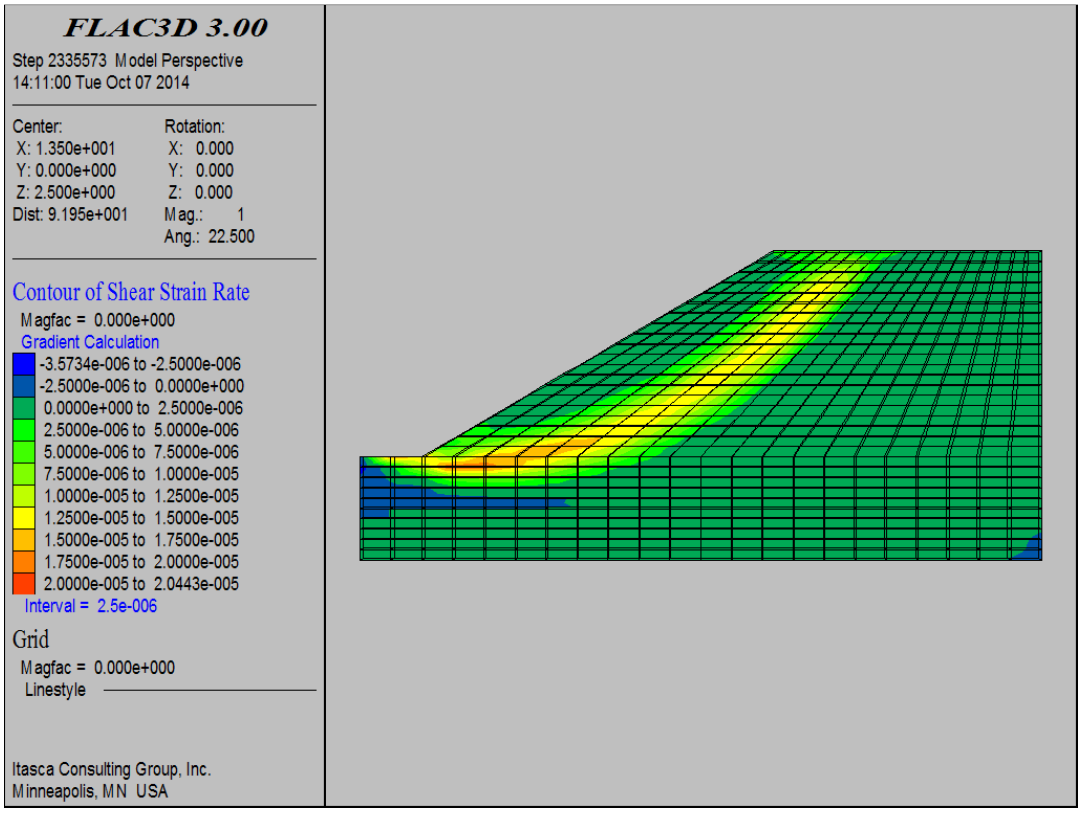

Figure 2.7: Shear strain distribution in the soil mass

Table 2.2 provides the values of the *FoS* for all the configurations. Analysis of these results shows that for all the configurations, the *FoS* decreases with the increase in the slope inclination and the water table level. For the first case with β = 30°, *FoS* decreases from 1.83 to 0.31 when the height of the water table (h_w) increase from 0 to *H*. For the same case with h_w =0.75*H*, *FoS* decreases from 1.24 to 1.04 when the slope inclination increases from 30 to 40°.

We observe also that the increase in the cohesion of the non-saturated zone from 10 to 20 *kPa* leads to an increase in the factor of safety for the configurations with low water-table. As example, for the slope inclination β= 30°, the increase in the cohesion between case 2 and 4 leads to an increase in *FoS* from 1.78 to 2.3. For the slope inclination β= 40°, the same increase in the cohesion leads to an increase of *FoS* from 1.43 to 1.88.

The comparison of case 1 with case 2 and case 3 with case 4 shows that the consideration of the tensile strength does not affect the *FoS*.

Table 2.2: Factor of Safety for the 4 cases used in the deformation analysis.

Case 1 Not Use	FoS	30	35	40
	0	1.83	1.62	1.45
	25	1.64		1.37
	50	1.24		1.26
	75	1.24		1.04
	100	0.31		
C Non Sat	10	kPa		
C Sat	5	kPa		
Ten	100	kPa		

Case 2	FoS	30	35	40
	0	1.78	1.6	1.43
	25	1.64	1.49	1.34
	50	1.49	1.36	1.23
	75	1.24	1.13	1.06
	100	0.88	0.84	0.83
C Non Sat	10	kPa		
C Sat	5	kPa		
Ten	0	kPa		

Case 3 Not Use	FoS	30	35	40
	0	2.33	2.1	1.88
	25	1.82		1.55
	50	1.61		1.39
	75	1.31		1.17
	100	0.41		
C Non Sat	20	kPa		
C Sat	5	kPa		
Ten	100	kPa		

Case 4	FoS	30	35	40
	0	2.3	2.08	1.88
	25	1.8	1.67	1.55
	50	1.59	1.48	1.39
	75	1.26	1.21	1.17
	100	0.88	0.85	0.86
C Non Sat	20	kPa		
C Sat	5	kPa		
Ten	0	kPa		

2.5.3 Distribution of the pore pressure

Figure 2.8 shows the variation of the water pressure in the soil mass with the increase in the water table for the case 2 with slope inclination β = 30°. We observe that the water-table surface (free surface) is quasi linear in the soil mass with an inclination, which increases with the increase in the water table. Above this surface the pressure is equal to zero. Below this surface, the pressure increases quasi-linearly with the depth.

Figure 2.9 shows the pore pressure distribution for the case 4 with slope inclination β = 30° and water table height h_w = 0.75H. The comparison of this distribution with that of the case 2 (figure 2.8 c), shows that the pressure distribution is not affected by the soil strength. This result is expected, because the pore pressure distribution is mainly affected by the hydraulic conditions.

Figures 2.10 and 2.12 show the results obtained for the slope inclinations β = 30°, 35° and 40°, respectively. Analyses were conducted with the soil properties of cases 2 and 4. For the two configurations of the slope, we observe that the soil strength does not affect the pore pressure distribution. This result confirms that obtained with the slope inclination β= 35°.

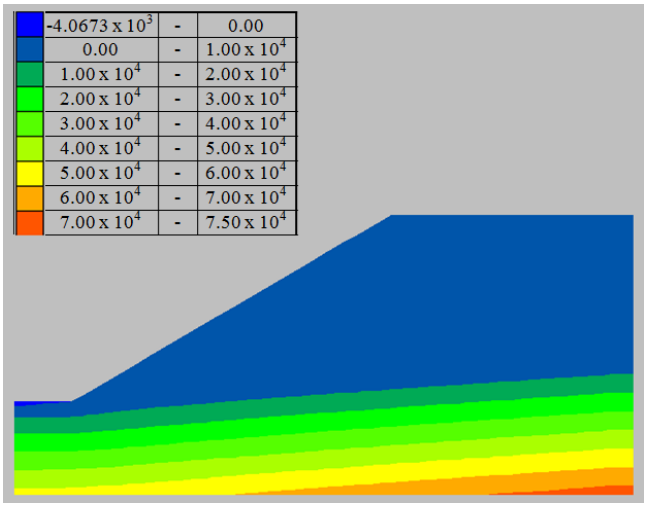

(A) h_w/H **= 0.25**

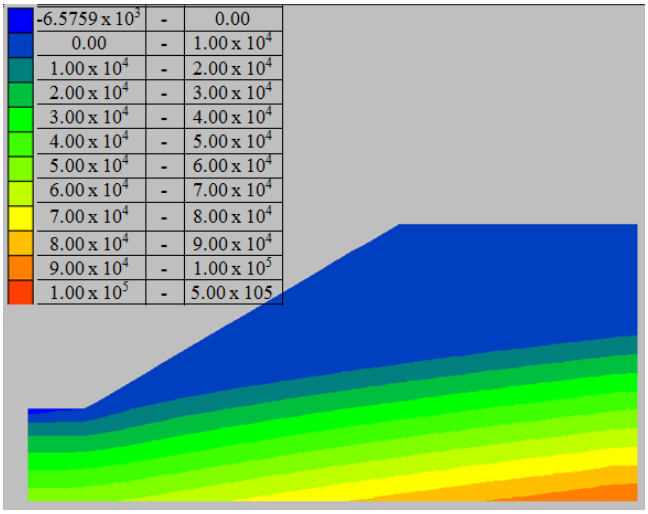

(B) h_w/H **= 0.50**

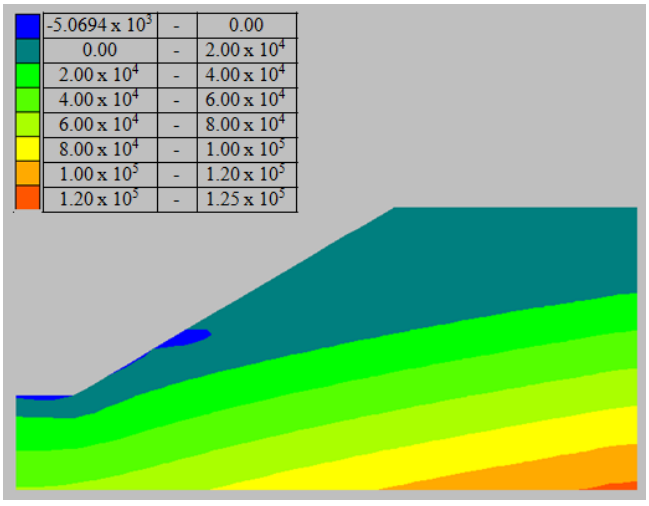

(C) h_w/H **= 0.75**

Figure 2.8: Variation of the pore pressure with the increase in the water table (Case 2, β **= 30°)** h_w/H **= 0.25, 0.5 and 0.75**

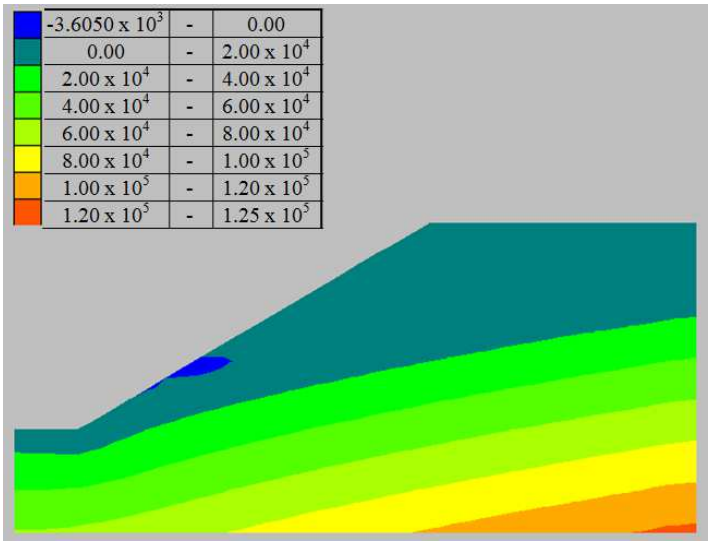

Figure 2.9: Pore pressure distribution with the increase in the water table

(Case 4, β = 30°) h_w/H = 0.75

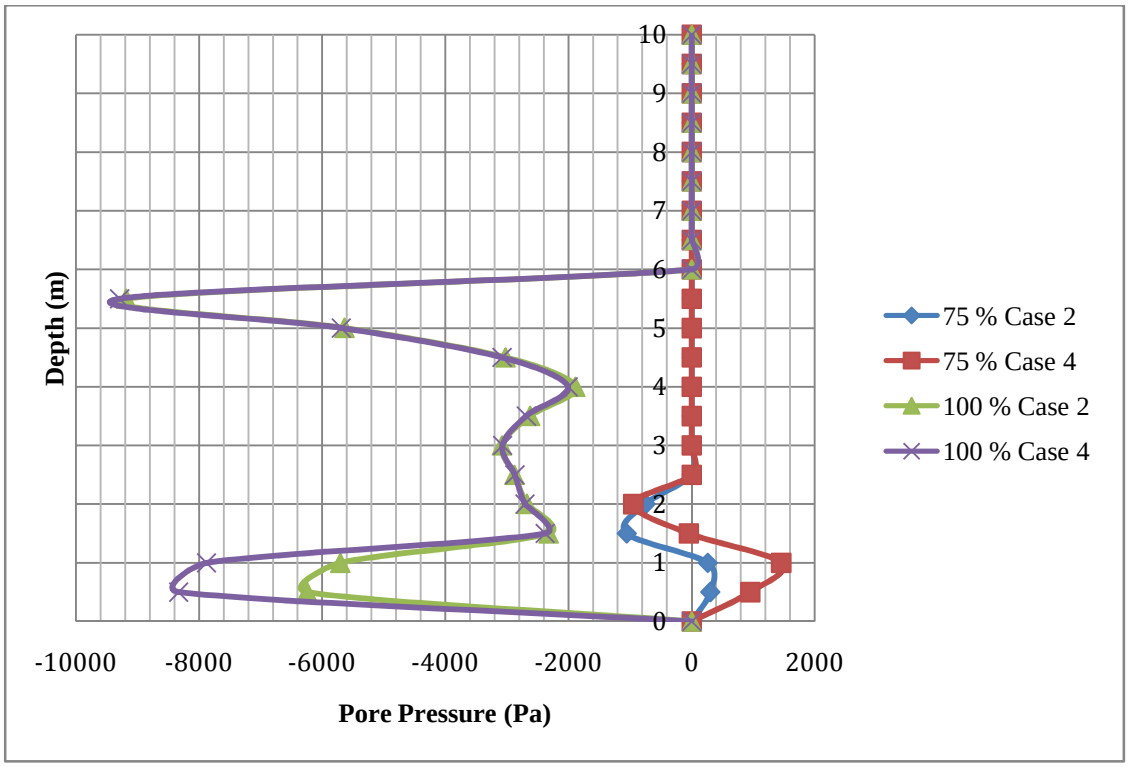

Figure 2.10: Influence of the soil strength on the distribution of the pore pressure

(Cases 2 and 4, β= 30°)

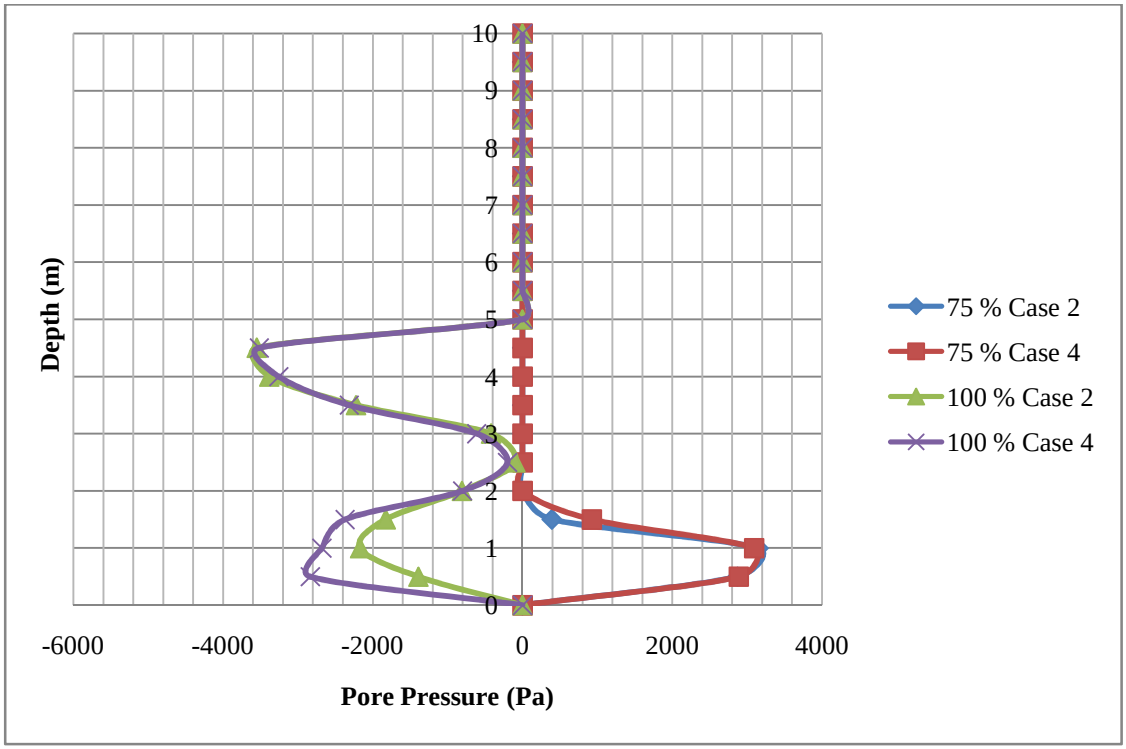

Figure 2.11: Influence of the soil strength on the distribution of the pore pressure (Cases 2 and 4, β= 35°)

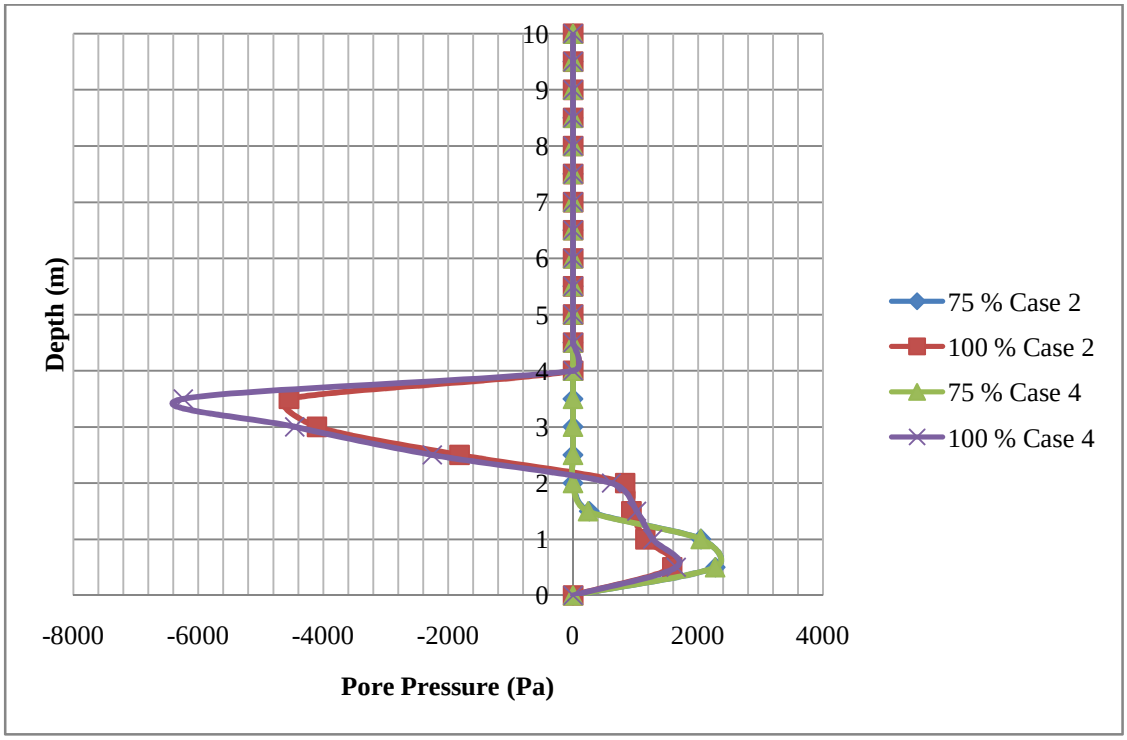

Figure 2.12: Influence of the soil strength on the distribution of the pore pressure (Cases 2 and 4, β = 40°)

2.5.4 Displacement

A. Lateral displacement

Figure 2.13 shows point observation of displacement. This post will be different every models, is depend zone change with small displacement change to large displacement.

Figure 2.14 shows point observation of the variation lateral displacement in the soil mass with the increase in the water table for the case 2 with slope inclination β = 30°. We observe that in the absence of the water table (h_w = 0), the lateral displacement is close to zero. This situation corresponds to the initial value of the soil mass. The increase in the water table induces an increase in the lateral displacement. For $h_w = 0.25H$, we observe a quasi rigid movement with a lateral displacement $0.1m$.

The increase of the water table from $0.25H$ to $0.50H$ induces an important increase in the lateral displacement, in particular at the slope bottom, where the displacement attains 0.4 *m*. At the top of the soil mass the lateral displacement is equal to 0.3 *m*. The variation of the displacement with depth is quasi-regular.

For h_w = 0.75 *H*, we observe a high lateral displacement at the soil bottom, which attains about 1 *m*. This high value indicates large displacement, which could correspond to the slope instability. The displacement at the top of the soil mass is equal to 0.1 *m*, which is lower than that obtained with h_w = 0.50 *H*. This decrease in the lateral displacement indicates a rotation of the sliding bloc towards the interior of the soil mass.

Results obtained with $h_w = H$ are close to that obtained with h_w = 0.75 *H*. The safety factor in this case is equal to 0.88. This result confirms that the lateral displacement obtained at the water level h_w = 0.75 *H* corresponds to the initiation of the slope instability.

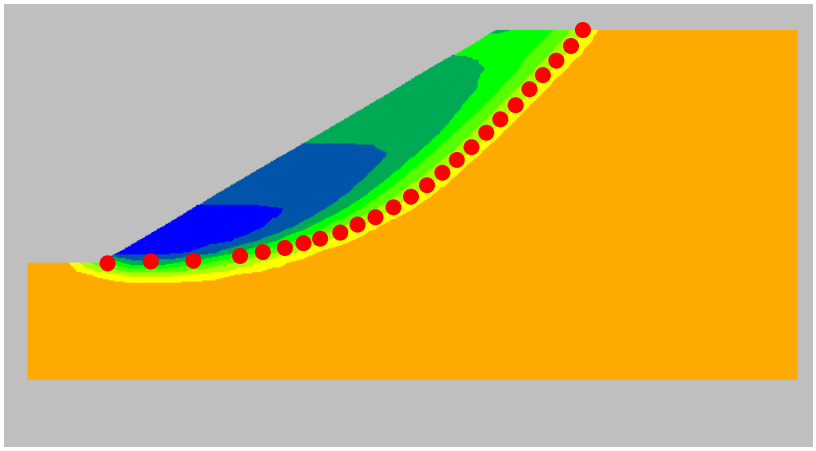

Figure 2.13 : Point observation of displacement

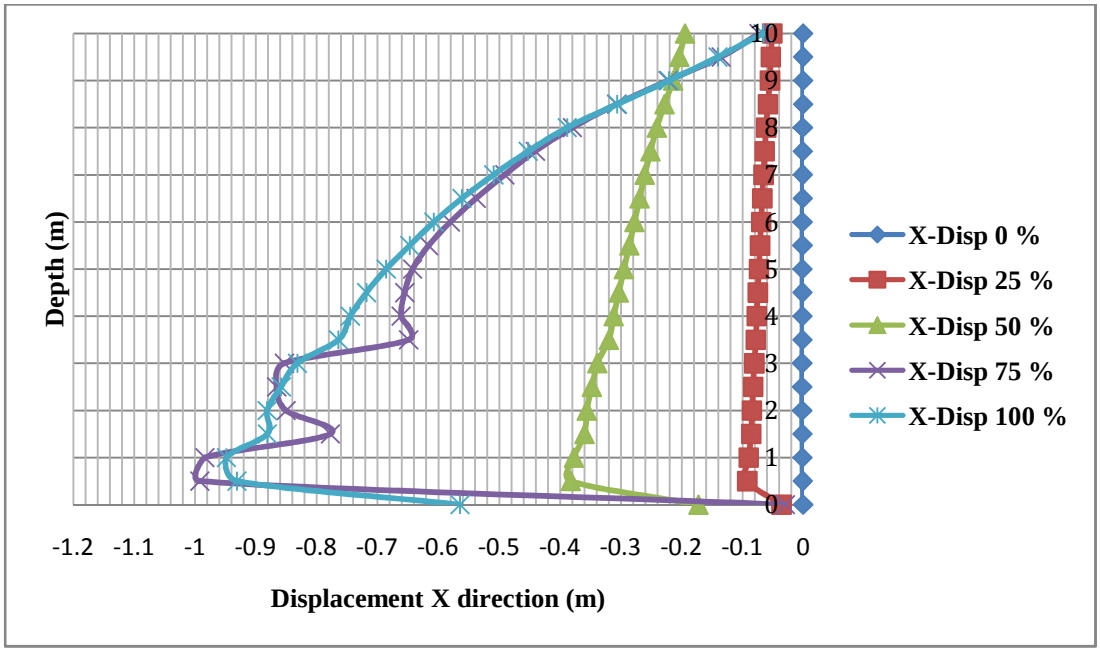

Figure 2.14: Influence of the water-table level on the lateral displacement

(Case 2, β = 30°) *hw/H* = 0.25, 0.5, 0.75 and 1.0

B. Vertical displacement

Figure 2.15 shows the variation of the vertical displacement in the soil mass with the increase in the water table for the case 2 with slope inclination β = 30°. We observe that in the absence of the water table (h_w = 0), the vertical displacement is close to zero. The increase in the water table induces an increase in the lateral

displacement in the central part of the soil mass. For h_w = 0.25 H, we observe a small downward displacement of the bloc. The increase of the water table to h_w = 0.50 H induces an increase in the downward displacement which attains about 0.4 m at z = 9 m. For h_w = 0.75 H and h_w = H, we observe a high downward displacement in the central part, which attains about 1.75 m. This high value indicates a slope instability in this part.

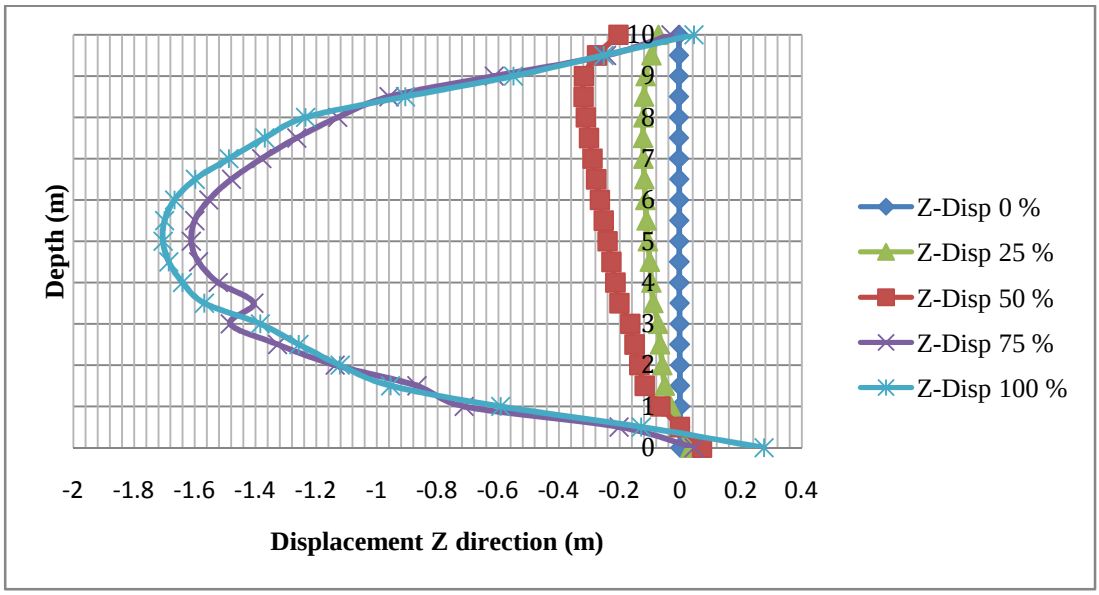

Figure 2.15: Influence of the water-table level on the vertical displacement

(Case 2, β = 30°) hw/H = 0.25, 0.5, 0.75 and 1.0

C. Lateral displacement in the soil mass

Figure 2.16 shows the variation of the lateral displacement in the soil mass with the increase in the water table for the case 2 with slope inclination β = 30°.

For h_w = 0.25 H, we observe that the maximum lateral displacement occurs in the lower part of the bloc but with large extension to the interior of the soil mass. This displacement decreases when going from the bottom to the top of the soil mass. The increase of the water table level to h_w = 0.50 H induces an extension of the large displacement to the top of the soil mass.

At h_w = 0.75 H, we observe the apparition of quasi uniform lateral movement in a bloc delimited by an inclined line from about 3 m to the right of the slope edge down to the slope bottom. This movement confirms the slope instability at this level of loading.

D. Vertical displacement in the soil mass

Figure 2.17 shows the influence of the increase in the water table on the vertical displacement in the soil mass.

For h_w = 0.25 H, we observe that the maximum vertical displacement occurs in an area close to the top of the slope with moderate extension to the interior of the soil mass. The augmentation of the water table level to h_w = 0.50 H induces an increase in the displacement and its extension downward the soil slope.

At h_w = 0.75 H, we observe a translation of the maximum downward displacement towards the central part of the slope.

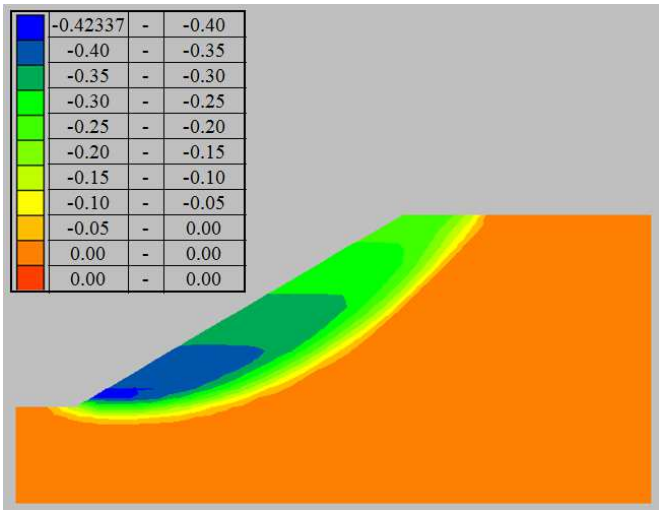

(A)hw* = 0.25 *H

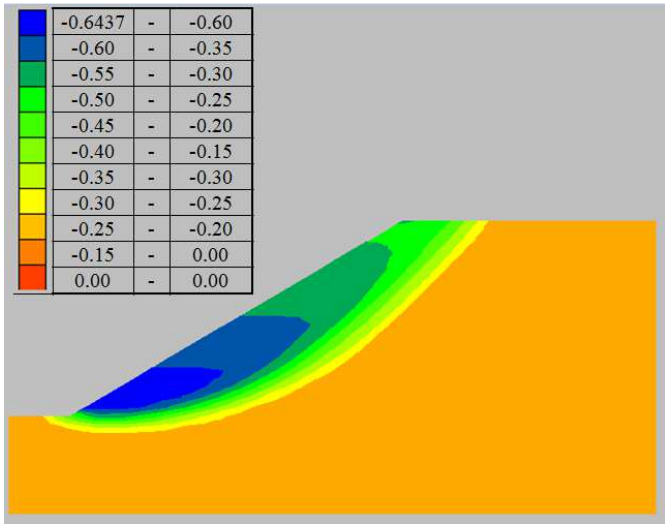

(B)hw* = 0.50 *H

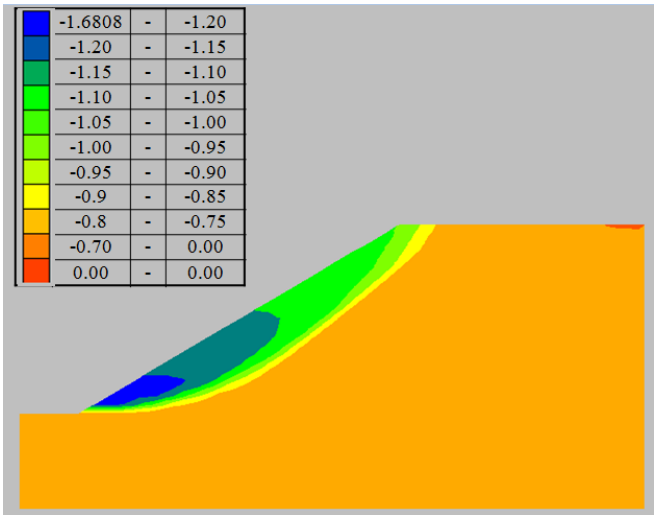

(C)hw* = 0.75 *H

Figure 2.16: Influence of the water-table level on the lateral displacement (Case 2, β = 30°) *hw/H* = 0.25, 0.5, 0.75

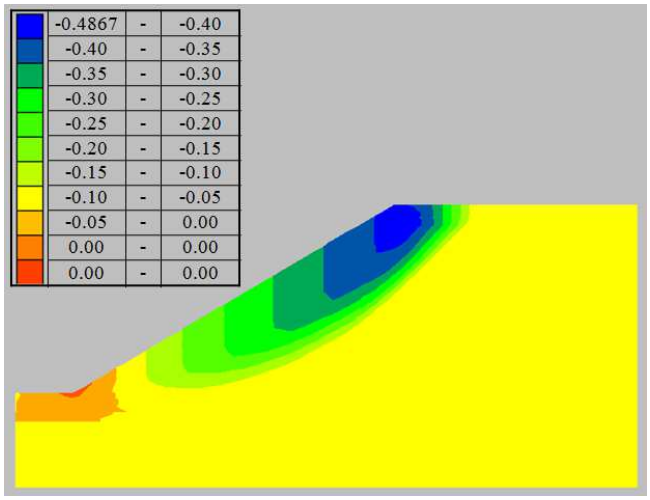

hw = 0.25 *H*

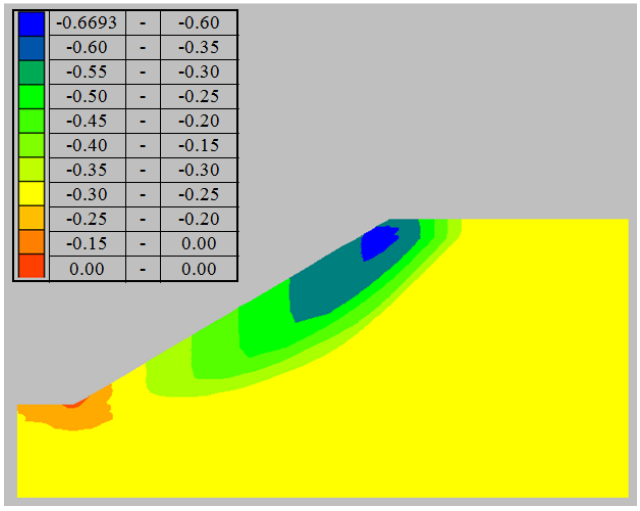

hw = 0.50 *H*

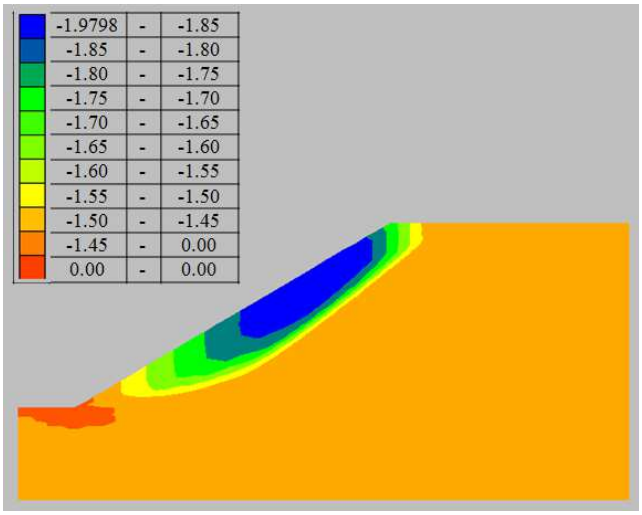

hw = 0.75 *H*

Figure 2.17: Influence of the water-table level on the vertical displacement (Case 2, β = 30°) *hw/H* = 0.25, 0.5, 0.75

E. Influence of the soil cohesion in the non-saturated area

Figures 2.18 and 2.19 show the variation of the lateral and vertical displacement with the increase in the water-table level for the soil properties of the case 4. In this case, the soil cohesion in the unsaturated area is equal to 20 *kPa*, while in the case 2 this cohesion is equal to 10 *kPa*. The comparison of these results with those obtained with the case 2 (Figures 2.14 and 2.15) shows that the increase in the cohesion does not affect the pattern of the lateral and vertical displacement, but reduces their values. At the water level h_w = 0.75 *H*, the maximum lateral displacement in case 2 is equal to 0.9 *m*, to be compared to 0.6 *m* which is obtained in the case 4.

Concerning the maximum vertical displacement, it decreases from 1.65 *m* to 1.3 *m* with the increase in the cohesion.

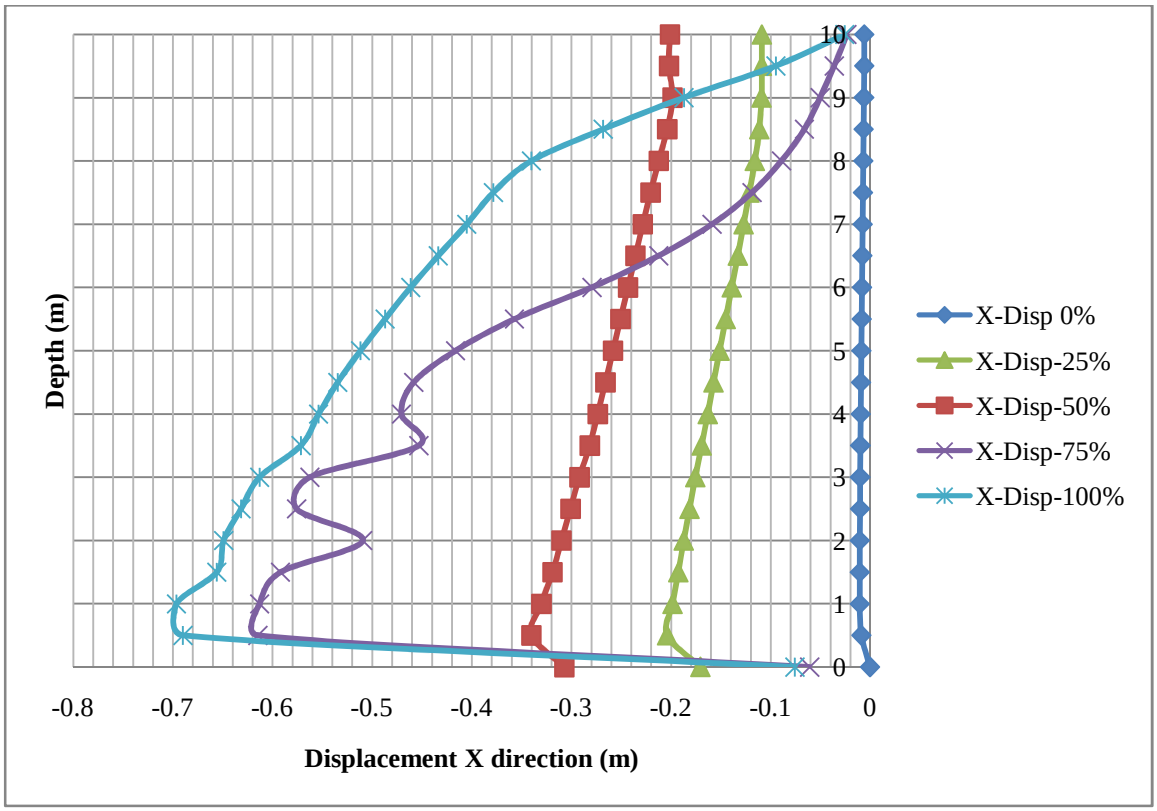

Figure 2.18: Influence of the water-table level on the lateral displacement

(Case 4, *β* = 30°) *hw/H* = 0.25, 0.5, 0.75 and 1.0

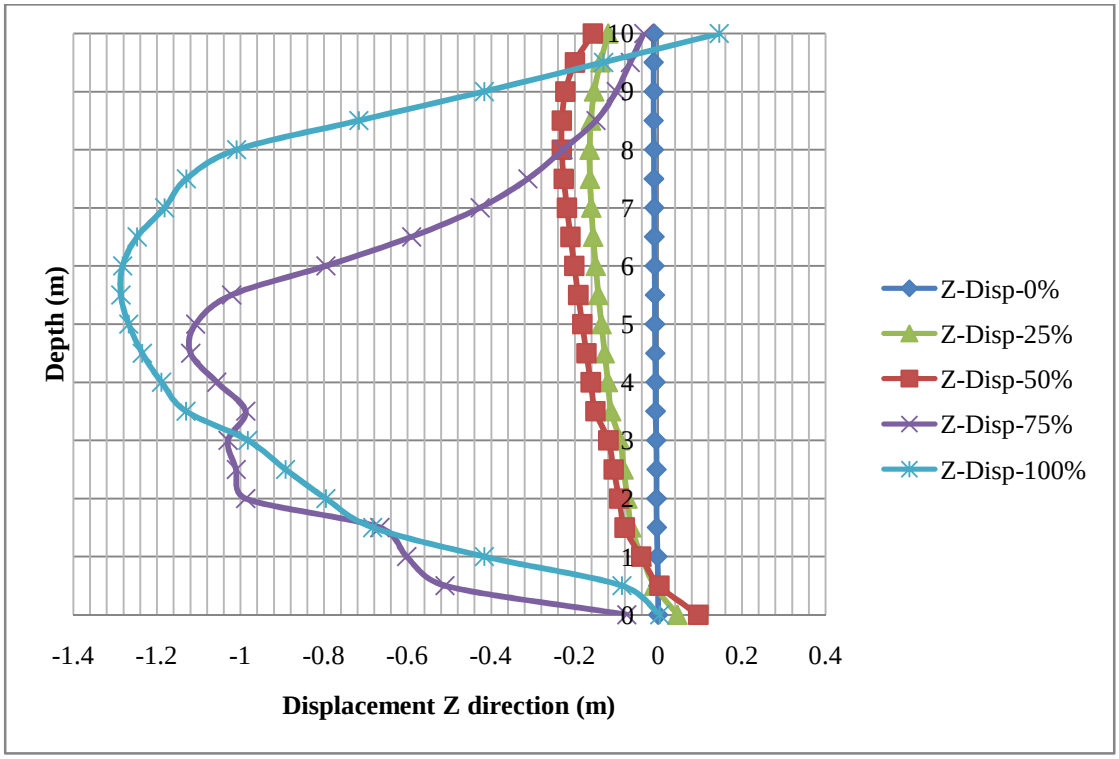

Figure 2.19: Influence of the water-table level on the vertical displacement

(Case 4, β= 30°) h_w/H = 0.25, 0.5, 0.75 and 1.0

F. Influence of the soil slope inclination

Figures 2.20 and 2.21 show the influence of an increase in the slope inclination on the lateral displacement resulting from an increase in the water table level. Analyses were conducted with the soil properties of case 2. We observe that the increase in the slope inclination does not affect the lateral displacement pattern for h_w/H = 0.25 and 0.5, but translates the location of the maximum lateral displacement upward for h_w/H = 0.75 and 1.0. It leads also to a high increase in the displacement: for the slope β = 35° and h_w/H = 0.75, the maximum lateral displacement is equal to 1.8 *m*, while this displacement is equal to 3.2 *m* with β = 40°.

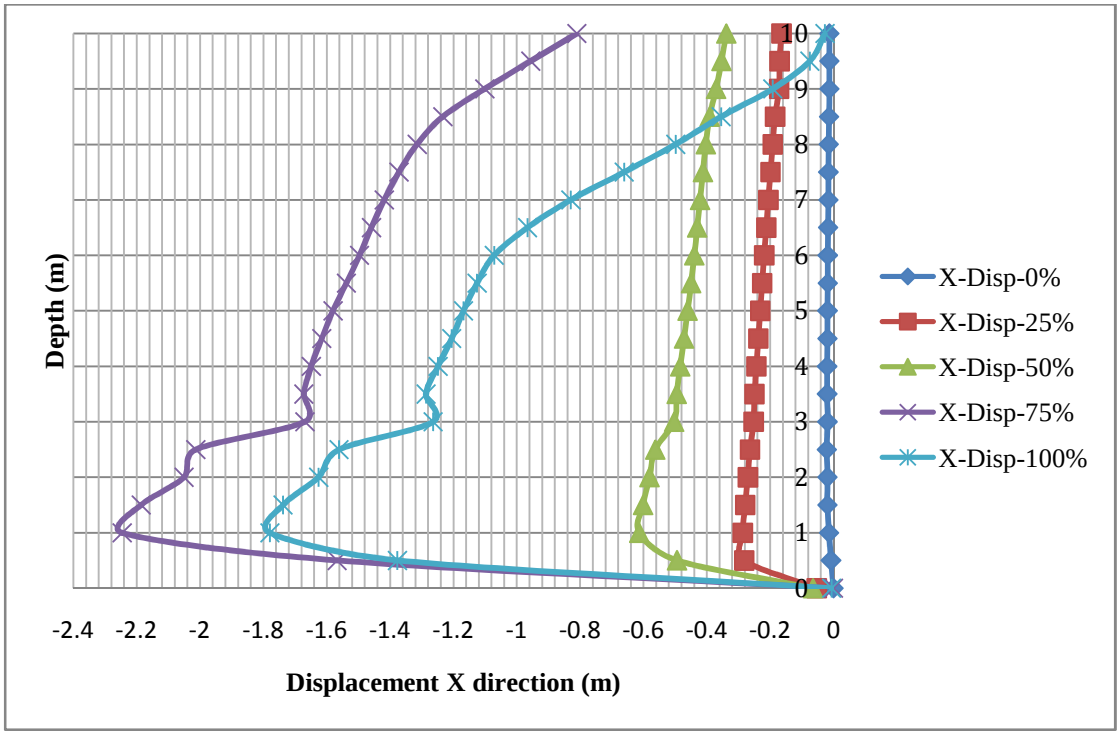

Figure 2.20: Influence of the increase in the water table on the lateral displacement

(Case 2, β = 35°) *hw/H* = 0.25, 0.5, 0.75 and 1.0

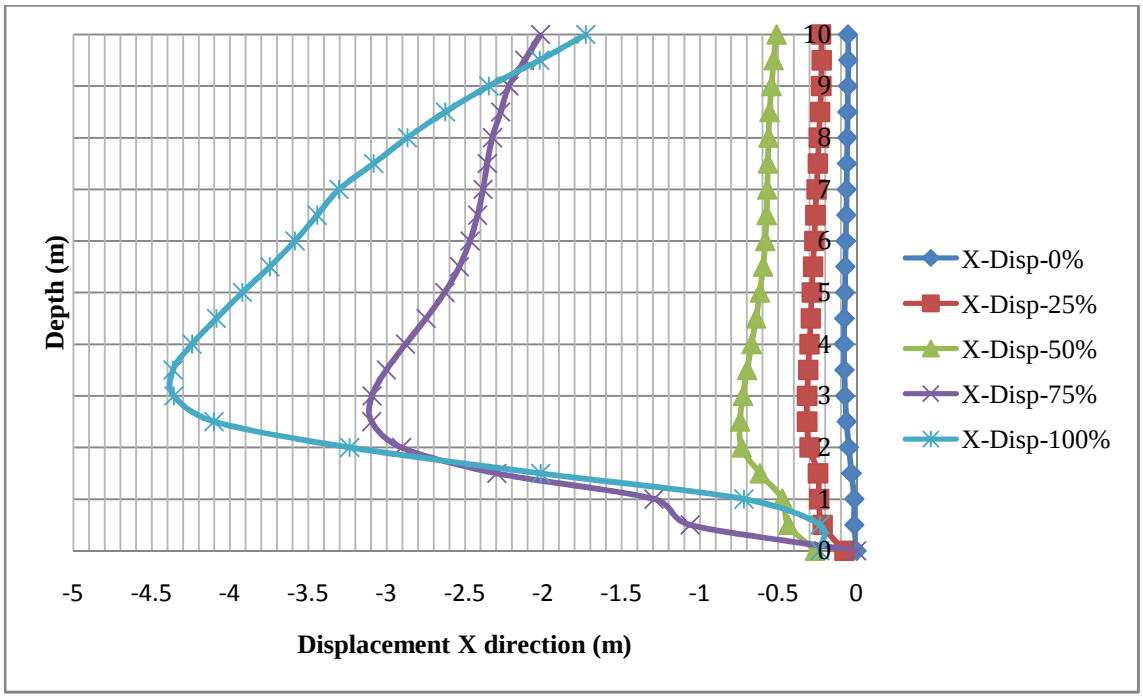

Figure 2.21: Influence of the increase in the water table on the lateral displacement

(Case 2, β = 40°) *hw/H* = 0.25, 0.5, 0.75 and 1.0

Figures 2.21 and 2.22 show the influence of an increase in the slope inclination on the vertical displacement. We observe that the increase in the slope inclination does not affect the lateral displacement pattern for h_w/H = 0.25 and 0.5, but translates the location of the maximum displacement upward for h_w/H = 0.75 and 1.0. It leads also to an increase in the vertical displacement amplitude: for the slope β= 35° and h_w/H = 0.75, the maximum vertical displacement is equal to 2.1 *m*, while this displacement is equal to 2.2 *m* with β= 40°. For more figure displacement will be found in appendix.

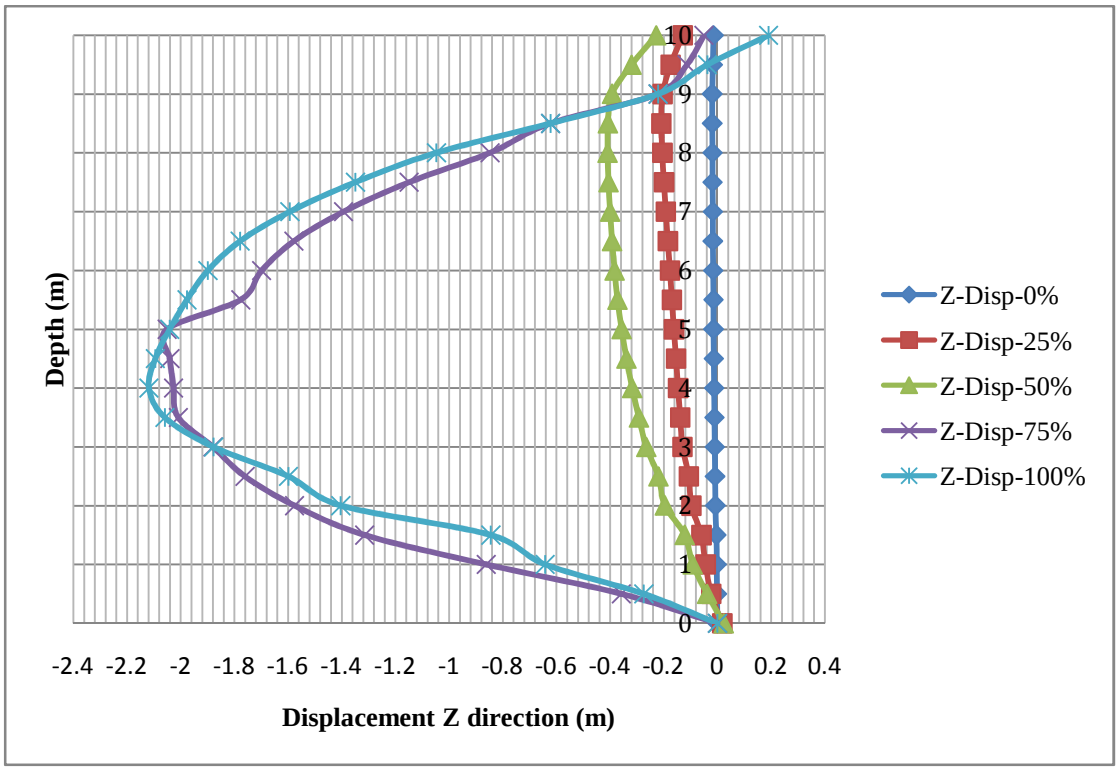

Figure 2.21: Influence of the water-tablelevel on the vertical displacement

(Case 2, β = 35°) h_w/H = 0.25, 0.5, 0.75 and 1.0

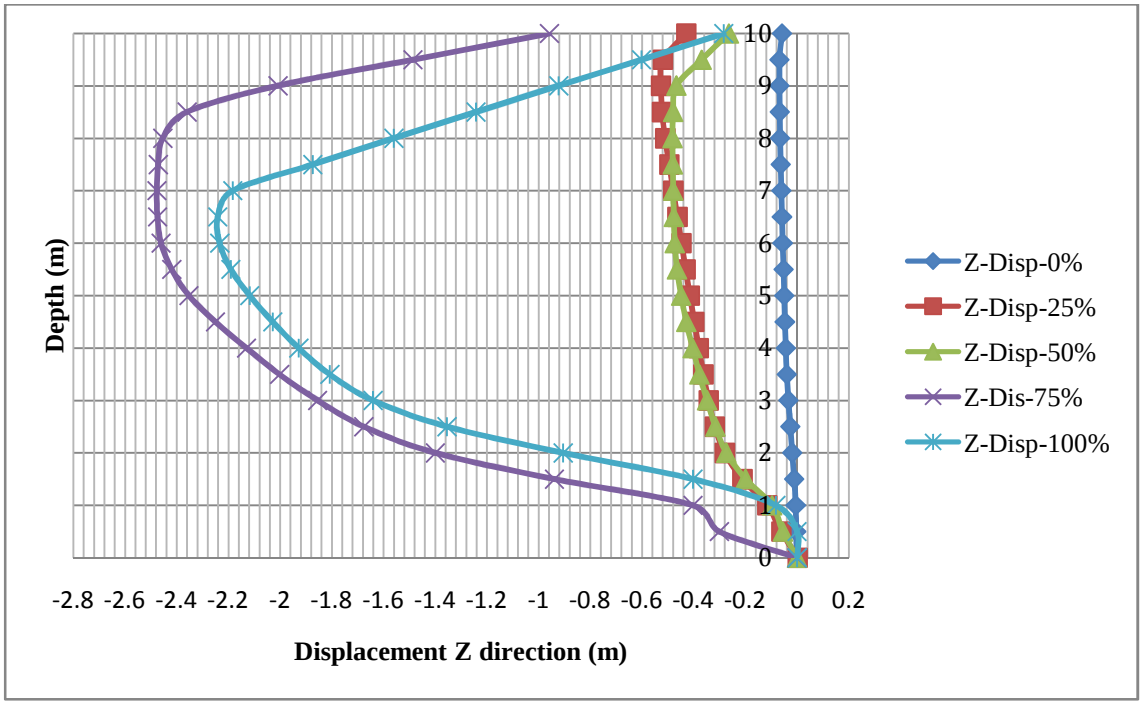

Figure 2.22: Influence of the water-tablelevel on the vertical displacement

(Case 2, β = 40°) h_w/H = 0.25, 0.5, 0.75 and 1.0

2.6 Conclusion

This chapter included analysis of the soil slope stability subjected to a variation of the water-table. Below the water table, the soil was assumed fully saturated, while above the water-table, it was assumed partially saturated.

Analyses were conducted using a full-coupled hydro-mechanical model implemented in the FLAC 3D program. The soil behaviour was assumed to be governed by the non-associated Mohr-Coulomb criterion. The *FoS* was determined using the Strength Reduction Method implemented in FLAC 3D.

Analyses were conducted for different values of both the water-table level and the slope inclination. The influence of the soil strength in the unsaturated zone was also considered.

The main results of the Analyses conducted in this chapter could be summarized as follows:

- The increase in the water – table level leads to a decrease in the slope *FoS*. For the slope included 30° to the horizontal, the *FoS* decreased from 1.86 to 0.27 when the water-table height h_w increased from 0.25H to H (H is the height of the soil mass). Based on the numerical analysis, a chart was proposed for the determination of the critical water-table level from the slope inclination. This chart could be constructed for cases encountered in engineering practice.
- For the configurations considered in this study, the increase in the cohesion in the non-saturated zone from 10 to 20 *kPa* leads to an increase in the factor of safety for the configurations with low water table. The tensile strength does not affect the slope stability.
- The pore pressure distribution is mainly governed by the hydraulic condition. The influence of the soil strength parameters on this distribution is negligible.
- The increase in the water-table level leads to an increase in the lateral and vertical displacements with the formation of a quasi-bloc movement including lateral and vertical displacement as well as rotation. At high water level (h_w/H > 0.7), large displacements were observed, which indicate the presence of slope instability. The amplitude of the displacement increased with the increase in the slope inclination.

Analyses conducted in this chapter are based on advanced conventional hydro-mechanical methods. In the following chapter, we will use the method of nonlinear dynamic for the analysis of this stability.

CHAPTER 3: Analysis the slope stability using the nonlinear dynamic theory

3.1 Introduction

Chapter 2 included analysis of the slope stability using the coupled hydro-mechanical numerical model. The use of this approach allows requires huge numerical computations.

In this chapter we propose to analyze the slope stability using the nonlinear dynamic theory, which constitutes a powerful tool for the analysis of discontinuous phenomena, such as landslides.

Analysis of the slope stability was conducted on a simplified configuration of a slope, which consists in the movement of a rigid bloc over a plan-sliding surface. The influence of the water table will considered through the behavior of the interface. The chapter includes three parts. The first one establishes the system governing equation from the balance equation. The second part includes analysis of the slope stability using the balance equation. The last part includes a generalization of the study by the use of the energy approach. Analyses aim at the determination of the zone of stability of the slope trough the construction of charts.

3.2 Problem statement

Figure 3.1 shows the problem under consideration. It concerns a soil mass with a potential sliding bloc along a surface, inclined β to the horizontal axis. The height of the soil mass is H while the height of the water table is h_w. For simplification, the soil mass is assumed to be homogeneous. However, above the water table, the soil is assumed unsaturated, while below the water table, it is assumed to be saturated. Since the soil saturation largely affects its resistance, the soil mass will be considered as bi-layer.

The water pressure under the water table and the suction above the water table are assumed to follow a linear variation with depth.

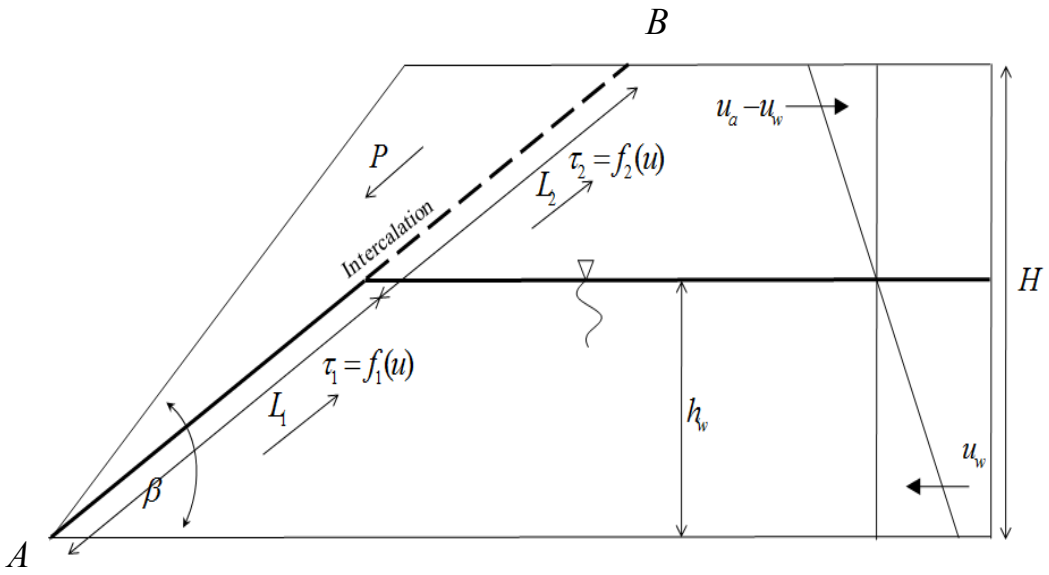

Figure 3.1:Problem under consideration: slope stability due to the fluctuation of the water table

3.2.1 Deformation process

The deformation of the soil mass is assumed to occur by the sliding of the upper bloc, considered as rigid, along the sliding surface *A* - *B*. In this example, the weight of the bloc is the unique driving force, while the shear resistance at the sliding surface constitutes the unique resistance force.

3.2.2 Interface constitutive relation

The relation between the shear stress and the shear strain at the interface *A* - *B* is non linear. Figure 3.2 shows typical variations of the shear stress with the variation in the shear strain:

- For “compact/rough interface”, we observe generally a rapid increase in the shear stress with the increase in the shear strain up to a peak, followed by a decrease down to the residual shear strength.

- For “loose /smooth interface”, the increase in the shearing strain causes a regular increase in the shear stress up to the shear strength.

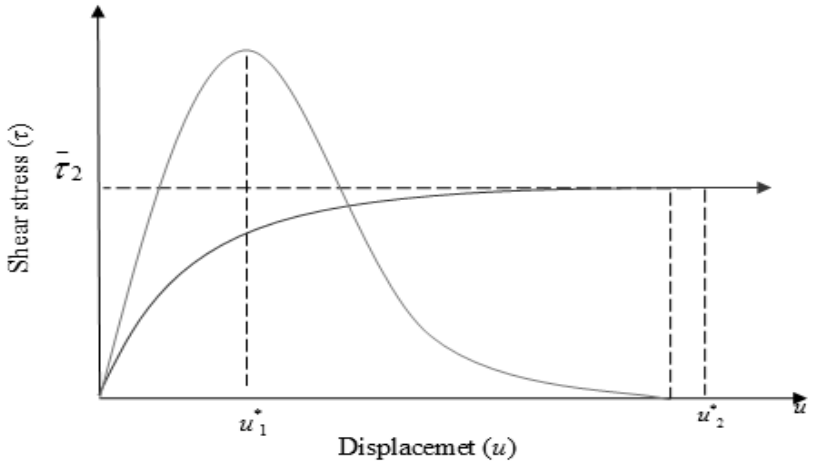

Figure3.2:Constitutive model of the interface

The behaviour at the "rough interface" (medium 1) including the peak phenomena is described using the Weibull's function (Hudson and Fairhurst, 1969):

$$\tau_1 = G_{s1}.u.e^{\left(-u/u^*_1\right)^m} \tag{3.1}$$

- G_{si} is the initial shear modulus
- u^*_i corresponds to the displacement at the shear peak.

The parameter *m* controls the variation of the shear stresses with the change in the shear strain (displacement). Figure 3.3 summarizes the influence of the parameter *m* on the variation of the shear stress. The increase in *m* leads to an increase in the peak magnitude as well as an increase in the rate of variation of the shear stress with the shear strain.

The parameter *m* is a measurement of the local strength variability. It is considered as a homogeneity index: the increase in *m* leads to an increase in the soil homogeneity (Tang, 1993). Analysis were conducted with the following values:

- G_s= 10 *MPa*
- u^* = 0.1 *m*

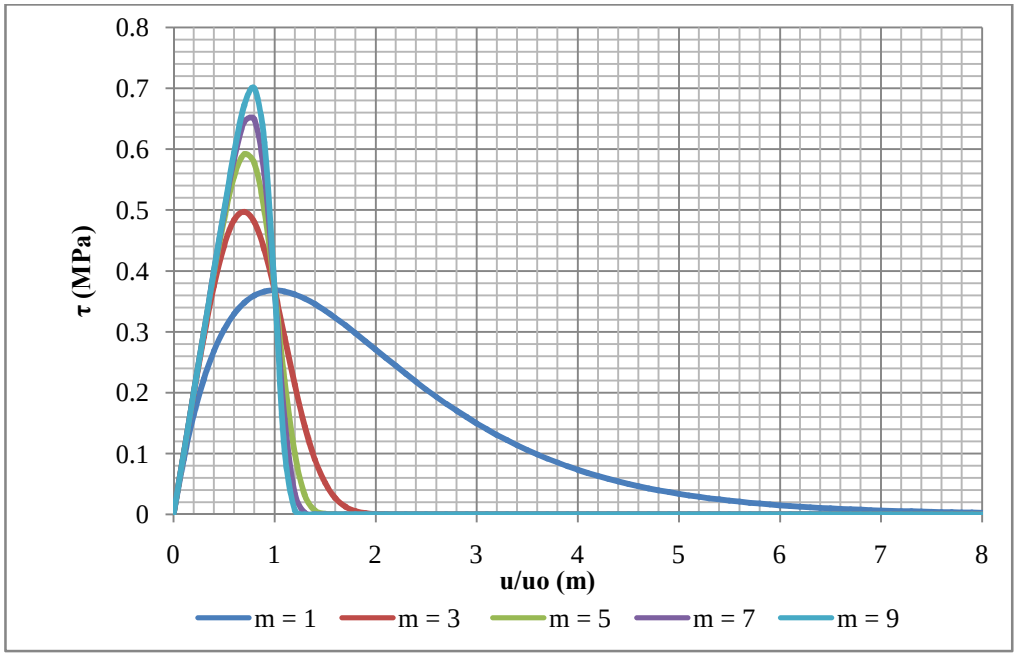

Figure 3.3 : Weibull's distribution constitutive curve

For medium 2 above the water table, the soil is partially saturated. The shear strength of the unsaturated soil can be formulated in terms of independent state variables (Fredlund et al. 1978). The shear strength of the interface is this area is assumed to be governed by that of the unsaturated soils. It could be written as follows:

$$\overline{\tau_2} = c' + (\sigma_n - u_a)\tan\phi' + (u_a - u_w)\tan\phi^b \qquad (3.2)$$

where :

$(\sigma - u_a)$: The net normal stress state on the failure surface (sliding surface).

$(u_a - u_w)$: The matric suction

(ϕ'): The friction angle associated to contribution of the normal net stress to the shear strength.

(ϕ^b): The friction angle associated to the contribution of the suction to the shear strength.

c : the cohesion.

The mobilization of the friction in this layer is described using the following relation:

$$\tau_i = \left(1 - e^{-k_i u}\right)\overline{\tau_i} \tag{3.3}$$

k_i is a constitutive parameter of the interface which controls the rate of variation of the shear stress with the shear strain.

3.3 Governing equation

The weight of the upper bloc constitutes the driving force of the bloc movement. Its value is given by the following expression:

$$P = \rho.g.\left(\frac{h.(L_1 + L_2)}{2}\right)\sin\beta \tag{3.4}$$

- P is the volume mass.
- L_1 and L_2 denote the length of the interface in the lower and upper parts of the soil mass, respectively (Figure 3.1).

Considering a sliding movement (u) of the upper bloc, the potential energy of the system is calculated by the sum of the :

- Strain energy $\left(f_1(u).L_1 + f_2(u).L_2\right)$ of the upper and lower interfaces
- Energy related to the bloc weight (P).

The balance of the forces applied on the bloc gives the following equation:

$$V' = f_1(u).L_1 + f_2(u).L_2 - P = 0 \tag{3.5a}$$

$$V' = G_{s1}.u.e^{\left(-u/u^*_1\right)^m}.L_1 + \bar{\tau}_2.\left(1 - e^{-k_2.u}\right).L_2 - \rho.g.\left(\frac{h.(L_1 + L_2)}{2}\right)\sin\beta = 0 \tag{3.5b}$$

Considering

$$G_s = k_i\overline{\tau_i} \tag{3.6a}$$

$$k_i = \frac{1}{u^*_i} \tag{3.6b}$$

$$\tau_2 = G_{s2}.u^*_2.\left(1 - e^{-\frac{u}{u^*_2}}\right) \tag{3.6c}$$

equation 3.5 could be re-written as follows:

$$V' = G_{s1}.L_1.u.e^{\left(-u/u^*_1\right)^m} + G_{s2}.u^*_2.L_2.\left(1 - e^{-\frac{u}{u^*_2}}\right) - \rho.g.\left(\frac{h.(L_1 + L_2)}{2}\right)\sin\beta = 0 \tag{3.7}$$

By introducing the new parameters A and B:

$$A = \frac{G_{s2}.L_2}{G_{s1}.L_1} \tag{3.8a}$$

$$B = \frac{\rho.g.h.(L_1 + L_2).\sin\beta}{2.G_{s1}.L_1} \quad \text{or} \quad B = \frac{P}{G_{s1}.L_1} \tag{3.8b}$$

equation 3.7 could be re-written under the simplified expression:

$$u.e^{\left(-u/u^*_1\right)^m} + A.u^*_2\left(1 - e^{-\frac{u}{u^*_2}}\right) - B = 0 \tag{3.9}$$

This equation involves the following parameters:

- The interface constitutive parameters m, u^*_1 *and* u^*_2
- The parameter A, which corresponds to the ratio between the stiffness of the upper part of the sliding bloc to that of the lower part.
- The parameter B, which stands for the driving forces.

The values of parameters A and B are positive.

3.4 Analysis of the bloc stability

3.4.1 Balance equation (equation 3.9)

Figure 3.4 illustrates the influence of the variation of parameters A and B on the bloc response (displacement u, solution of equation 3.9). Analyses were conducted with the following values of the interface parameters:

- $m = 3$
- $u^*_1 = 0.05\ m$
- $u^*_2 = 0.5\ m$.

The response was determined for a variation of B between 0 and 0.2 and various values of A in the interval [0.10 and 1.08]. Results are illustrated for a response value (u) up to 0.3 *m*.

Analysis of figure 3.4 shows that the response of the bloc largely depends on the value of the parameter A.

Concerning the bloc stability, we observe two trends in the response (Figure 3. 5):

- Stable response (trend B): for each value of B (driving force), the system has a unique response.
- Unstable response (trend A): for some values of B (driving force), the system has tow possible responses.

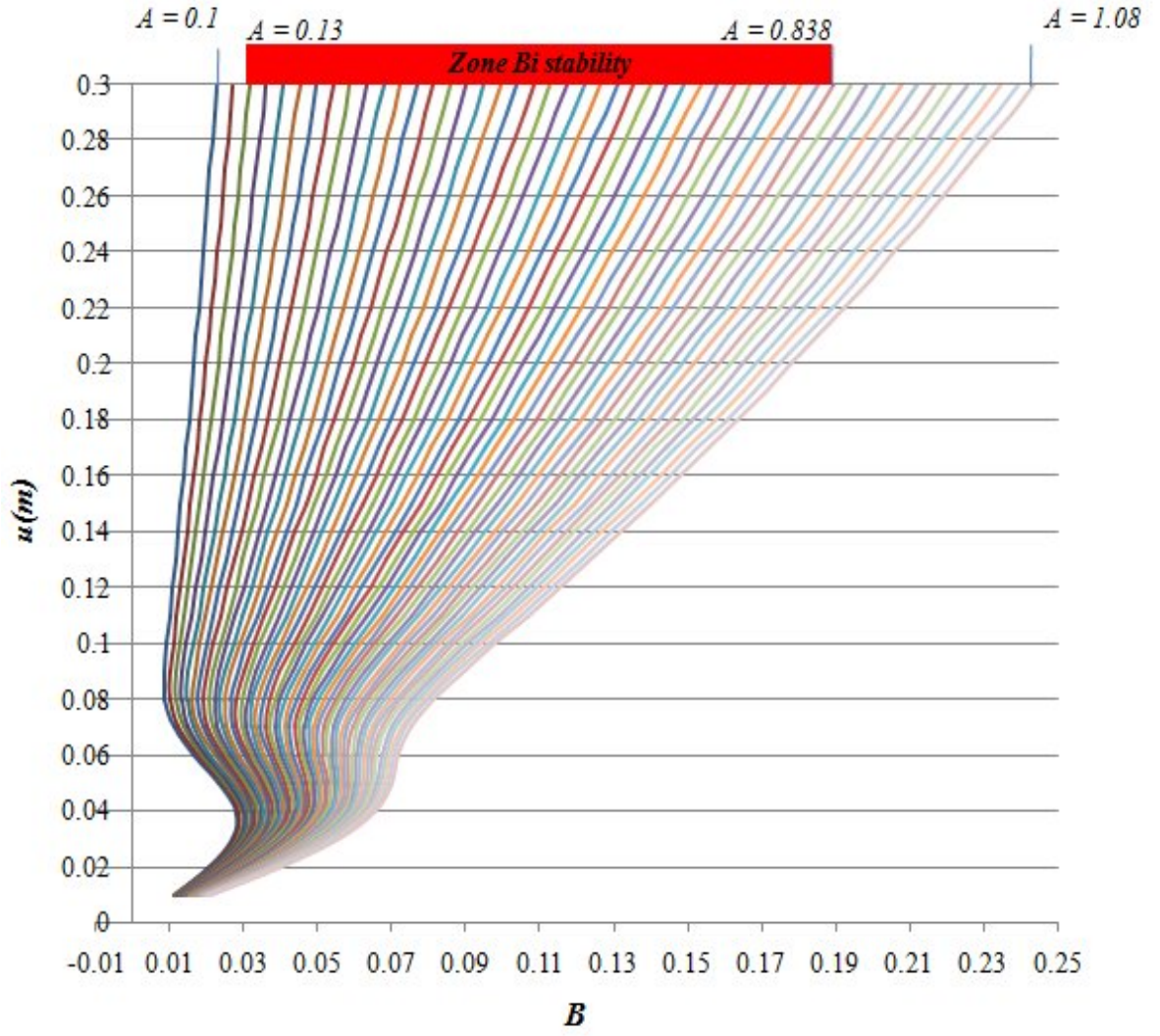

Figure 3.4 : Influence of the variation of parameters A and B on the bloc response (displacement u, solution of equation 3.9)

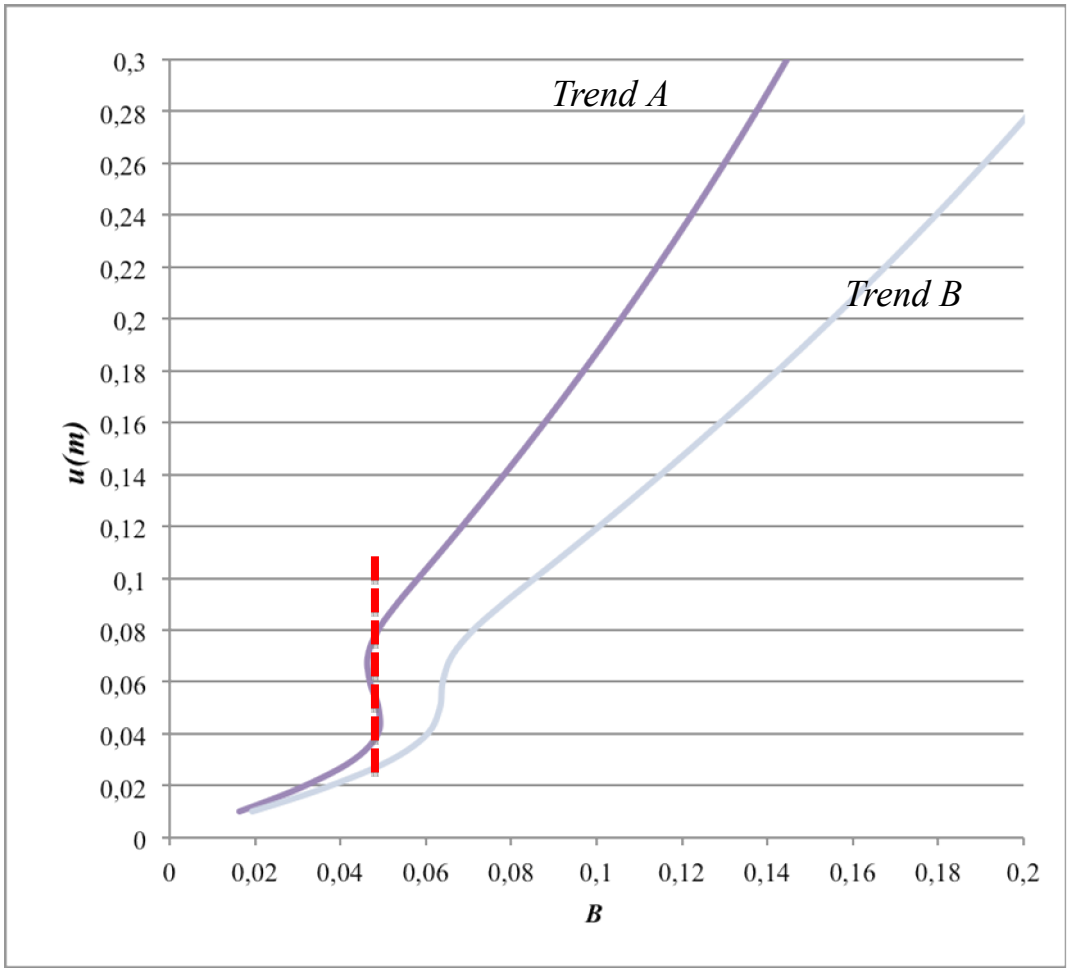

Figure 3.5: The bloc response trends to the variation of parameters B and A

- A: Instable response (possibility 2 solutions for a given value of B)
- B: Stable response (unique response for each value of B).

Figure 3.6 illustrates in the three dimensional space (*A, B, u*) the influence of the variation of parameters A and B on the bloc response (*u*). This figure permits to localize in the three dimensional space the stable zone of the bloc. This zone is shown in Figure 3.7.

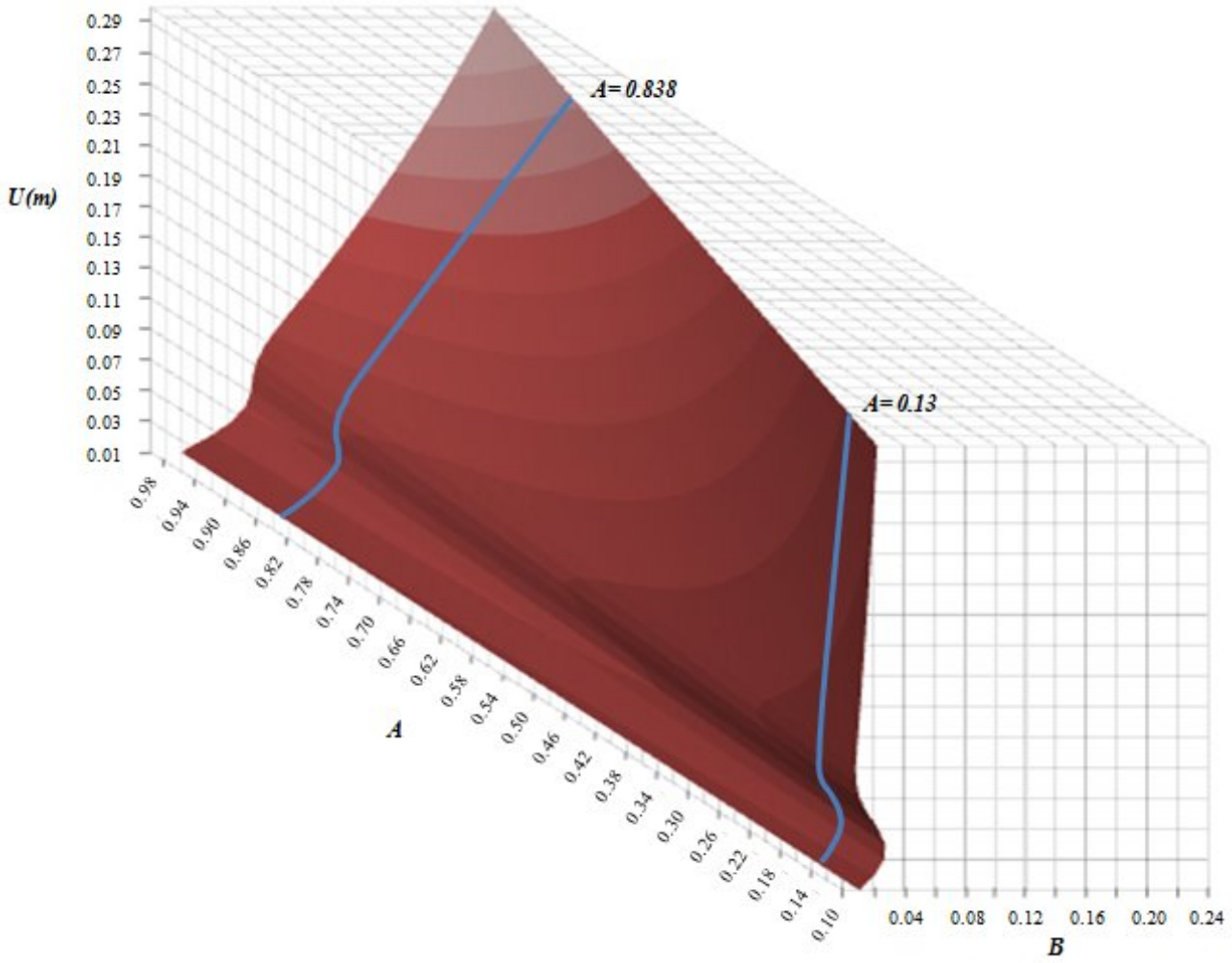

Figure 3.6: Three dimensional illustration of the influence of the variation of parameters A and B on the bloc response

(displacement u, solution of equation 3.9)

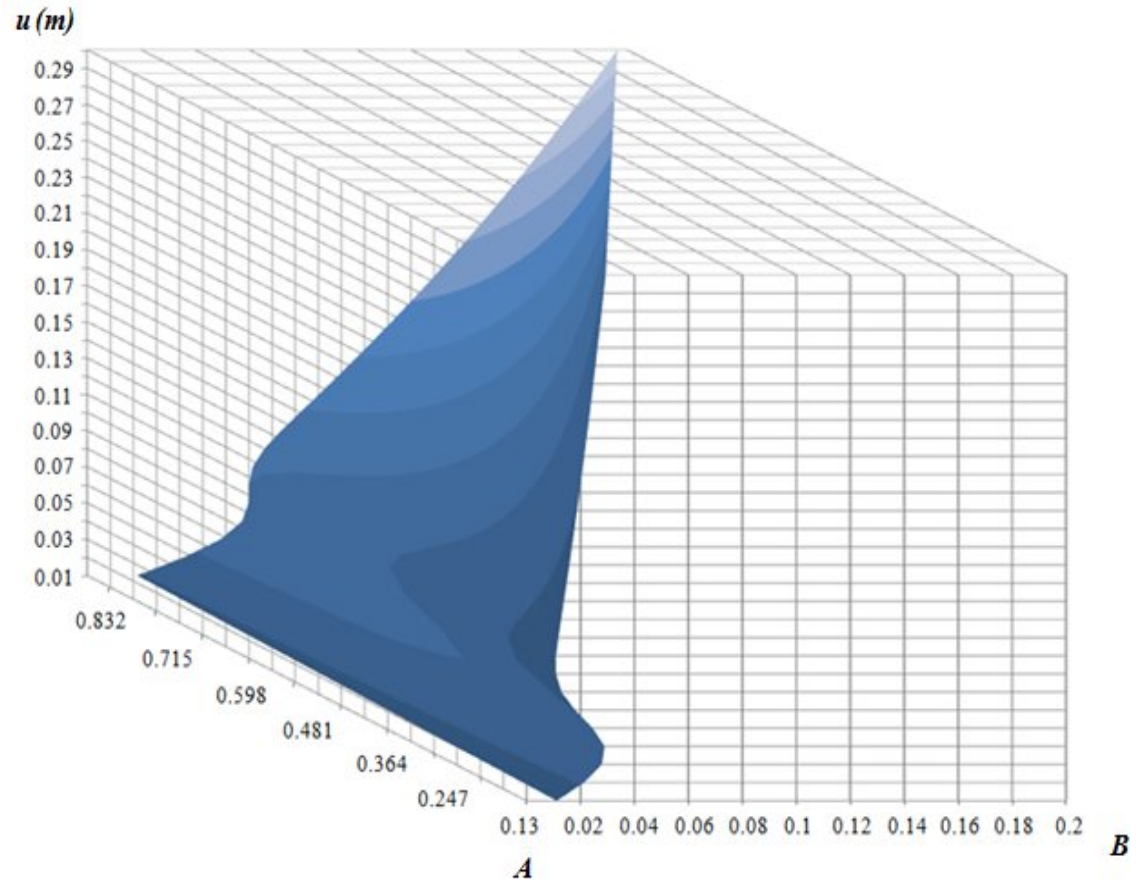

Figure 3.7: Zone limit *A* = 0.13 – 0.838 in the three dimensional space

3.4.2 Energy analysis

The stability analysis using the energy approach requires the calculation of the 2nd and 3rd derivatives of the energy of the system. From equation 3.1 (1st derivative of the potential energy), we obtain the following expressions:

$$v'' = e^{\left(-u/u^*_1\right)^m} + \left(-u/u^*_1\right)^m .m.e^{\left(-u/u^*_1\right)^m} + A.e^{\left(-u/u^*_2\right)} = 0 \qquad (3.10)$$

$$v''' = \left(-u/u^*_1\right)^m .\frac{m}{u}.e^{\left(-u/u^*_1\right)^m} + \left(-u/u^*_1\right)^m .\frac{m^2}{u}.e^{\left(-u/u^*_1\right)^m} + \left(\left(-u/u^*_1\right)^m\right)^2 .\frac{m^2}{u}.e^{\left(-u/u^*_1\right)^m} - \frac{A}{u^*_2}.e^{\left(-u/u^*_2\right)} = 0$$

(3.11)

In order to illustrate the energy approach of the system instability, we show in figures 3.8a and 3.8b the variation of the 2nd and 3rd derivates of the energy of the system with the variation of the displacement (*u*). Figure 3.8c shows the corresponding value of B for each value of the displacement (*u*) (according to the the equlibrium equation 3.9).

Figure 3.8a shows that the 2nd derivative has a minimum and a maximum in the studies interval (*u* between 0 and 0.5 *m*) with opposite sings (the minimum is negative, while the maximum is positive). This change in the sign is confirmed by the annulation of the 3rd derivative of the energy of the system (Figure 3.8b). The latter condition leads to the trend "A" of the system response, which indicates system instability.

.

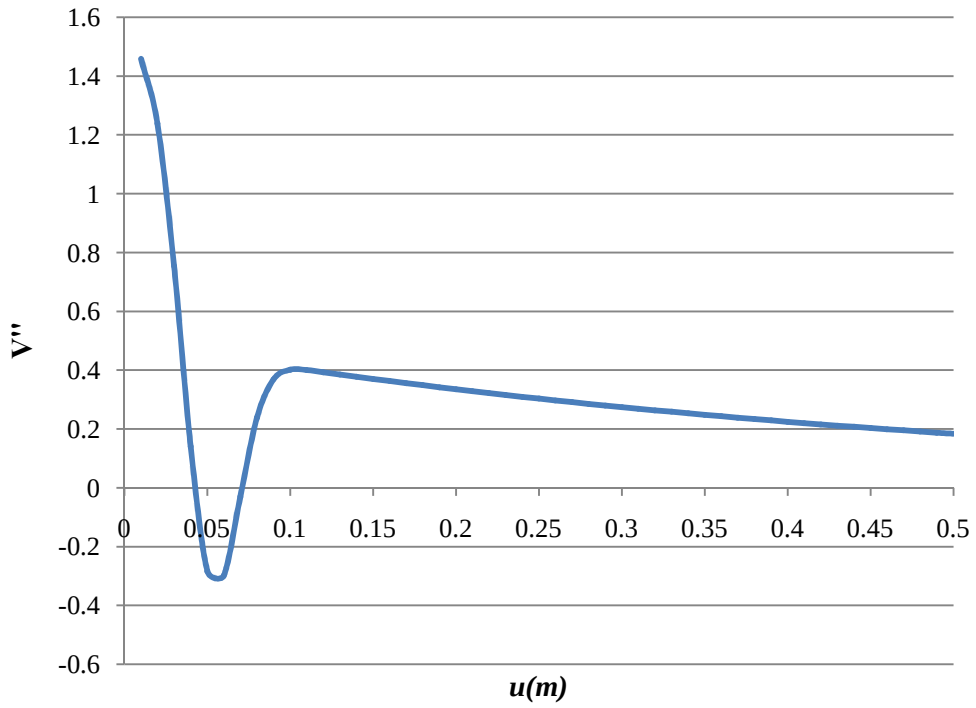

Figure 3.8a: Variation *the 2nd derivative of the energy of the system* with displacement u (Equation 3.10)

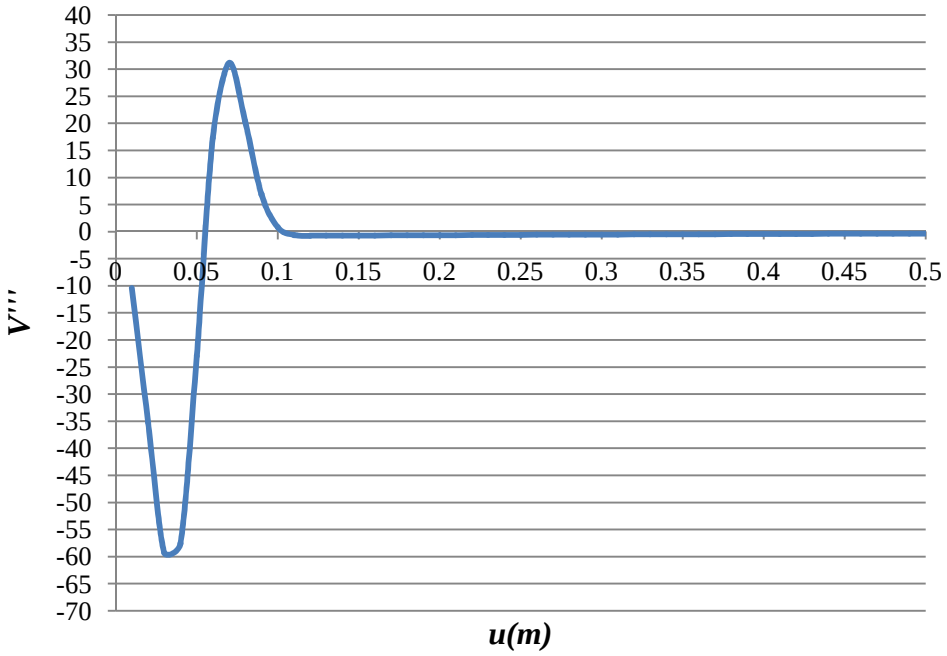

Figure 3.8b: Variation *the 3nd derivative of the energy of the system* with displacement u (Equation 3.11)

Figure 3.9 shows that the increase in the response (u) in this case is accompanied by an irregular variation of the parameter B (the driving force). The figure shows the domaine of instability, which is limited by the values of u corresponding to the extrema of B.

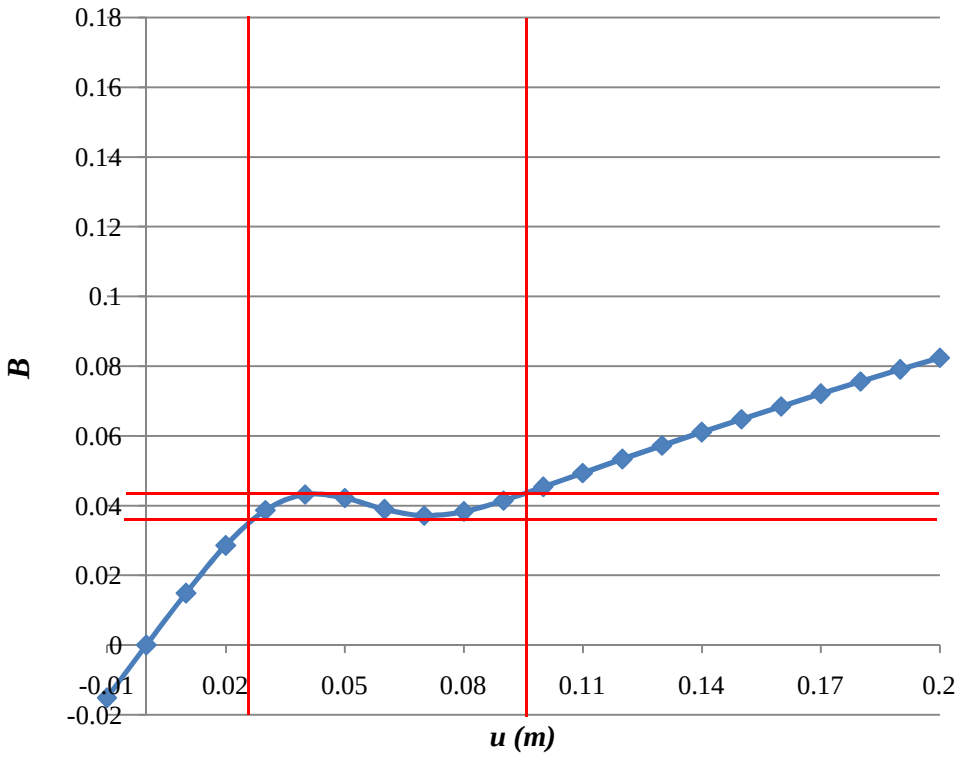

Figure 3.9: Variation of B with the value of (*u*) (According to the equilibrium equation 3.9)

Figure 3.10 summarizes the influence of the increase in the displacement (*u*) on the variation of the 2nd and 3rd derivatives of the energy of the soil bloc as well as that of the paramter B (driving force). For a good illustration of this graph, the values the 2nd and 3rd derivatives of the energy of the soil bloc of were nomalized. This figure allows the determination of the zone of instability which cooresponds to the interval of u limited by the extrema of B, which includes a zero of the 3rd derivate of the energy of the system as well as the minimum and maximum of the 2nd derivative.

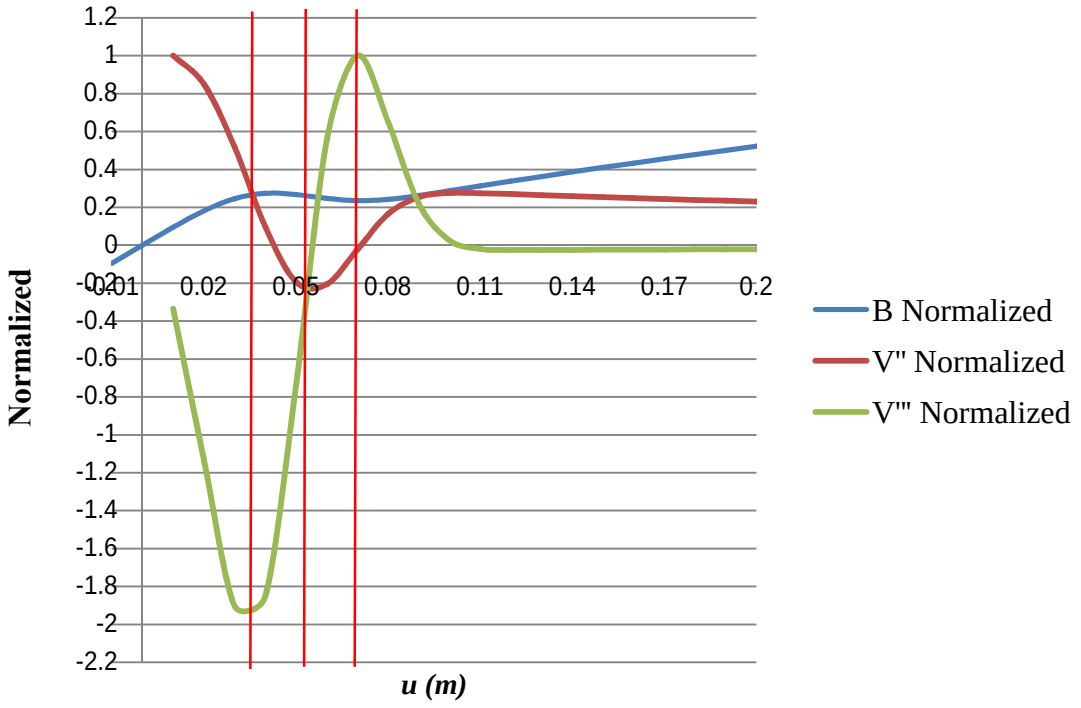

Figure 3.10: Variation of the 2nd and 3rd derivatives of the energy of the system and that of parameter B with the bloc response

3.4.3 Energy analysis (Zero of the 3rd derivative)

The determination of the zero of the 3rd derivative is very complex. In order to overcome this difficulty, we determine the value of the parameter A corresponding to this zero from the response of the system (displacement *u*):

$$A = \frac{\left(-u/u^*_1\right)^m . \frac{m}{u} . e^{\left(-u/u^*_1\right)^m} . u^*_2 . \left(1 + m + \left(-u/u^*_1\right)^m . m\right)}{e^{\left(-u/u^*_2\right)}} \quad (3.12)$$

Figure 3.12 shows the variation the normalized values of the parameters A and B with *u* (zero of the 3rd derivative). We observe an interval of u delimited by the extreme of the parameter B (driving force) with u with positive values of A. This zone corresponds to the zone of instability of the bloc.

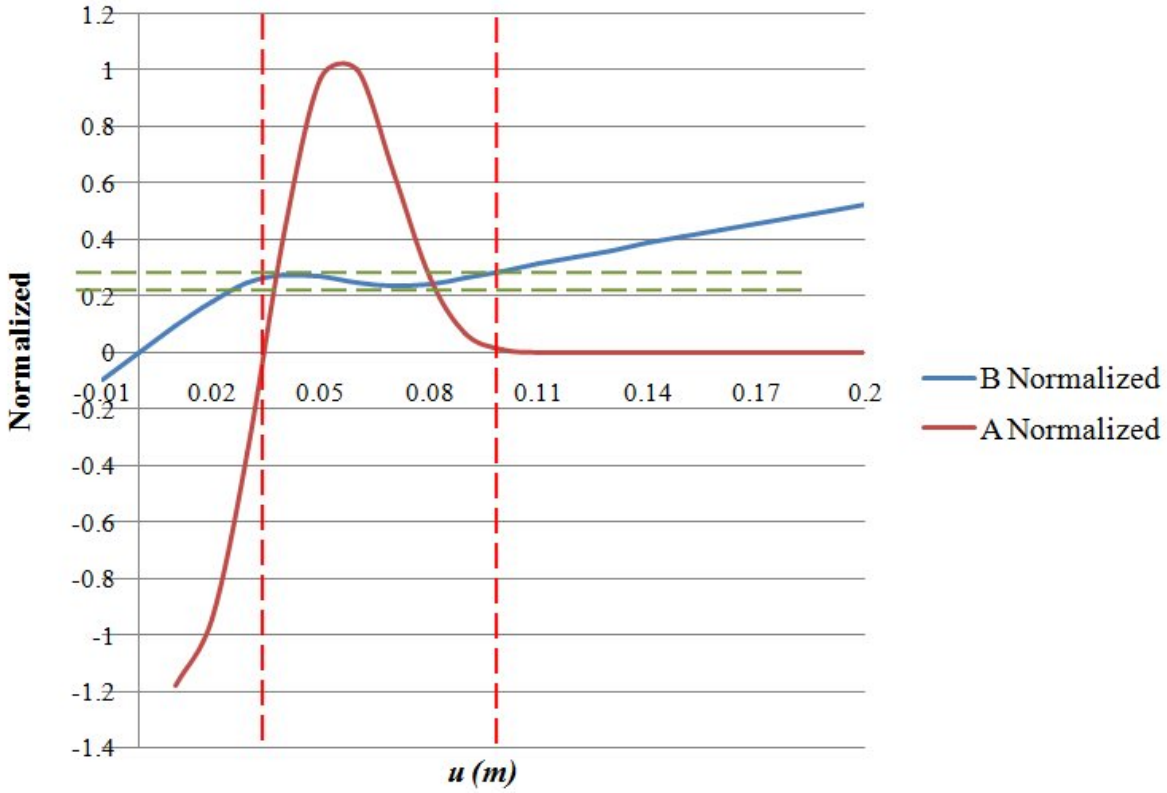

Figure3.11 : Development Limit Analysis

3.5. Instability domain

The bloc behavior depends on the values of the three parameters, which control the mode of mobilization of the shear stress at the interface:

- u^*_1
- u^*_2
- m

The domain of instability will be determined by the determination of the upper and lower values of the parameter A as illustrated in figure 3.11. Analyses were conducted for 4 values of the parameter m (3, 5, 7, 9).

Figure 3.12a shows the results obtained with $m = 3$. The surface in red color designates the upper limit, while the blow color denotes the lower limit. We can observe that the lower and upper parts largely depend on the values of u^*_1 and u^*_2, in

particular for the low values of u^*_2. The domain of instability shows a general trend of increase with the increase in u^*_2 andthe decrease in u^*_1.

Results obtained with m = 5 are illustrated in figure 3.12b. We observe the same trends as in the case m = 3, but with high irregularities at low values of u^*_2.

Figure 3.12c shows the results obtained with m = *7*. We observe a regular variation in the boundary of the instability domain with regard to the boundaries obtained with m = 3 and 5.

Figure 3.12d shows the results obtained with m = *9*. We observe an increase in the domain of instability with regard to previous results, accompanied by a translation towards the higher values of the parameter A.

This analysis allows the construction of charts for the instability domain of the soil slope in terms of parameters which control the rate of variation of the shear stress at the bloc interface.

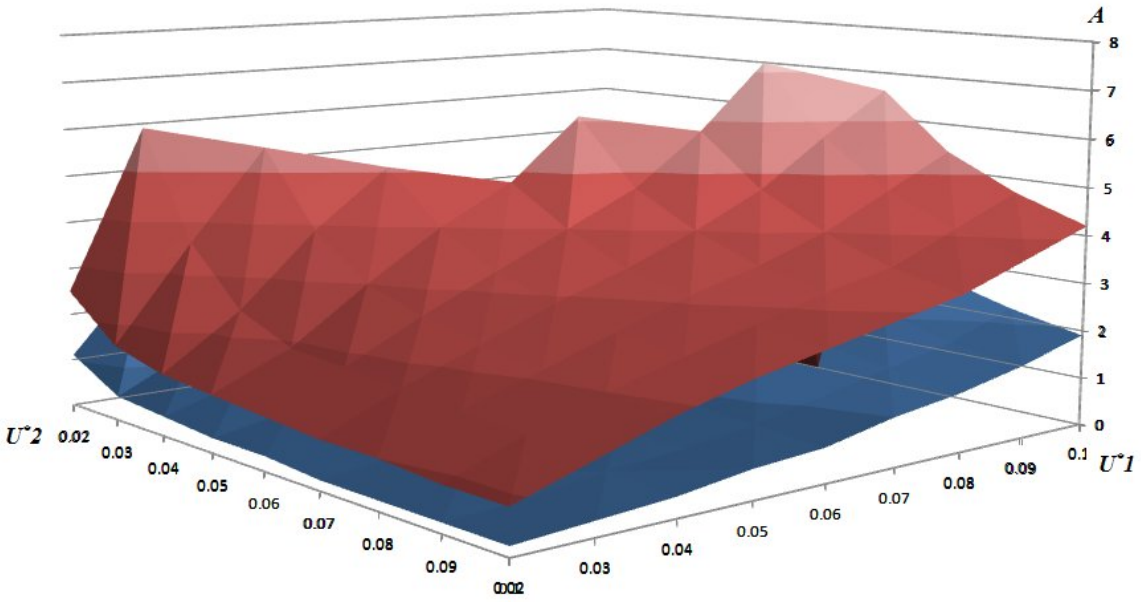

Figure 3.12a : Upper and lower limits of the instability domain (m = 3)

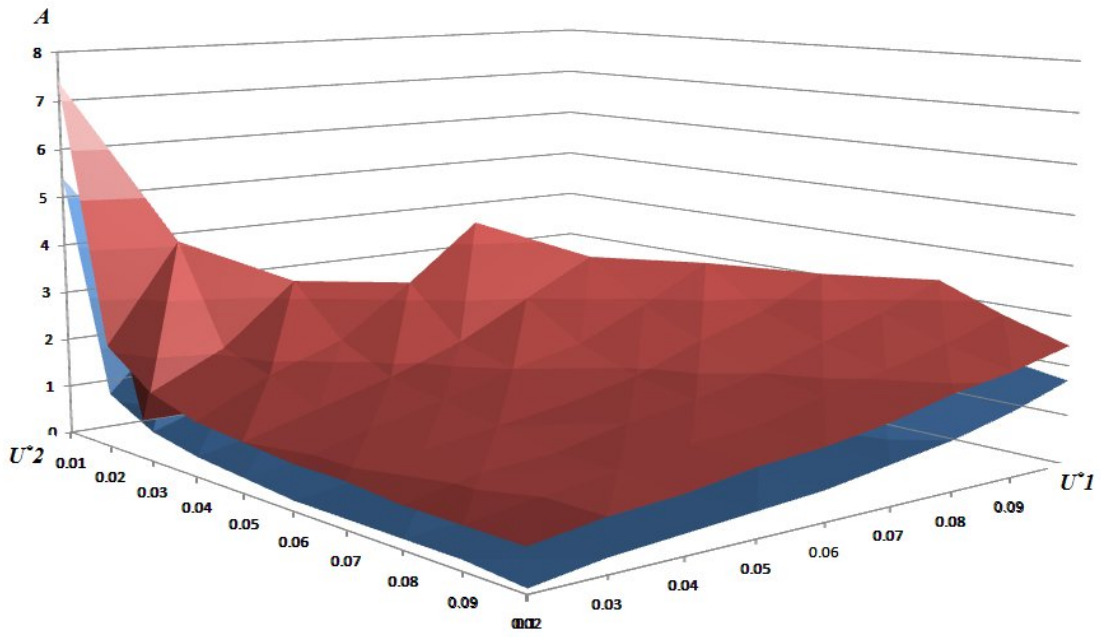

Figure 3.12b: Upper and lower limits of the instability domain (m = 5)

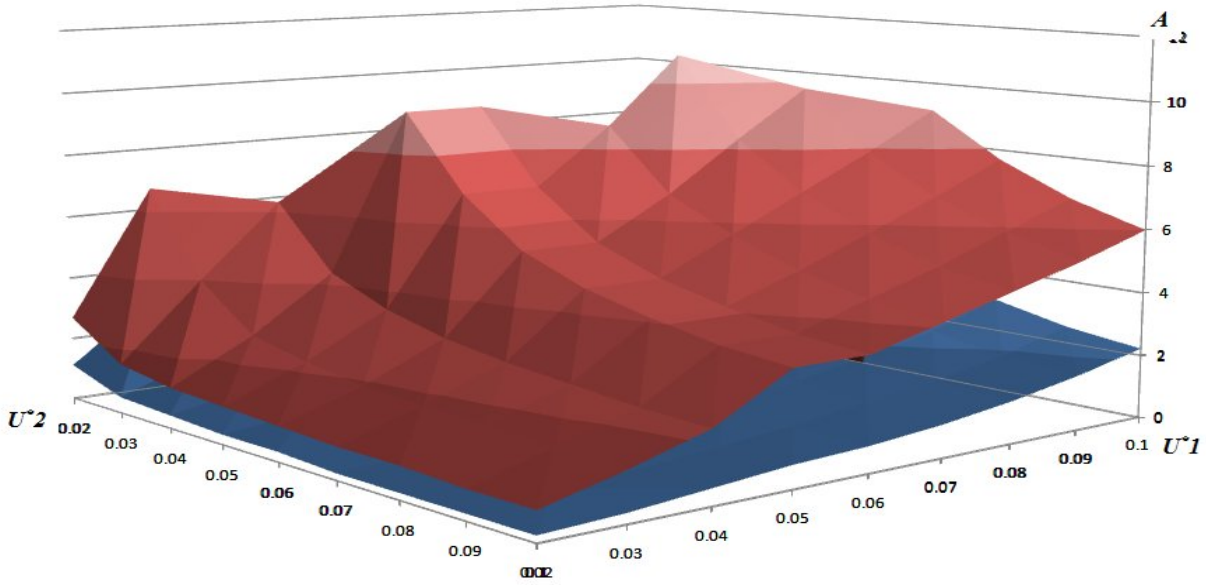

Figure 3.12a: Upper and lower limits of the instability domain (m = 7)

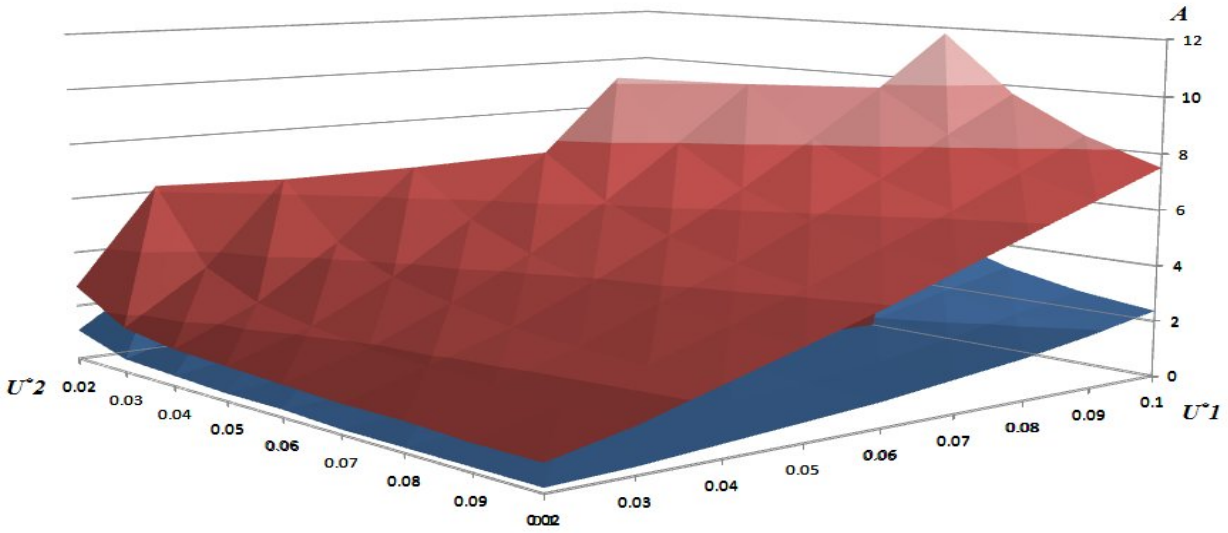

Figure 3.12 d: Upper and lower limits of the instability domain (m = 9)

3.6 Conclusion

The nonlinear dynamic theory provides a powerful tool for the analysis of discontinuous phenomena, such as landslides, which constitute an important issue in geotechnical engineering. This theory allows taking into account complex process in physical phenomena including discontinuities.

The use of the nonlinear theory is based on the energy approach. Analysis of the slope stability was conducted on a simplified configuration of the slope, which consists in a movement of a rigid bloc over a surface composed of 2 parts. The first one includes the peak effect.

Analysis of the stability was first conducted using the balance equation. This analysis allowed the determination of the zone of slope instability.

The second analysis was conducted using the 2nd and 3rd derivatives of the energy of the system. This analysis allowed the determination of the domain of instability. Charts were constructed for the determination of the upper and lower limits of the instability domain using the parameters u^*_1, u^*_2 and m as input parameters.

REFERENCES

A.BACHTA.2011. Le modèle mathématique de la Morphogenèse chez R. Thom. Université de Tunis.

Andreas C.W. Baas.2002. Chaos, fractals and self-organization in coastal geomorphology: simulating dune landscapes in vegetated environments. Geomorphology. Vol. 48, PP. 309–328.

A. Rahimi, H. Rahardjo, E. C. Leong. 2011. Effect of Antecedent Rainfall Patterns on Rainfall-Induced Slope Failure. Journal of geotechnical and geoenvironmental engineering ASCE. May 2011.

A. Rahimi, H. Rahardjo, E. C. Leong. 2010. Effect of hydraulic properties of soil on rainfall-induced slope failure. Engineering Geology. Vol. 114, PP. 135–143.

B. D. Collins, D. Znidarcic. 2004. Stability Analyses of Rainfall Induced Landslides. Journal of geotechnical and geoenvironmental engineering ASCE. April 2004.

C.W.Lin, S.H.Liu, S.Y.Lee, C.C.Liu.2006.Impac of the chi-chi earthquake on subsequent rainfall-induced landslide in central Taiwan. Engineering Geology. Vol.86, PP.87-101.

C. W. W. Ng, Q. Shi.1998. A Numerical Investigation of the Stability of Unsaturated Soil Slopes Subjected to Transient Seepage. Computers and Geotechnics , Vol. 22, No. 1, pp. 1-28.

D.G. Fredlund, H. Raharjdo.1993. Soil Mechanics for unsaturated soils. John wiley & Sons, inc.

D.G. Fredlund, A. Xing. 1994. Equations for soil-water characterictic curve. Can Geotech J Vol.31, PP. 521-532.

D. Liu2, F. Zheng, S. Hu. 2013. Soil slope stability analysis under rainfall infiltration. Journal of Food, Agriculture & Environment Vol.11, PP.713-717.

D. yang, G. Li.2009.Chaotic dynamics analysis and control of iterative procedure of capacity spectrum method.Soil dynamic and earthquake engineering. Vol. 29, PP.459-468.

D. Liu, Fugang Zheng, Shaowei Hu. Soil slope stability under rainfall infitration.Journal of food, argiculture and environment. Vol.11,PP. 713-717.

E. C. Leong, H. Rahardjo. 1997. Review of soil-water characteristic curve equations. Journal of geotechnical and geoenvironmental engineering. December 1997.

E. Damiano, P. Mercogliano.2013.Potential effects of climate change on slope stability in unsaturated pyroclastic solis.The second world landslide forum. Vol.4.

F. Cai, K. Ugai. 2004. Numerical Analysis of Rainfall Effects on Slope Stability. international journal of geomechanics ASCE. June 2004.

F. Guzzetti, S. Peruccacci, M. Rossi, C. P. Stark.2007. Rainfall thresholds for the initiation of landslides in central and southern Europe. Meteorol Atmos Phys. Vol. 98, PP. 239–267

G. Biondi, E. Cascone, M. Maugeri. 2002. Flow and deformation failure of sandy slopes. Soil Dynamics and Earthquake Engineering. Vol. 22, PP.1103–1114.

G.B. Crosta.2001. Failure and flow development of a complex slide: the 1993 Sesa landslide. Engineering Geology. Vol. 59, PP. 173-199.

G. Biondi, E. Cascone, M. Maugeri. 2002. Flow and deformation failure of sandy slopes. Soil Dynamics and Earthquake Engineering. Vol. 22, PP. 1103–1114.

G.W. Jia, Tony L.T. Zhan, Y.M. Chen, D.G. Fredlund. 2009. Performance of a large-scale slope model subjected to rising and lowering water levels. Engineering Geology . Vol. 106, PP. 92–103.

G. Furuya, A. Suemine, K. Sassa, T. Komatsubara, N. Watanabe, H. Marui. 2006. Relationship between groundwater flow estimated by soil temperature and slope failures caused by heavy rainfall, Shikoku Island, southwestern Japan. Engineering Geology. Vol. 85, PP. 332–346.

H. Rahardjo, T. H. Ong, R. B. Rezaur, E. C. Leong.2007. Factors controlling instability of homogeneous soil slopes under rainfall. Journal of geotechnical and geoenvironmental engineering ASCE. december 2007.

H. Rahardjo, E. C. Leong, R. B. Rezaur. 2008.Effect of antecedent rainfall on pore-water pressure distribution characteristics in residual soil slopes under tropical rainfall. Hydrol. Process. Vol. 22, PP. 506–523.

H. Rahardjo, X.W. LI, D. G. Toll, E. C. Leong. 2001. The effect of antecedent rainfall on slope stability. Geotechnical and Geological Engineering. Vol. 19, PP. 371-399.

H. Chen, C. F. Lee, K. T. Law. 2004. Causative Mechanisms of Rainfall-Induced Fill Slope Failures. Journal of geotechnical and geoenvironmental engineering © ASCE. June PP. 593.

I. Tsaparas, H. Rahardjo, D.G. Toll, E.C. Leong.2002. Controlling parameters for rainfall-induced Landslides. Computers and Geotechnics. Vol. 29, PP. 1–27.

J. D. Philips.2006.Deterministic chaos and historical geomorphology : A review and look forward. Geomorphology. Vol. 76, PP.109-121.

J.D. Phillips.1993.Instability and chaos in hill slope evolution. American Journal of science. Vol. 293, PP.25-48.

J.D.Phillips. 1995. Nonlinear dynamic and the evolution of relief. Geomorphology. Vol. 14, PP.57-64.

J. Kim, S. Jeong, S. Park, J. Sharma. 2004. Influence of rainfall-induced wetting on the stability of slopes in weathered soils.Engineering Geology. Vol. 75,PP. 251–262.

J.J. Jiao, X. S. Wang, S. Nandy.2005. Confined groundwater zone and slope instability in weathered igneous rocks in Hong Kong. Engineering Geology. Vol . 80, PP. 71–92.

J.Sulem.2010.Bifurcation theory and localization phenomena. European Journal of Environmental and civil engineering. Vol 14:8-9, PP.989-1009.

K. Gavin, J. Xue.2007. A simple method to analyze infiltration into unsaturated soil slopes. Computer and geotechnics. Vol.35, PP.185-208.

K. Millington, F.J. Wright. Algebraic computations in elemntary catastrophe theory. Queen Mary College University of London.

K.T.Chau. 1994. Lanslide modeled as bifurcation of creeping slopes with nonlinear friction law. Int. J. Solids structure. Vol. 32, PP. 3451-3464.

K. T. CHAU.1999. Onset of natural terrain landslides modeled by linear stability analysis of creeping slopes with a two-state variable friction law. Int. J. Numer. Anal. Meth. Geomech. Vol. 23, PP. 1835-1855.

K.T. Chau. 1995. Landslides modeled as bifurcations of creeping slope with nonlinear friction law. Solid Structures. Vol. 32, PP.3451-3464.

L.Lam, D.G.Fredlund. 1993. A general limit equilibrium model for three-dimensional slope stability analysis. Can Geotech. Vol. 30, PP. 905-919.

L. M. Lee, N. Gofar, H. Rahardjo. 2009. A simple model for preliminary evaluation of rainfall-induced slope instability. Engineering Geology. Vol. 108, PP. 272–285.

Marc Chaperon. Catastrophes un temoignage .

Miao X., Li. S, Chen. Z.2009.Bifurcation and catastrophe of seepage flow system in broken rock.Mining science and technology. Vol.19, PP.0001-0007.

M.T.V. Genuchten.1980.A close-form equation for predicting the hydraulic conductivity of unsaturated soils. Soil Sci Soc. Vol. 44, PP. 892-898.

M. Calvello, L. Cascini, G. Sorbino. 2008. A numerical procedure for predicting rainfall-induced movements of active landslides along pre-existing slip surfaces. Int. J. Numer. Anal. Meth. Geomech. Vol. 32, PP.327–351.

M. D. Fredlund, G. W. Wilson, D. G. Fredlund.1997. Indirect procedures to determine unsaturated soli property function.Procceding of the 50th Canadian geotechnical conference Golden Jubille Conference Ottawa, Ontaria, Canada, 1997.

N.E. Fettouhi, J. Zemmouri, B. Segard, B. Macke.1995.Dynamical hysteresis of bistable systems : from the deterministic to the fluctuation-dominated case.Physics Letters A.PP. 251-254.

P. Aleotti. 2004. A warning system for rainfall-induced shallow failures. Engineering Geology Vol. 73, PP. 247–265.

P. Frattini, G. Crosta, R. Sosio. 2009. Approaches for defining thresholds and return periods for rainfall-triggered shallow landslides. Hydrol. Process. Vol. 23, PP. 1444–1460.

P. T. Saunders.1980.Catastrophe theory.London.Cambridge university press.

R. K. Dahal, S. Hasegawa,A. Nonomura, M. Yamanaka,T. Masuda, K. Nishino.2009. Failure characteristics of rainfall-induced shallow landslides in granitic terrains of Shikoku Island of Japan. Environ Geol Vol. 56, PP. 1295–1310.

Robet C. Hilborn. Chaos and nonlinear dynamics an introduction for sceintists and engineers. Oxford Univercity press.

R. Schnellmann, M. Busslinger, H.R. Schneider, H. Rahardjo. 2010. Effect of rising water table in an unsaturated slope. Vol. 114, PP.71-83.

Robert W. D.,Fellow. 1997. State of the art: limit equilibrium and finite-lement

R. M. Iverson.2005. Regulation of landslide motion by dilatancy and pore pressure feedback. Journal of geophysical research. VOL. 110, F02015.

Steven H. Strogatz.1994. Nonlinear synamics and chaos with application to physics, biology, chemistry and engineering. Advance book program perseus books reading, massachusetts.

S.E. Cho, S.R. Lee.2001. Instability of unsaturated soil slopes due to infiltration. Computer and geotechnics. Vol.28, PP.185-208.

S.E. Cho, S.R. Lee. 2001.Instability of unsaturated soil slopes due to infiltration.Computers and Geotechnics. Vol. 28, PP. 185-208.

S.E.Cho. 2009. Infiltration analysis to evaluate the surficial stability of two-layered slopes

considering rainfall characteristics. Engineering Geology. Vol. 105 PP. 32–43.

Analysis of slopes. Journal of geotechnical and geoenvironmental engineering . September 1997.

S.Q. Qin 7 J.J. Jiao 7 S.J. Wang. 2000. The predictable time scale of landslides. Bull Eng Geol Env. Vol. 59, PP. 307–312.

S.Q. QIN, J. J. JIAO, Z.G. Li.Nonlinear of istability of plane-shear slope : catastrophe, bifurcation, cahos and physical prediction.Rock Mechanic and Rock engineering.Vol. 39,PP.59-76.

S. Qin, Jiu Jimmy Jiao, Sijing Wang, Hui Long.2001.A nonlinear catastrophe model of instability of planar-slip slop and chaotic dynamical mechanisms of its evolutionary process.Solid and Structures.Vol. 38,PP. 8093-8109.

S.Qin, J.J. Jiao, S. Wang. 2002. A nonlinear dynamical model of landslide evolution. Geomorphology. Vol. 43, PP. 77-85.

S.Qin, J.J. Jiao, S.Wang.2002.A Nonlinear dynamical model of landslide evolution.geomorphology.Vol.43, PP.77-85.

S.Qin, J.J. Jiao, S.Wang.2000.The predictable time scale of landslide. Bull Eng Geol Env. Vol.59, PP.307-312.

S.W.C. Au. 1998. Rain-induced slope instability in Hong Kong. Engineering Geology. Vol. 51, PP. 1–36.

T. L. Tsai, H. E. Chen, J. C. Yang. 2008. Numerical modeling of rainstorm-induced shallow landslides in saturated and unsaturated soils. Environ Geol. Vol. 55, PP. 1269–1277.

T.W.J. v. Asch, J.P. Malet, L.P.H.v. Beek.2006. Influence of landslide geometry and kinematic deformation to describe the liquefaction of landslides: Some theoretical considerations. Engineering Geology. Vol. 88, PP. 59–69.

Valdimir I. Arnold.1992.Catastrophe theory.Berlin.Springer.

Y. Kun, W. Tongxu, M. Zhitao.Application of cups catastrophe theory to reliability analysis of slope in open-pit mines. Mining science and technology.Vol. 20,PP. 0071-0075.

Y. Tao, J. Cao, J. Hu, Z. Dai.2013.A cusp catastrophe model of mid-long-term landslide evolution over low latitude highlands of China.Geomorphology.Vol.187,PP.80-85.

Zhenya Yan. 2007. Hopf bifurcation in the Lorenz-type chaotic system. Chaos, Solitons and Fractals. Vol. 31, PP. 1135–1142.

Z. Huang, K. T. Law, H. Liu, T. Jiang.2009.The chaotic characteririsctics of landslide evolution : a case study of Xintan landslide.Environ Geol. Vol.56, PP.1585-1591.

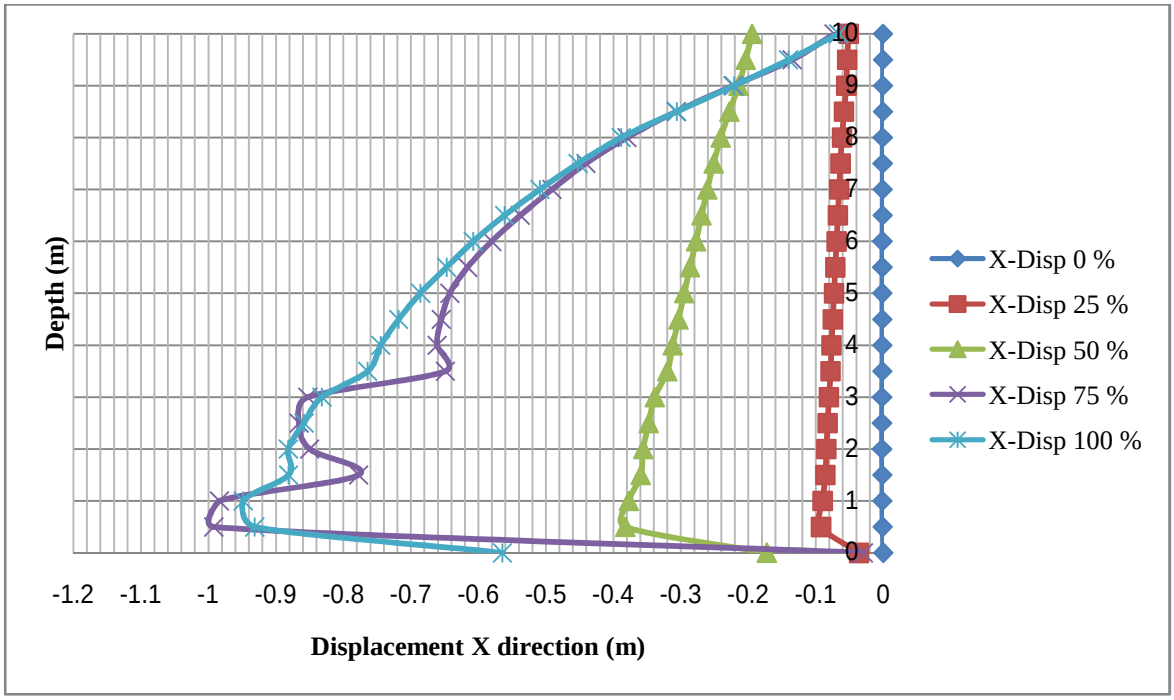

Figure A.1: Influence of the water-table level on the lateral displacement

(Case 2, β = 30°) *hw/H* = 0.25, 0.5, 0.75 and 1.0

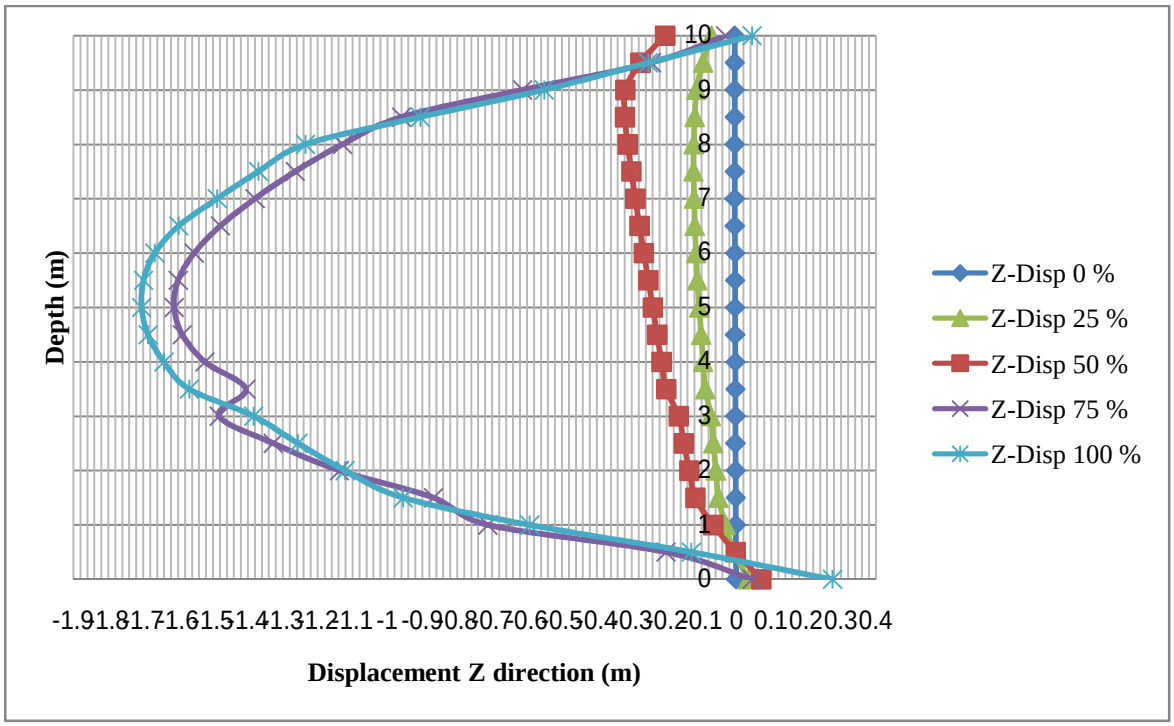

Figure A.2: Influence of the water-table level on the vertical displacement

(Case 2, β = 30°) *hw/H* = 0.25, 0.5, 0.75 and 1.0

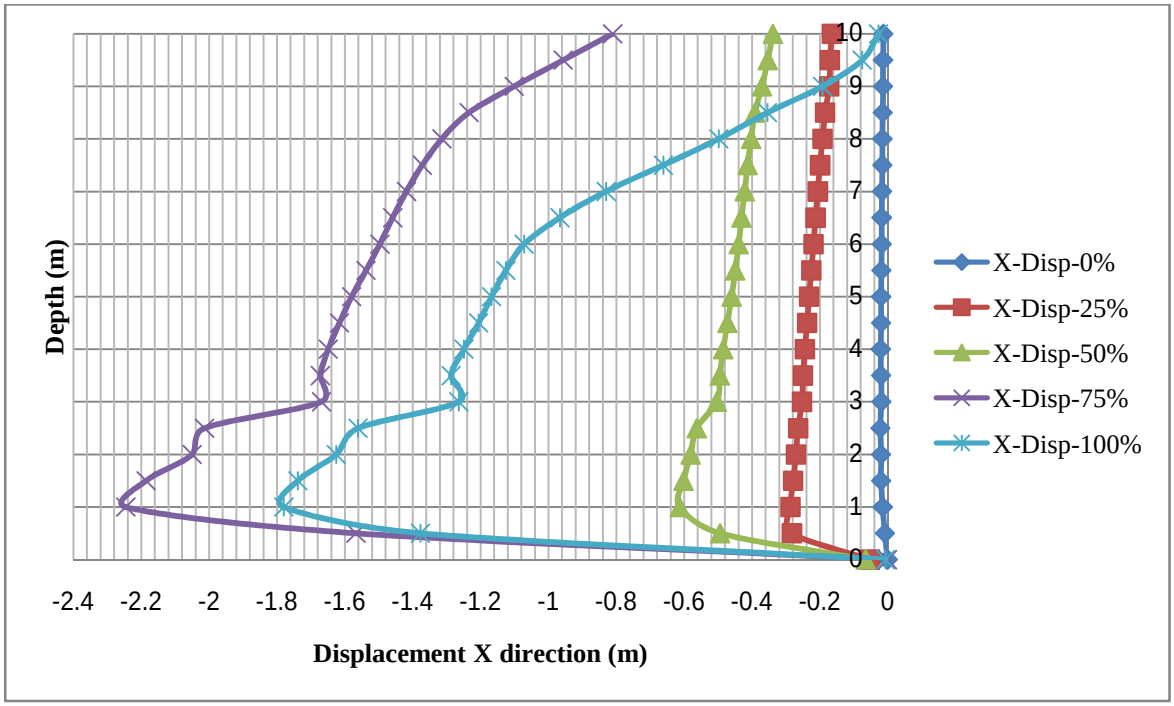

Figure A.3: Influence of the water-table level on the lateral displacement

(Case 2, β = 35°) *hw/H* = 0.25, 0.5, 0.75 and 1.0

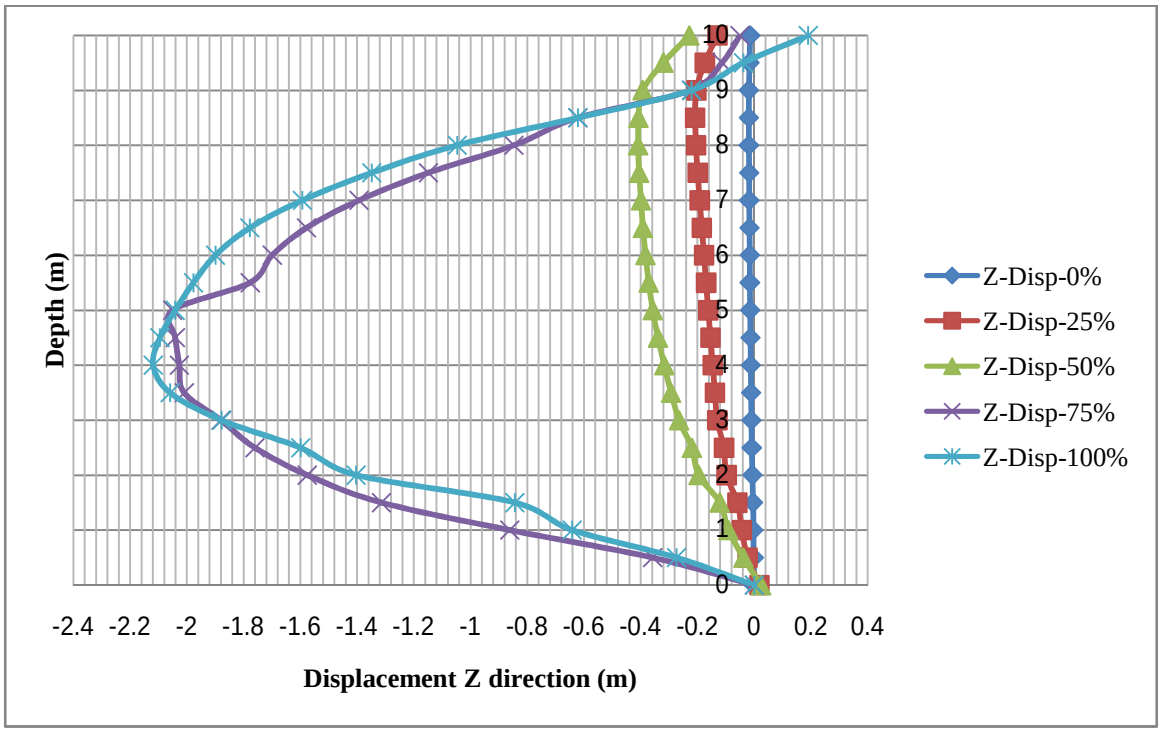

Figure A.4: Influence of the water-table level on the vertical displacement

(Case 2, β = 35°) *hw/H* = 0.25, 0.5, 0.75 and 1.0

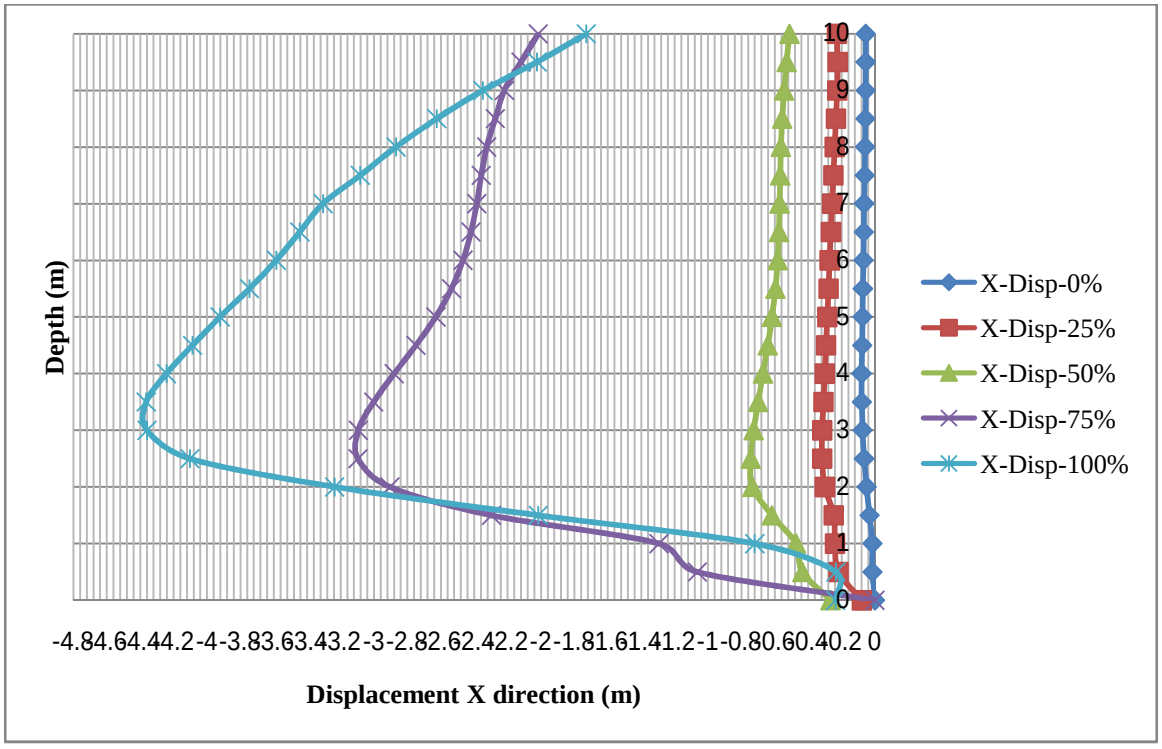

Figure A.5: Influence of the water-table level on the lateral displacement

(Case 2, β = 40°) *hw/H* = 0.25, 0.5, 0.75 and 1.0

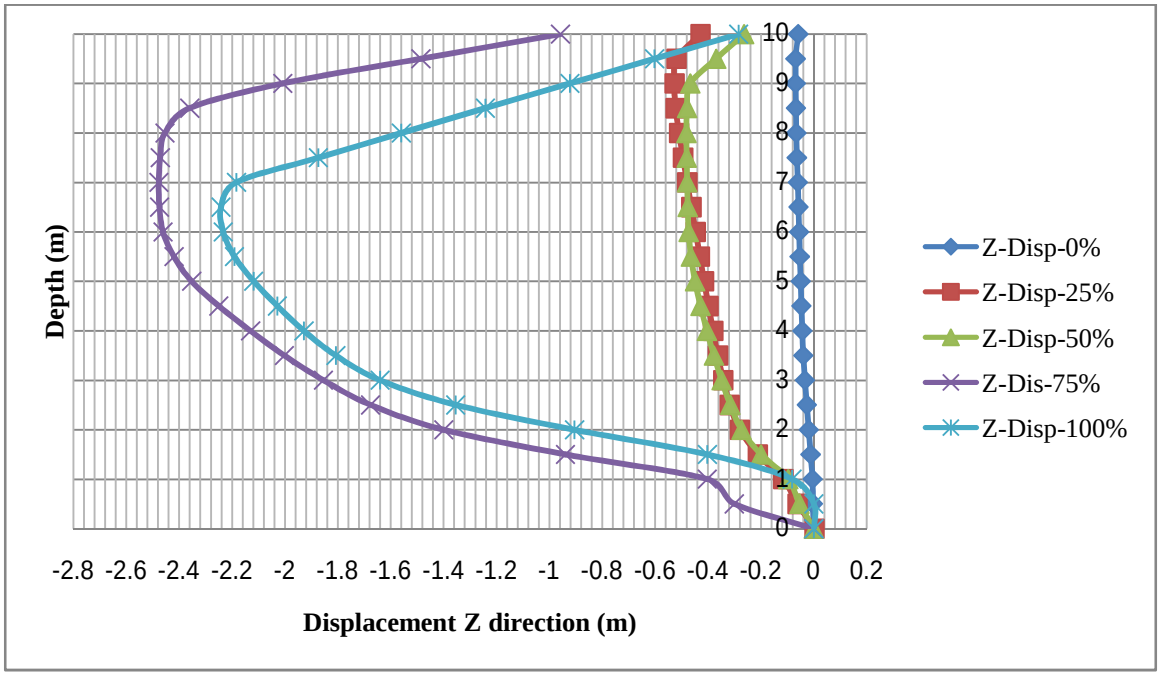

Figure A.6: Influence of the water-table level on the vertical displacement

(Case 2, β = 40°) *hw/H* = 0.25, 0.5, 0.75 and 1.0

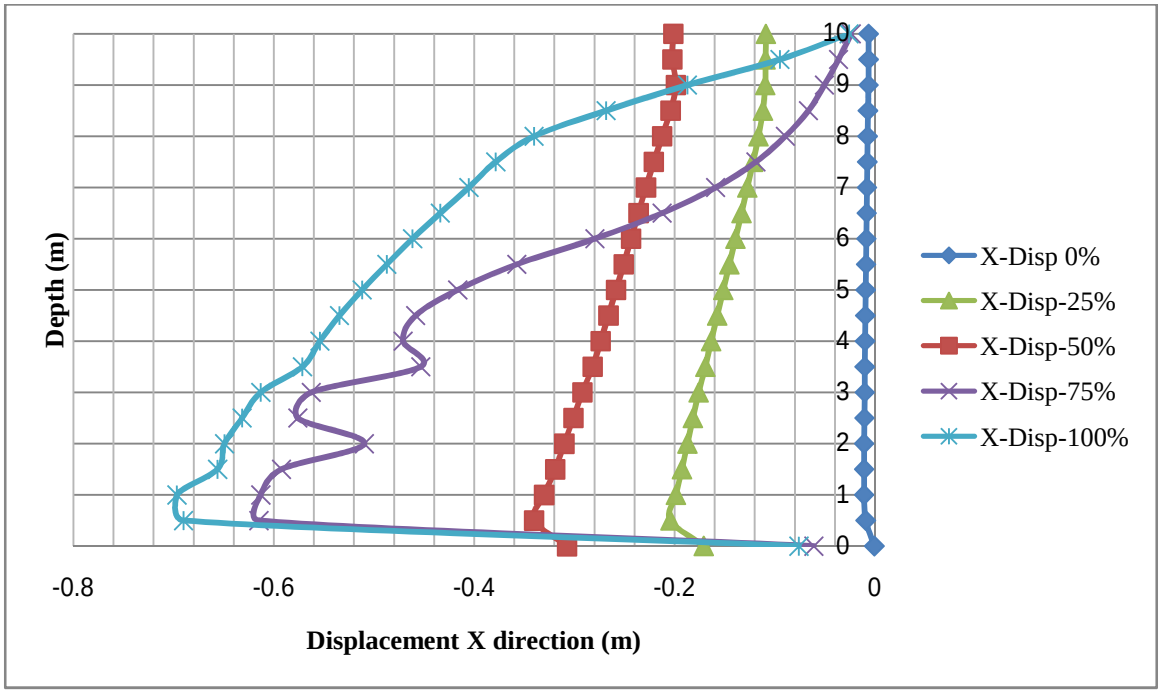

Figure A.7: Influence of the water-table level on the lateral displacement

(Case 4, β = 30°) *hw/H* = 0.25, 0.5, 0.75 and 1.0

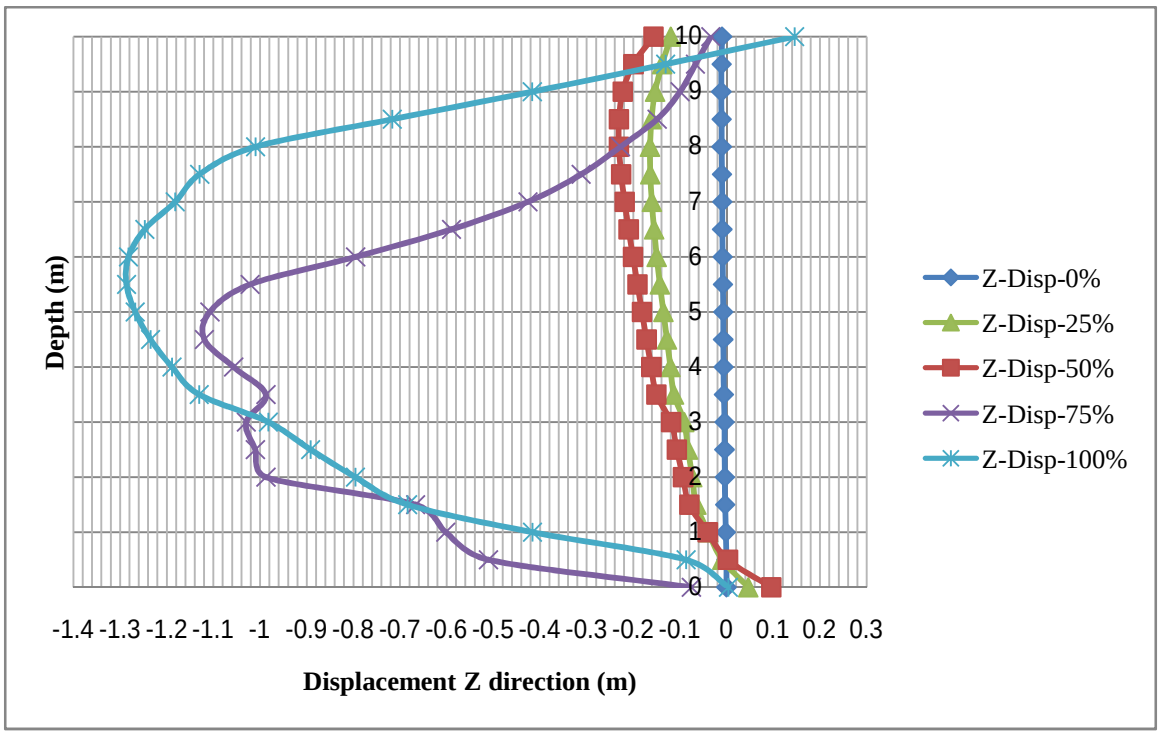

Figure A.8: Influence of the water-table level on the vertical displacement

(Case 4, β = 30°) *hw/H* = 0.25, 0.5, 0.75 and 1.0

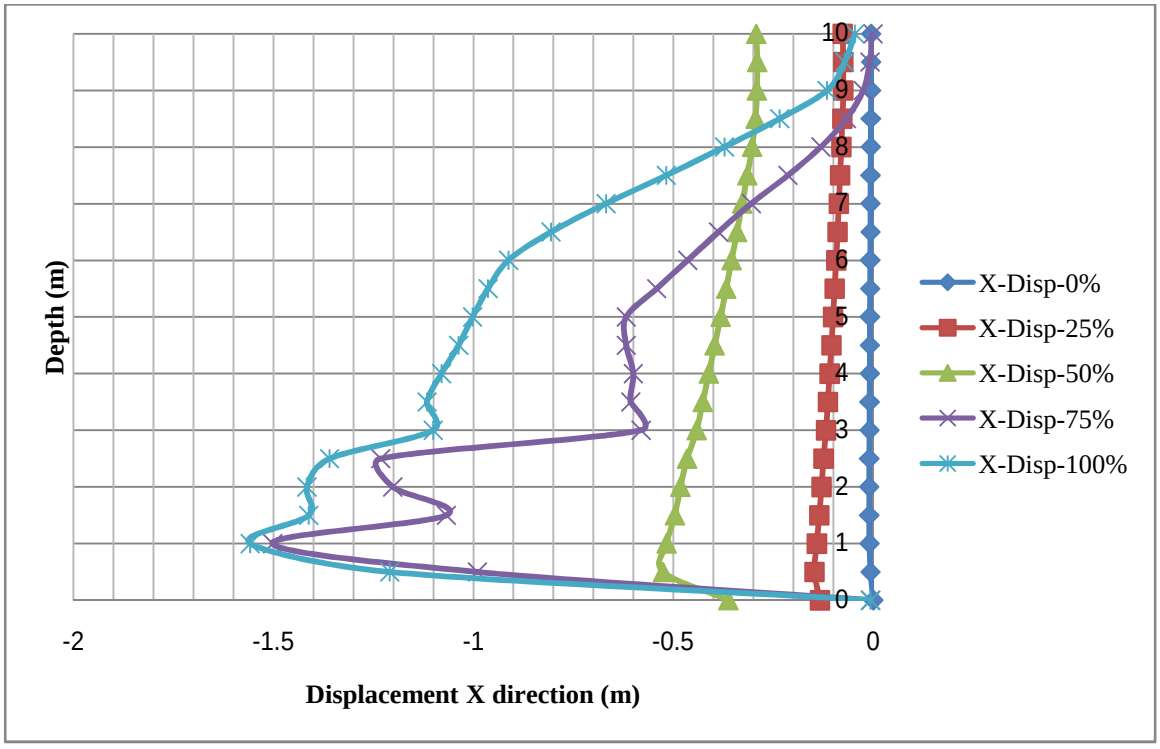

Figure A.9: Influence of the water-table level on the lateral displacement

(Case 4, β = 35°) *hw/H* = 0.25, 0.5, 0.75 and 1.0

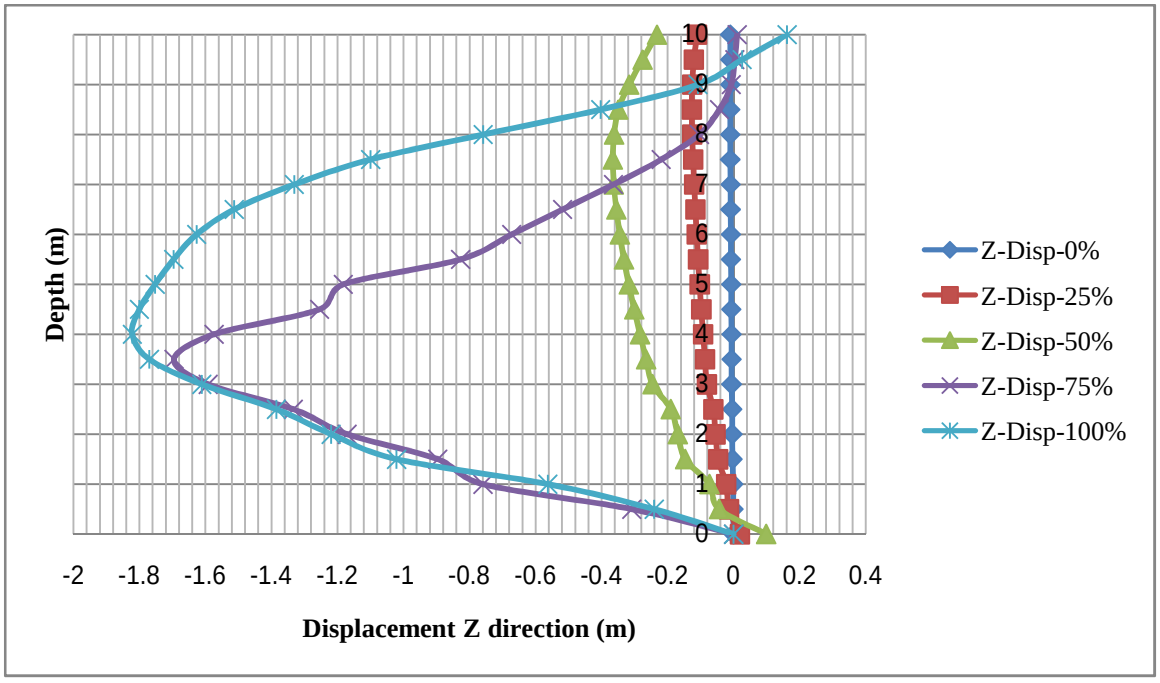

Figure A.10: Influence of the water-table level on the vertical displacement

(Case 4, β = 35°) *hw/H* = 0.25, 0.5, 0.75 and 1.0

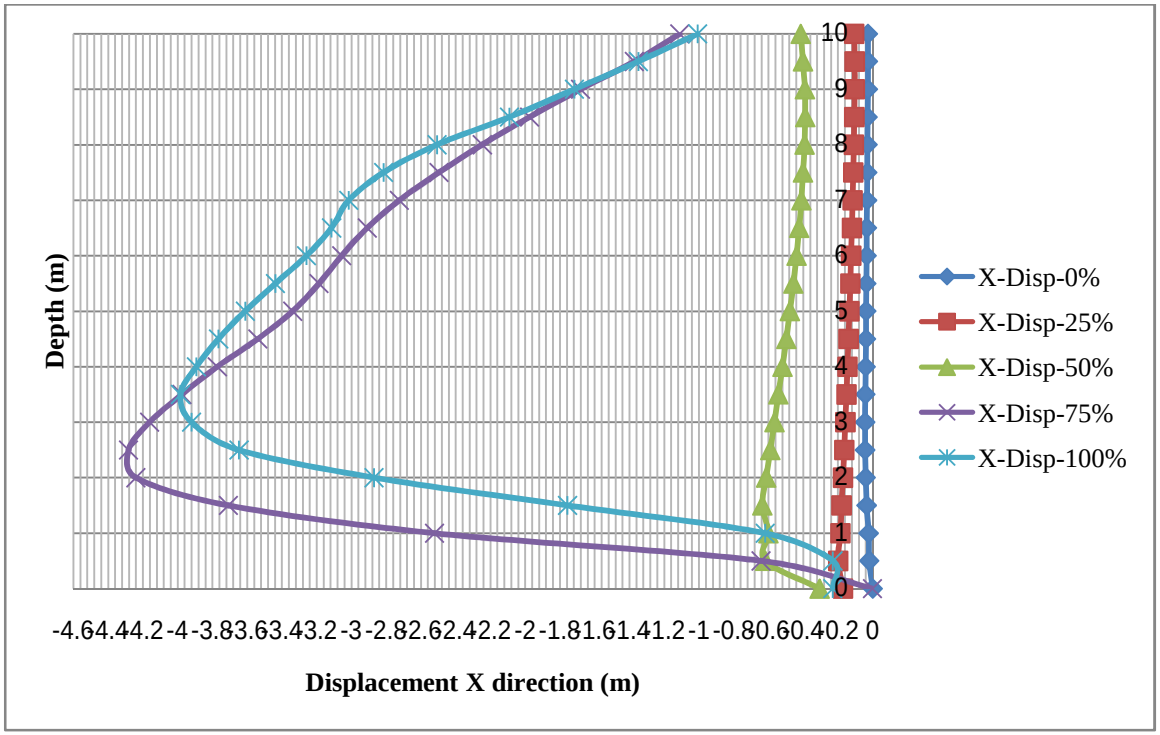

Figure A.11: Influence of the water-table level on the lateral displacement

(Case 4, β = 40°) *hw/H* = 0.25, 0.5, 0.75 and 1.0

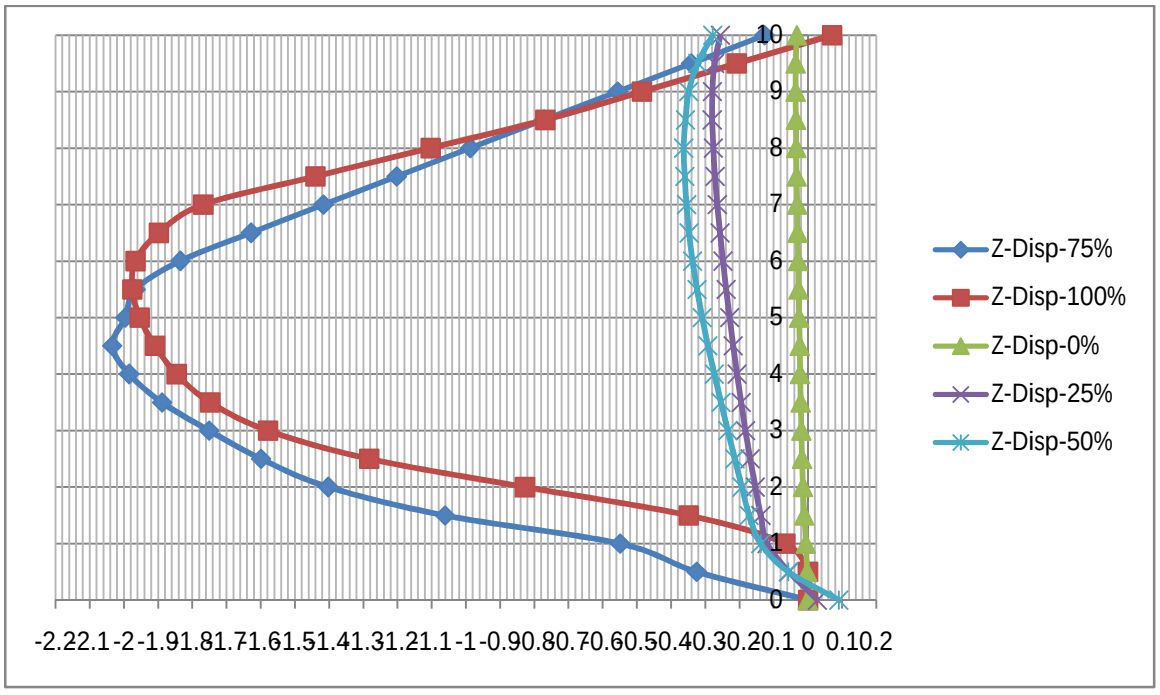

Figure A.12: Influence of the water-table level on the vertical displacement

(Case 4, β = 40°) *hw/H* = 0.25, 0.5, 0.75 and 1.0

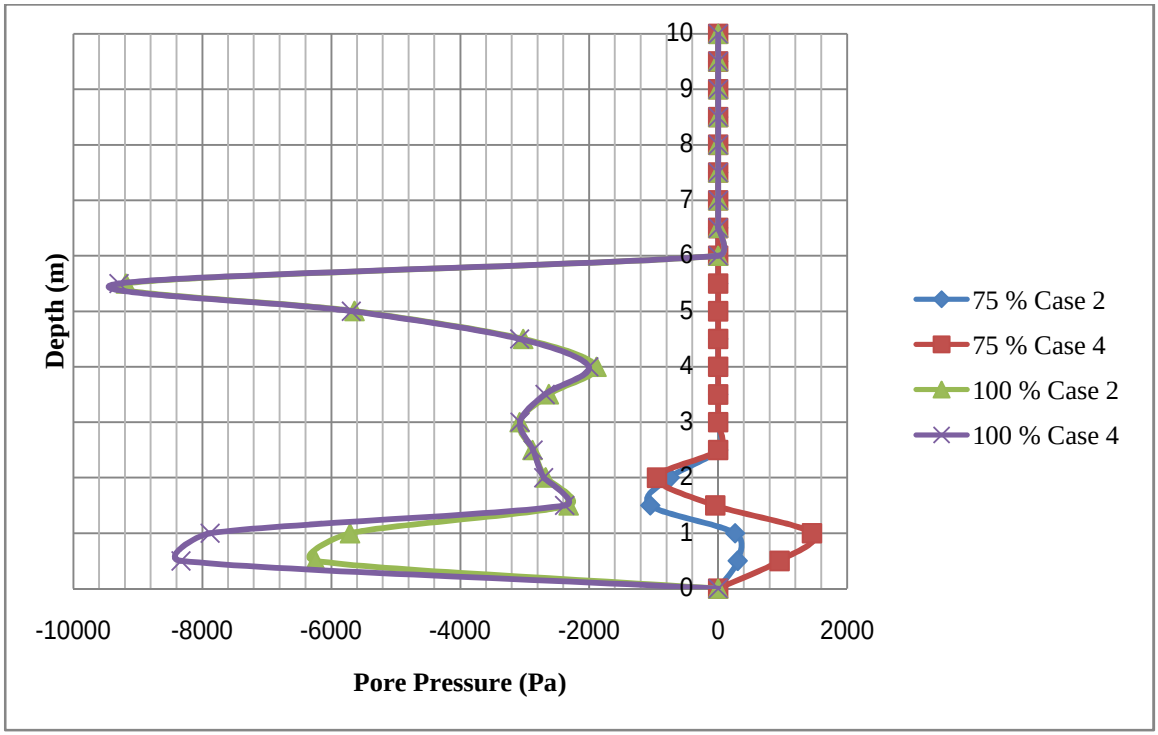

Figure A.13 : Influence of the soil strength on the distribution of the pore pressure (Cases 2 and 4, β= 30°)

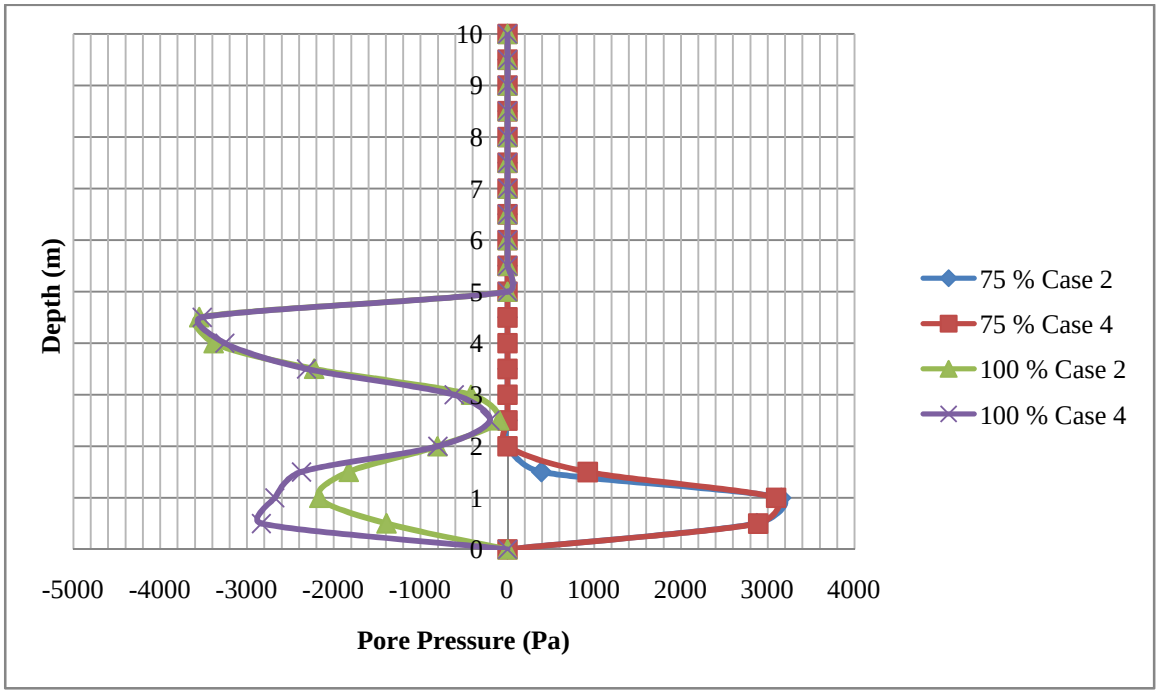

Figure A.14 : Influence of the soil strength on the distribution of the pore pressure (Cases 2 and 4, β= 35°)

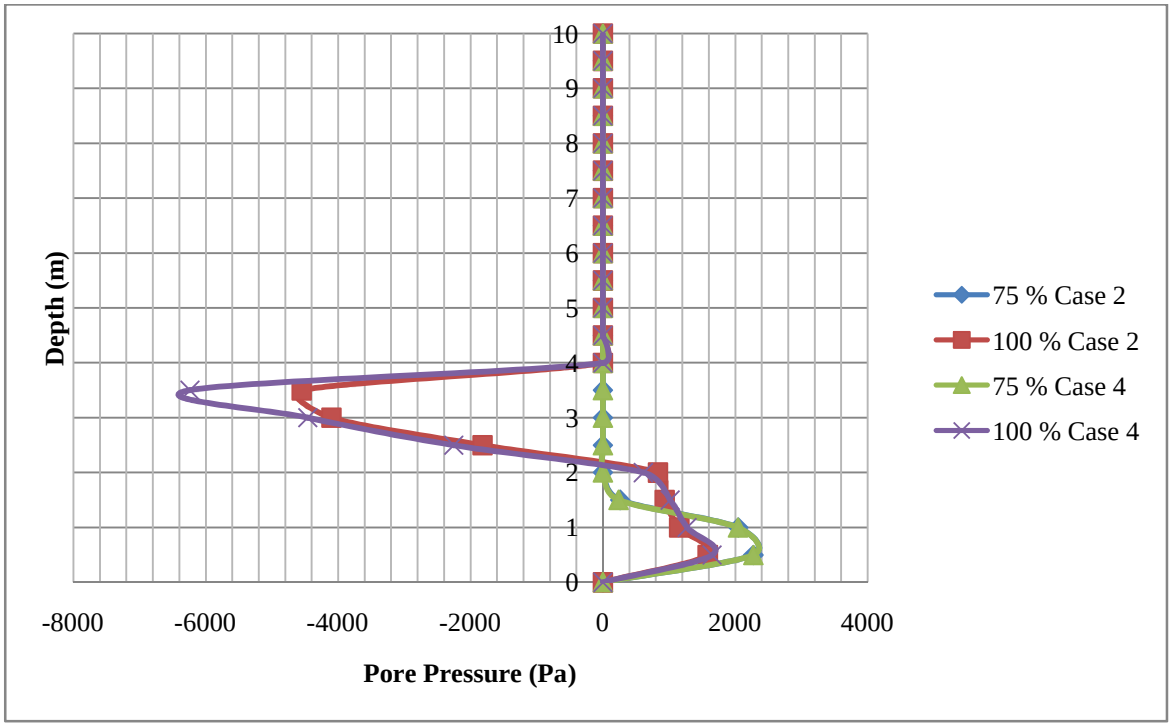

Figure A.15: Influence of the soil strength on the distribution of the pore pressure (Cases 2 and 4, β = 40°)